University of Nevada, Reno

Estimating Free Field Seismic Settlement History in a Saturated Layered Soil Profile

A dissertation submitted in partial fulfillment of the

requirements for the degree of Doctor of Philosophy in

Civil & Environmental Engineering

by

Nima Mojtahedzadeh

Dr. Rajaratnam Siddharthan/Dissertation Advisor

May 2021

THE GRADUATE SCHOOL

We recommend that the dissertation
prepared under our supervision by

Nima Mojtahedzadeh

entitled

Estimating Free Field Seismic Settlement History in a Saturated Layered Soil Profile

be accepted in partial fulfillment of the
requirements for the degree of

Doctor of Philosophy

Raj Sidharthan, PhD
Advisor

Ramin Motamed, PhD
Committee Member

John Anderson, PhD
Committee Member

Stephen E. Dickenson, PhD
Committee Member

Michael Gardner, PhD
Graduate School Representative

David W. Zeh, Ph.D., Dean
Graduate School

May, 2021

Abstract

Existing methods proposed for estimating the earthquake-induced one-dimensional free-field settlement in saturated soil, focus on the post-liquefaction permanent volumetric strain. These methods rely on undrained cyclic laboratory tests that subject the sandy samples to uniform cycles. A new method is presented to estimate the free-field one-dimensional settlement histories induced by random base motions. This approach uses an existing incremental volumetric strain model to determine the settlement history before and after liquefaction. The shear strain history of a layered profile was obtained from an effective stress-based response analysis available as an option in DEEPSOIL and was subsequently used as an input to the proposed method. A simple two-parameter porewater pressure generation model available in DEEPSOIL was employed. This model, which is capable of simulating strain-softening, was calibrated to an existing probabilistic liquefaction potential curve and acceptable rate of porewater pressure generation. The proposed method was then used to calculate the settlements at the Marina District after the 1989 Loma Prieta earthquake, at Port Island after the 1995 Kobe earthquake, and at 6 different sites located within Christchurch and Ferrymead after the 2011 Christchurch earthquake. The estimated settlements were compared to the measured values along with those estimated by existing methods.

Subsequently, the proposed incremental volumetric strain model is used to calculate the earthquake-induced one-dimensional free-field settlement in liquefiable three-layered profiles subjected to a variety of earthquake ground motions. The shear strain histories of these profiles, obtained from the effective stress-based response analysis using DEEPSOIL, were used as an input to the incremental volumetric strain model. A new simplified equation has been developed to estimate the free-field one-dimensional settlement based on the analytical results from the three-

layered profiles. This equation includes the influence of important earthquake parameters and soil layer configuration and properties. The proposed equation is compared to the predictions made by an established model. This equation is then used to estimate the free-field settlements at 7 locations in the Marina District after the 1989 Loma Prieta earthquake and at 3 different sites after the 2011 Christchurch earthquake. The evaluated settlements were found to be consistent to those observed at the site and the ones estimated by an existing method.

Keywords: Settlement, Soil liquefaction, DEEPSOIL, Volumetric strain, Earthquake

DEDICATION

This dissertation is dedicated to the victims of the Ukraine International Airlines Flight 752 tragedy, whose lives were taken innocently.

You shall never be forgotten.

ACKNOWLEDGEMENTS

I would like to express my appreciation to Professor Raj Siddharthan, my advisor, who guided me through my research. Much gratitude is also given to my committee members, Dr. Ramin Motamed, Dr. John Anderson, Dr. Stephen Dickenson, and Dr. Michael Gardner for their precious comments and guidance.

I would like to thank my family, specially my mother and father for their love and support. I would also thank Mahshid for her passionate support, and my friends Milad, Joe, Peyman, Mohammad, Mona, Fahim, Swasti and Oveis for their help and support.

Table of Contents

List of Tables

List of Figures

Chapter 1: Introduction

1.1. Overview of the study and objectives

Ground motion-induced settlements are among the most hazardous consequences of earthquakes, damaging both structures and infrastructures. Earthquake-induced settlements are basically the result of the densification and compaction of loose granular soils after an earthquake loading. In loose granular saturated deposits, where liquefaction can also be likely, significant deformations occur. This large permanent deformation also dominates the compaction of the non-liquefied layers. Liquefaction is the process whereby soil behaves as if it were a fluid, when the effective stress decreases close to zero. This phenomenon occurs when the porewater pressure increases and cannot get dissipated as fast as it increases during an earthquake. In recent years, events including the 1989 Loma Prieta Earthquake and 2011 Christchurch Earthquake have attracted widespread recognition for the earthquake-induced settlements, especially to those caused by liquefaction.

The importance of the earthquake-induced building settlement has caused many researchers to study different parameters affecting it. In general, volumetric-induced, shear-induced, and ejecta-induced settlements have been identified as the main mechanisms of liquefaction-induced building settlement. After calculating each term, the total building settlement is estimated as the sum of those components. Besides these mechanisms, lateral spread is the other primary component of ground settlement.

Several methods have been proposed to predict the volumetric-induced one-dimensional free-field settlement in layered deposits. These methods focus mainly on the post-liquefaction compaction of saturated soils and are based on laboratory and field test results. Numerical

methods suffer from a major limitation that the liquefaction-induced settlement cannot capture the sedimentation under zero effective stress (post-liquefaction). Therefore, semi-empirical methods are currently the most popular approaches for calculating the volumetric liquefaction-induced settlement. In many cases, these empirical methods tend to overestimate the settlement by a considerable margin, as discussed by Ziotopoulou and Boulanger (2013).

A variety of field tests have been developed for the evaluation of liquefaction resistance for sandy soils. The standard penetration test (SPT), the cone penetration test (CPT) and shear-wave velocity measurement are among the most widespread methods to obtain the liquefaction resistance of sandy soils. The SPT-based method had been the most popular practice to calculate earthquake-induced ground settlement. More recently, CPT-based methods have been developed and increasingly used to predict the liquefaction-induced settlement.

The main objective of this study is to propose a new practical numerical method to capture the volumetric-induced settlement history (caused by grain slip), during the developing liquefaction conditions for a layered soil profile that can be readily incorporated in the performance-based engineering (PBE) design methodology. This method can also be used to generate a new simplified equation to estimate the earthquake-induced free-field settlement in both liquefied and non-liquefied layered grounds.

1.2. Methodology

In order to calculate volumetric strain during and after an earthquake using the method proposed in this study, the strain history should be obtained in the layers of the site profile. DEEPSOIL can be used to develop the strain history of different layers, using an effective stress-based response analysis. DEEPSOIL is a one-dimensional layered soil response analysis

platform with options for both equivalent linear and nonlinear analyses. DEEPSOIL analysis treats the entire soil deposits as a continuum that is made of many sublayers and the soil response is evaluated based on boundary (base excitation and surface) and layer interface conditions (deformation and shear stresses). In this study, among the several soil models available on DEEPSOIL platform, a simple and popular dynamic sandy soil model (Seed and Idriss, 1970) and a porewater pressure generation model (General Berrill/Davis model) were chosen. The DEEPSOIL analysis model was calibrated with a single soil element to reproduce the rate of the porewater pressure generation similar to laboratory tests while matching the desired probability-based liquefaction potential curves for different relative densities. Such an approach enables the method to be incorporated in PBE.

Chapter 2: Literature review

In previous research, it has been recognized that sands densify as a result of ground motion. Shaking of saturated sands with no possibility of drainage (constant volume conditions) would result in generation of excessive porewater pressure. Once excess porewater pressure dissipates, settlement occurs. It can take anywhere between almost immediately to about a day for all settlement to develop depending on the porewater pressure dissipation characteristics of the soil layers and the length of the drainage path. In contrast, in dry sands, settlement occurs as a consequence of accumulated permanent volumetric strain during an earthquake shaking. Due to the fact that even modest settlements can result in noteworthy effects upon the performance of structures during an earthquake, recent research pertaining to the settlements of sands resulting from earthquake shaking has received considerable attention.

2.1. Previous studies on earthquake-induced settlement

Lee and Albaisa (1974) and Silver and Seed (1971) have suggested methods for evaluating the dry and saturated soil settlement. They studied the settlement of sands as a result of the excess porewater pressures dissipation developed during cyclic loading using laboratory cyclic loading. They concluded that he relative density, grain size and porewater pressure affect the amount of volumetric strain.

The post-liquefaction volumetric strain was studied by Tatsuoka, et al. (1984). They observed that settlement is influenced by the soil relative density and the induced maximum shear strain developed in the soil. Therefore, even though the maximum porewater pressure does not change much beyond the liquefaction stage, the maximum shear strain is an important parameter influencing the soil settlement. Tatsuoka, et al. (1984) summarized the relationships between relative density and volumetric strain after initial liquefaction from their studies in Figure 1, which includes the data points from the research conducted by Lee and Albaisa, Tatsuoka, et al. and Yoshimi et al. Even though different types of sands were used in these studies, overall, the results are consistent. It is obvious that as soil relative density decreases and induced strain increases, the volumetric strain increases significantly.

Tokimatsu and Seed (1987) proposed another method based on the previous studies to determine the volumetric strain of dry soil during an earthquake as a function of the cyclic shear strain amplitude, the corrected SPT blow counts, relative density and the equivalent number of cycles corresponding to the magnitude of the earthquake. They utilized relationship between volumetric strain and shear strain amplitude for sands at different relative densities suggested by Silver and Seed (1971) and presented the relationship between the $(N_1)_{60}$ values and the volumetric strain for

15 cycles, which is equivalent to an earthquake with the magnitude of 7.5 (Figure 2). For earthquakes with uniform cycles other than 15, a correction factor can be applied (Figure 3). They also listed a series of field observations for the earthquake-induced settlements in saturated sands and compared them to the tentative relationship between the cyclic stress ratio, $(N_1)_{60}$ and volumetric strain.

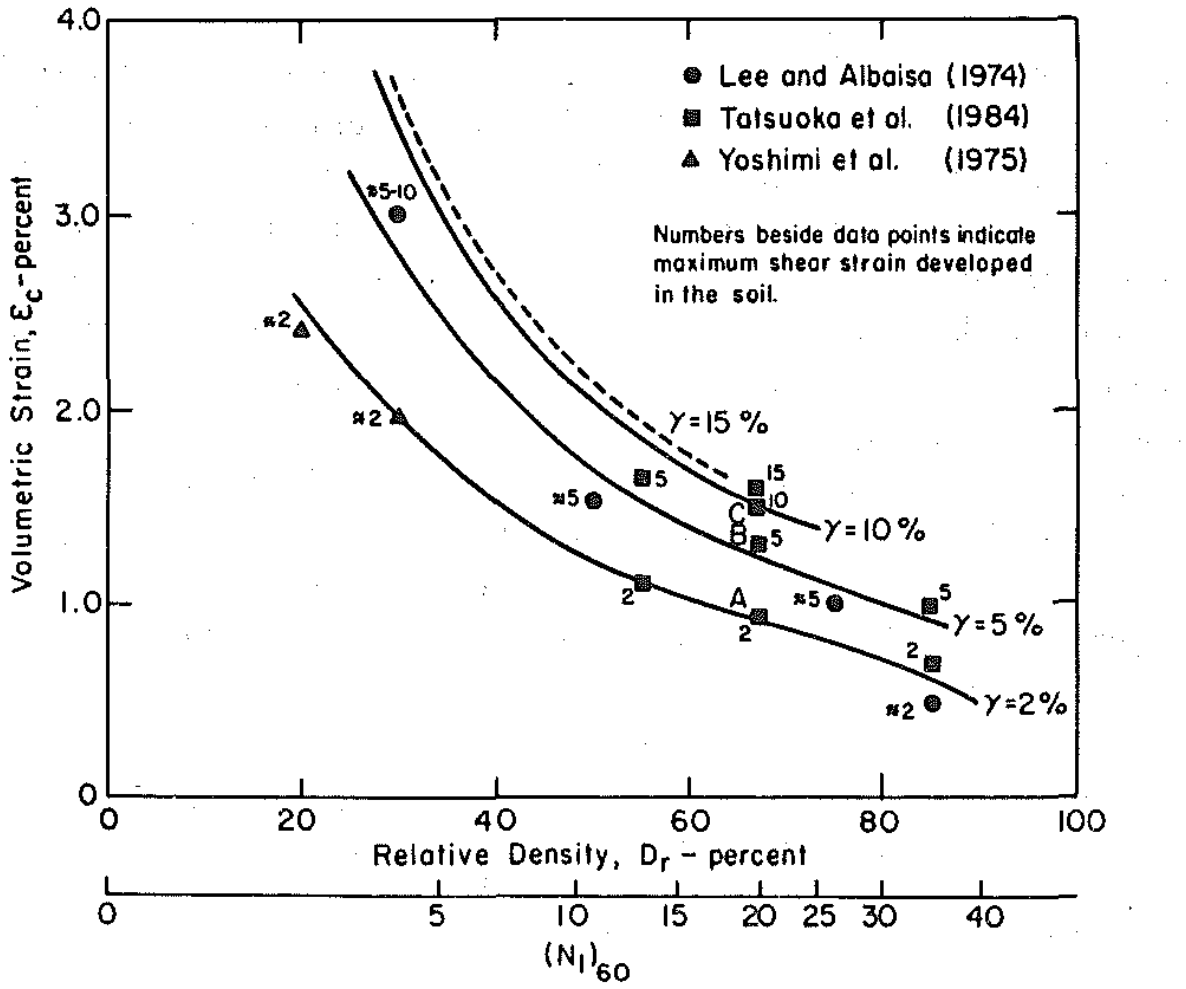

Figure 1. Relationship between volumetric strain, induced shear strain, and relative density for sands after Tatsuoka et al. (1984)

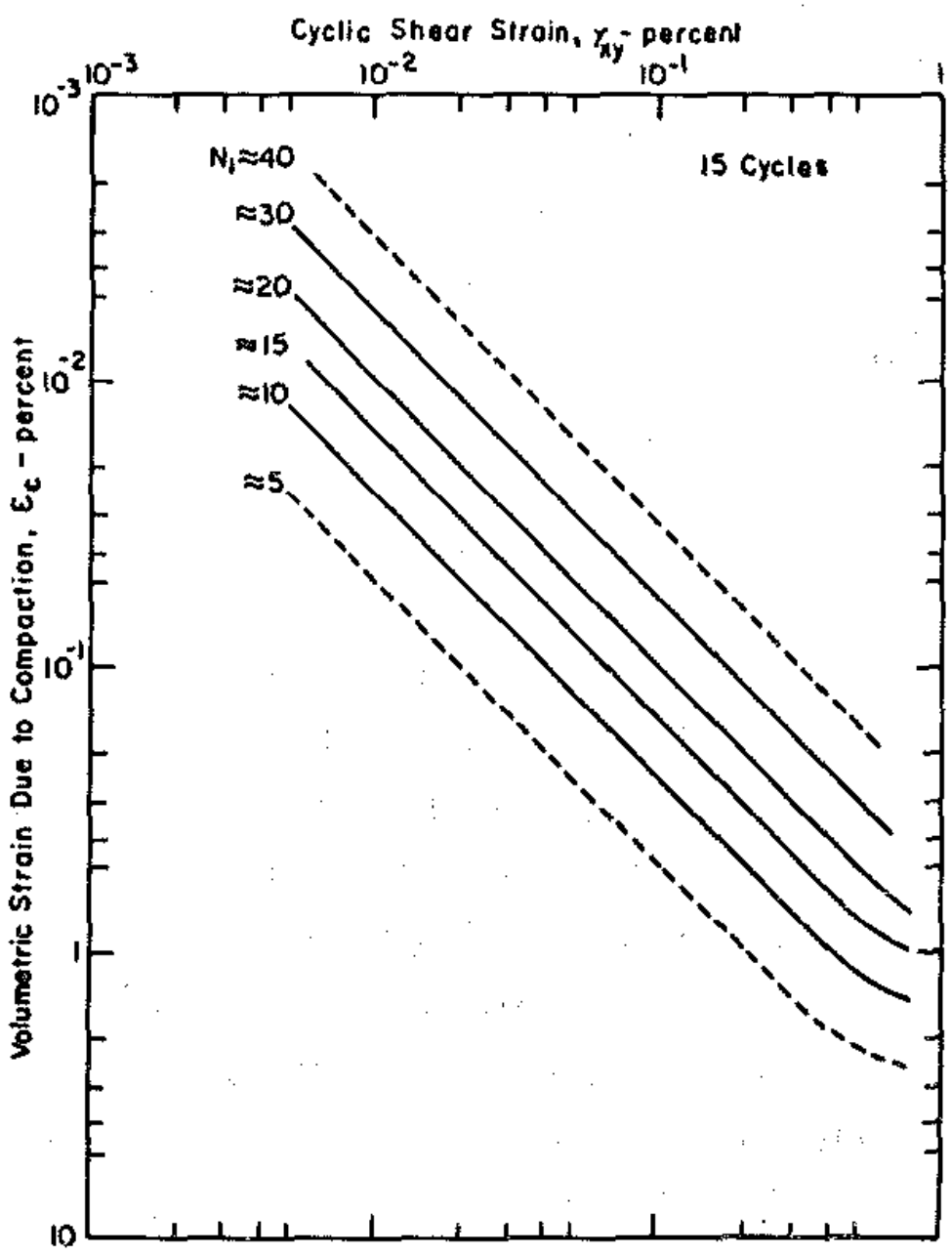

Figure 2. Relationship between volumetric strain, shear strain, and $(N_1)_{60}$ for dry sands after Tokimatsu and Seed (1987)

Table 1. Influence of earthquake magnitude on volumetric strain ratio for dry sands after Tokimatsu and Seed (1987)

Earthquake magnitude (1)	Number of representative cycles at 0.65 τ_{max} (2)	Volumetric strain ratio, $\epsilon_{C,N}/\epsilon_{C,N=15}$ (3)
8-1/2	26	1.25
7-1/2	15	1.0
6-3/4	10	0.85
6	5	0.6
5-1/4	2–3	0.4

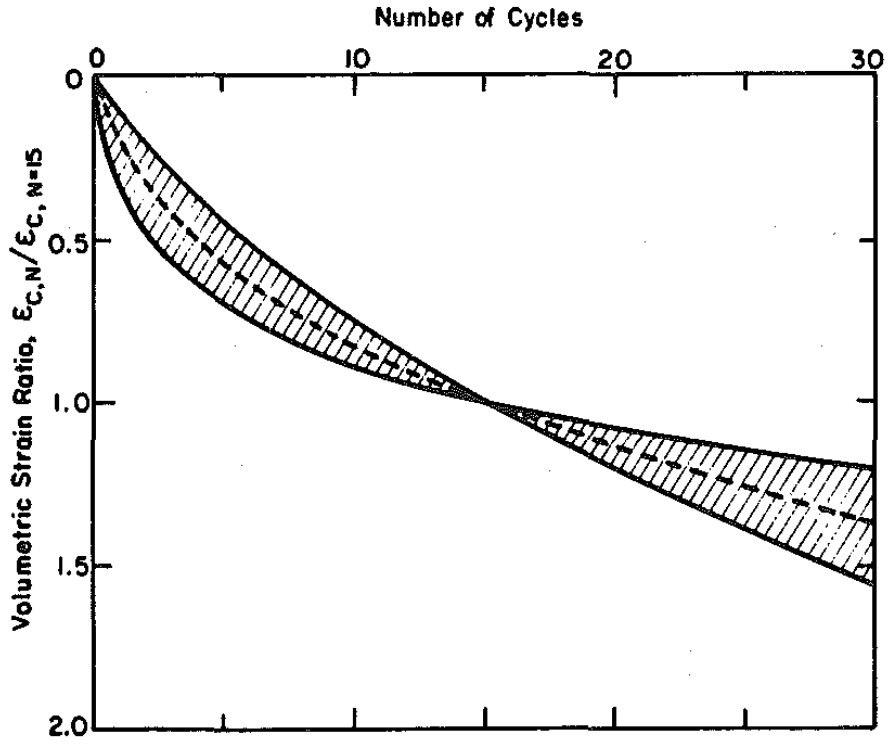

Figure 3. Relationship between volumetric strain ratio and number of cycles for dry sands after Tokimatsu and Seed (1987)

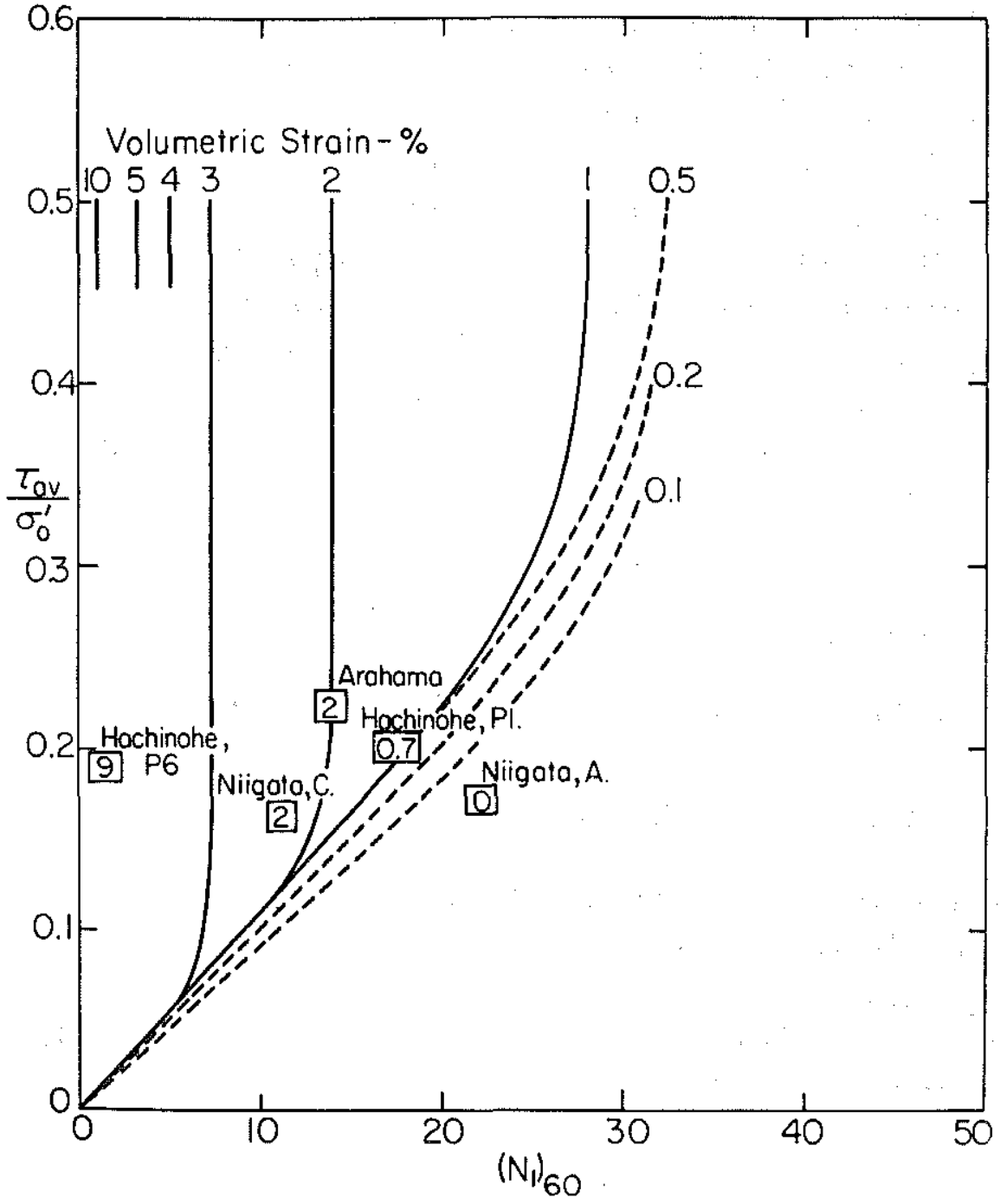

Figure 4. Comparison of proposed chart for determination of volumetric strain with field performance of saturated sands after Tokimatsu and Seed (1987)

Another widely accepted method to estimate the volumetric strain in sands was proposed by Ishihara and Yoshimine (1992). They conducted a series of simple shear tests on saturated sands and established a correlation between the post-liquefaction volumetric strain and the magnitude of the maximum shear strain. Another series of curves were developed that showed the relationship between the factors of safety against liquefaction versus the maximum shear strain. By combining these results they proposed a plot to obtain the post-liquefaction volumetric strain as a function of the factor of safety against liquefaction and the $(N_1)_{60}$ or the relative density (Figure 6). In a layered soil profile, the volumetric strain in each layer can be estimated using this method and then by summing up the values, the total free-field settlement can be measured. They evaluated this method using the measurements from the 1964 Niigata earthquake. Later, Ishihara et al. (1996) used this method to estimate the settlements measured in Port and Rokko Islands after the 1995 Kobe earthquake.

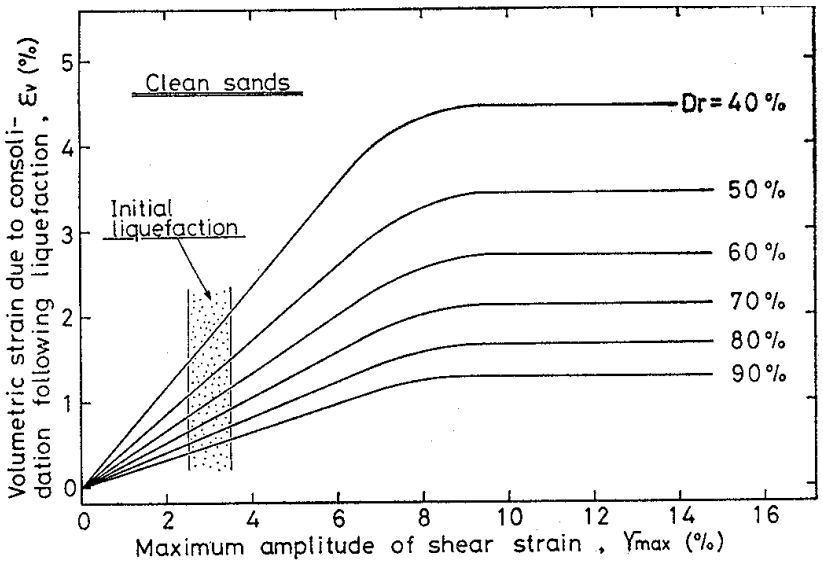

Figure 5. Reconsolidation volume change versus the maximum shear strain for different relative densities after Ishihara and Yoshimine (1992)

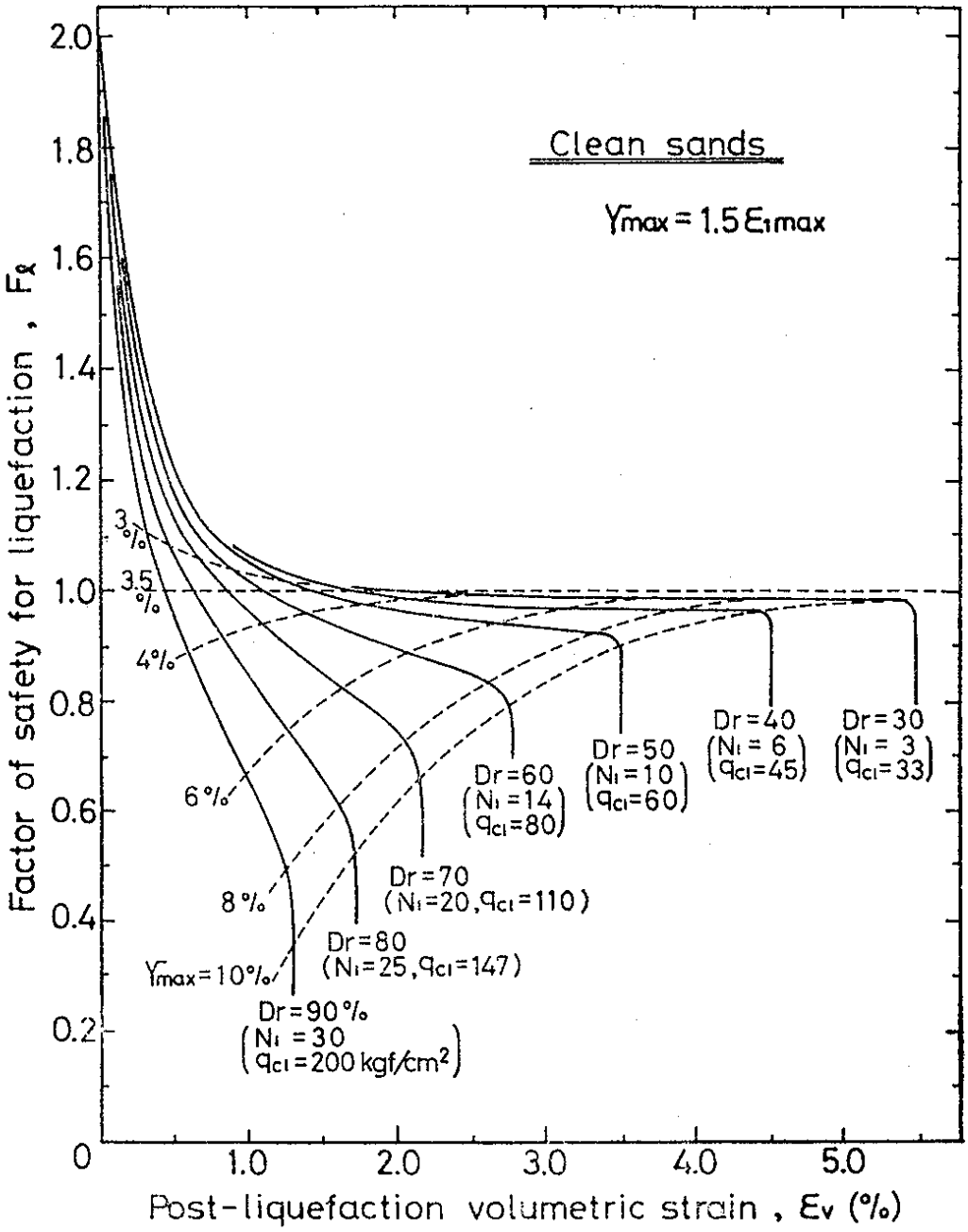

Figure 6. The chart proposed by Ishihara and Yoshimine (1992) for determining the volumetric strain

Zhang et al. (2002) proposed a new approach based on the work of Ishihara and Yoshimine to estimate liquefaction-induced ground settlements using CPT data for sites with level

ground. Prior to that, only SPT-based methods had been used to calculate the free-field earthquake-induced settlement. Due to the increasing popularity of the CPT measurements to characterize the soils and predicting liquefaction potential, Zhang et al. developed a CPT-based method. Their method combines the CPT-based approach for liquefaction potential analysis with laboratory test results from Nagase, Ishihara and Yoshimine to estimate the liquefaction-induced volumetric strains for sandy and silty soils. In this method, parameters needed to estimate the ground settlement are the CPT cone tip resistance and sleeve friction, moment magnitude of the earthquake, maximum surface acceleration, depth to the ground water table and the unit weights of the soil.

For evaluation of liquefaction potential and measuring the equivalent clean sand normalized cone penetration tip resistance ($(q_{c1N})_{cs}$), they used the flowchart proposed by Robertson and Wride (1998). Afterwards, they used a relationship between the relative density and the normalized tip resistance to translate the work of Ishihara and Yoshimine (Figure 5) to develop a plot showing the relationship between the $(q_{c1N})_{cs}$, factor of safety against liquefaction and the post-liquefaction volumetric strain. Similarly to Ishihara and Yoshimine, the free-field settlement in a layered profile can be obtained by estimating the values for each layer or sublayer and summing up the settlements. Zhang et al. used their method to evaluate two case history sites from the 1989 Loma Prieta earthquake: Marina District and Treasure Island. They found good agreement between the settlements estimated using their proposed method and the values measured at the sites.

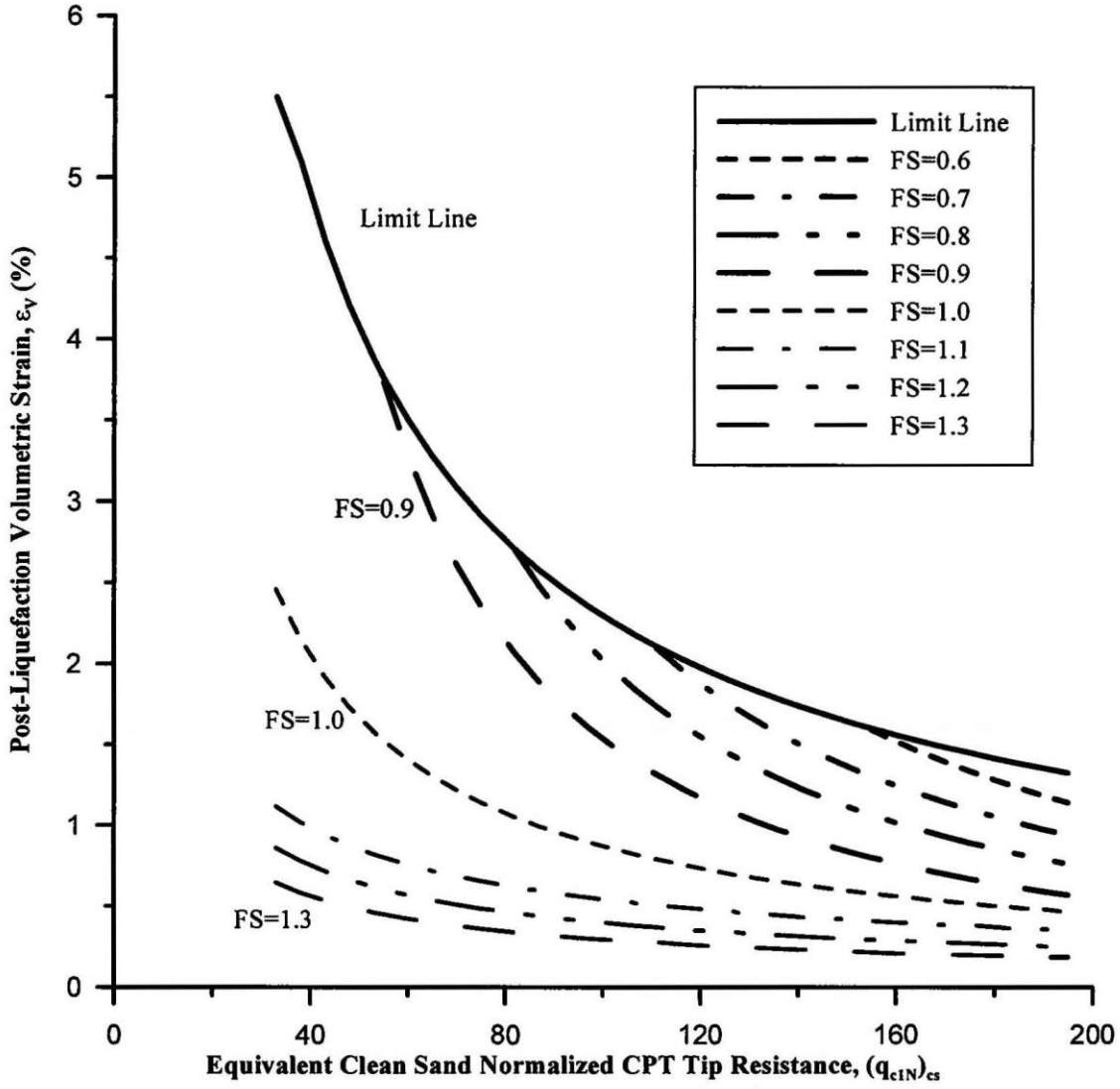

Figure 7. Relationship between post-liquefaction volumetric strain and normalized CPT tip resistance for different factors of safety after Zhang et al. (2002)

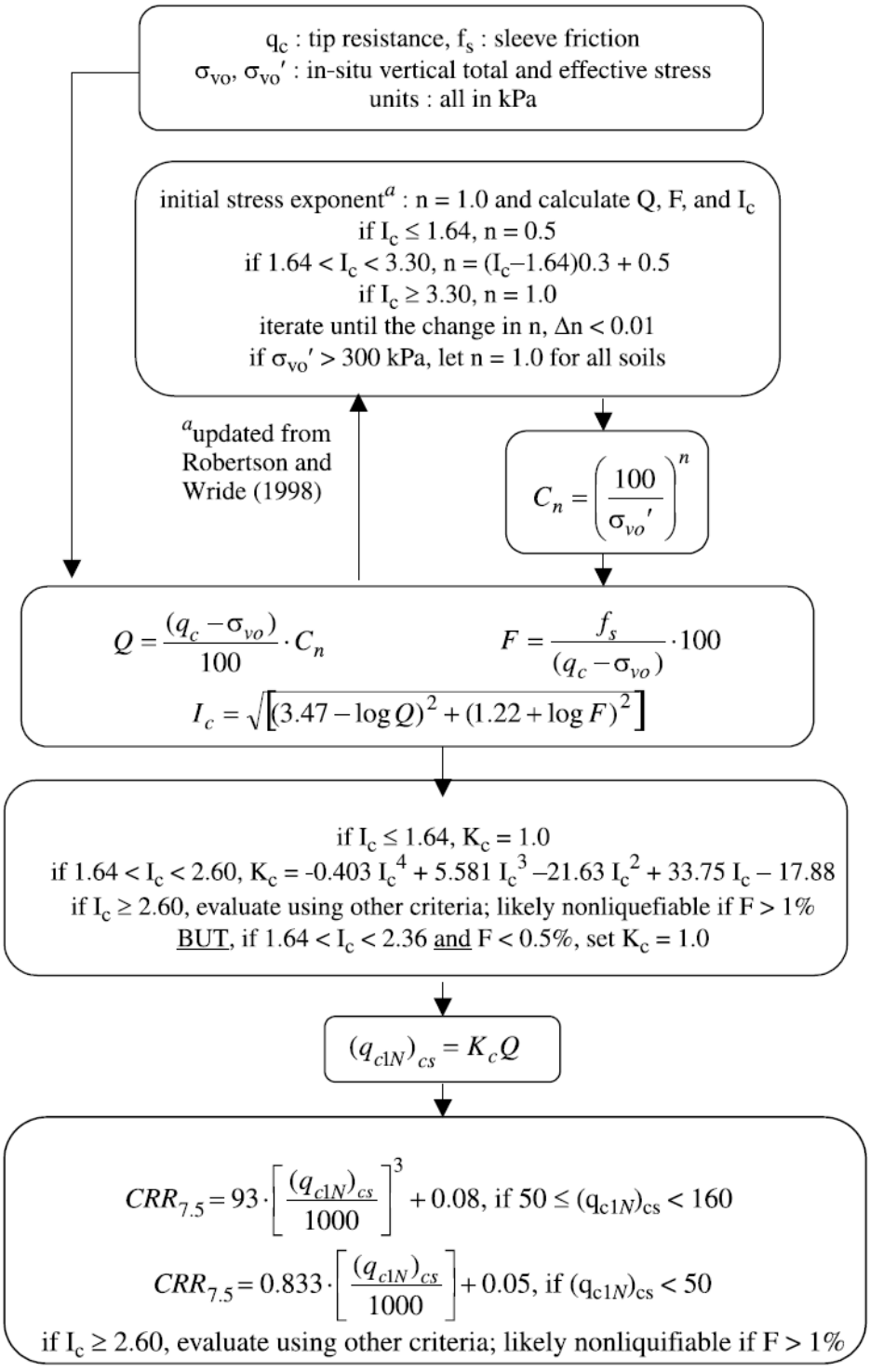

Figure 8. Robertson and Wride's (1998) CPT-based method to assess liquefaction potential and equivalent normalized CPT tip resistance after Zhang et al. (2008)

2.2. Settlement of building on liquefiable soils

Damages observed to the buildings located on liquefied grounds after the 1999 Kocaeli and the 2011 Christchurch earthquakes and the fact that the method used to estimate the liquefaction-induced building settlement has been largely based on neglecting the effect of the structures, triggered a series of researches evaluating the importance of other mechanisms that contribute to building settlement. Understanding the underlying mechanisms of soil liquefaction, the parameters affecting ground and building performance, and analytical procedures for carrying out practical assessments are critical to the evaluation of the building settlement. Bray and Dashti (2014) noted that the SSI-induced ratcheting and bearing capacity-type movements control seismically induced building movements through ground deformation caused by shear. They also investigated the effect of volumetric-induced ground settlement subsequent of localized partial drainage, sedimentation, post-liquefaction reconsolidation, and sediment ejecta on the building settlement. Bray and Macedo (2016) captured the effects of SSI-induced building settlement by inspecting different mechanisms of liquefaction-induced building movements and a suggested a simplified procedure, which defines the total settlement (D_t) as a sum of three separate components:

$$D_t = D_e + D_V + D_S \qquad \text{Equation 1.}$$

where, D_e is the amount of building settlement as a result of sediment ejecta, D_V is the volumetric-induced free-field settlement, and D_S is the shear-induced as a result of the building.

Bray and Macedo suggested that the volumetric-induced term of the equation could be calculated using a CPT-based approach. Among the available methods, the procedure

proposed by Zhang et al. was suggested by Bray et al. to estimate the free-field term. They evaluated the building settlement for a series of soil profiles consisted of 3 layers subjected to 36 different earthquakes. They also developed a predictive equation for D_s, based on the computed of the settlement values of a shallow foundation on top of a three-layered soil profile with thickness of 20m. Dashti and Karimi (2018) numerically computed the response of a similar layered profile and also measured the free-field and foundation settlement of these soil profiles using the Centrifuge tests and evaluated tilt of structures on liquefiable soils. Jahed Orang et al (2021) conducted a series of large-scale shaking table tests to evaluate the behavior of shallow foundations on top of similar 3-layer deposits.

.

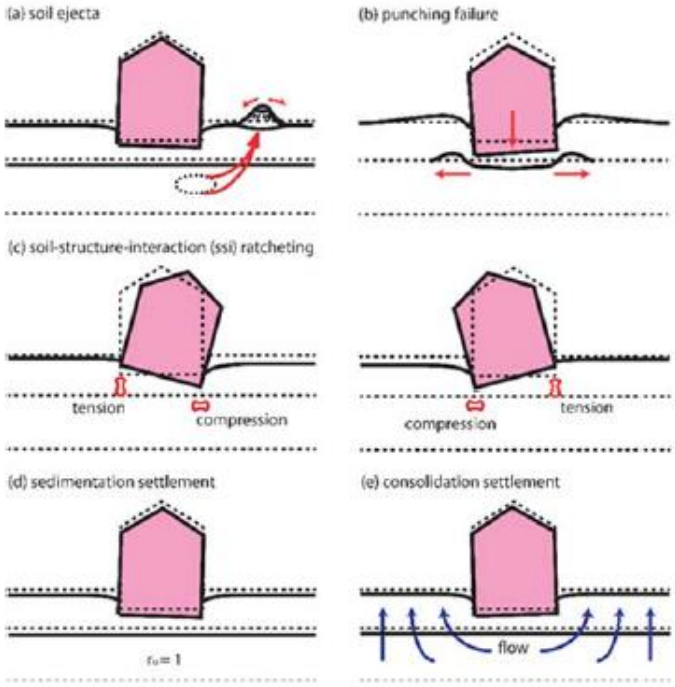

Figure 9. Liquefaction-induced building displacement mechanisms: (a) ground loss due to soil ejecta; shear-induced settlement from (b) punching failure, or (c) soil-structure-interaction (SSI) ratcheting; and volumetric-induced settlement from (d) sedimentation or (e) post-liquefaction consolidation after Bray and Macedo (2017)

2.3. Simplified methods to evaluate liquefaction assessment

One of the key parameters needed to estimate the free-field earthquake-induced settlement is the factor of safety against liquefaction. The simplified procedures to evaluate liquefaction has been discussed by many researchers since the disastrous earthquakes of Alaska and Niigata in 1964. Seed and Idriss (1967) introduced the stress-based procedure has been adopted widely by several other researchers including Seed and Idriss (1971), Shibata (1981), Tokimatsu and Yoshimi (1983), Seed et al. (1985), Youd et al. (2001), Cetin et al. (2004) and Idriss and Boulanger (2004). This method compares the earthquake-induced cyclic stress ratios (CSR) with the cyclic resistance ratios (CRR) of the soil to calculate the factor of safety against liquefaction. Under earthquake excitations, CSR is usually expressed equal to 65% of the maximum cyclic shear stress ratio at a given depth:

$$CSR = 0.65\frac{\tau_{max}}{\sigma'_v} \qquad \text{Equation 2.}$$

where τ_{max} is the maximum earthquake induced shear stress, σ'_v is thevertical effective stress. CSR is computed for a specific earthquake magnitude (M) and in-situ σ'_v. The maximum earthquake-induced shear stress can be estimated from dynamic response analyses with an adequate number of input acceleration time series and site characterization details. It can also be estimated using the equation developed as part of the simplified procedure suggested by Seed and Idriss:

$$CSR = 0.65\frac{\sigma_{max}}{\sigma'_v}\frac{a_{max}}{g}r_d \qquad \text{Equation 3.}$$

where σ_v is the vertical total stress at a given depth, a_{max} divided by g is the maximum horizontal acceleration at the ground surface as a fraction of gravity and r_d is the shear

stress reduction factor accounting for the dynamic response of the layered soil profile. This reduction factor can be obtained from the mean curve and the ranges suggested by Seed and Idriss (Figure 10). Golesorkhi (1989) suggested that it can be seen that the range of possible r_d increases with depth. The reduction factor can also be determined using the equations proposed by different researchers including Liao and Whitman (1986) and Blake (1996).

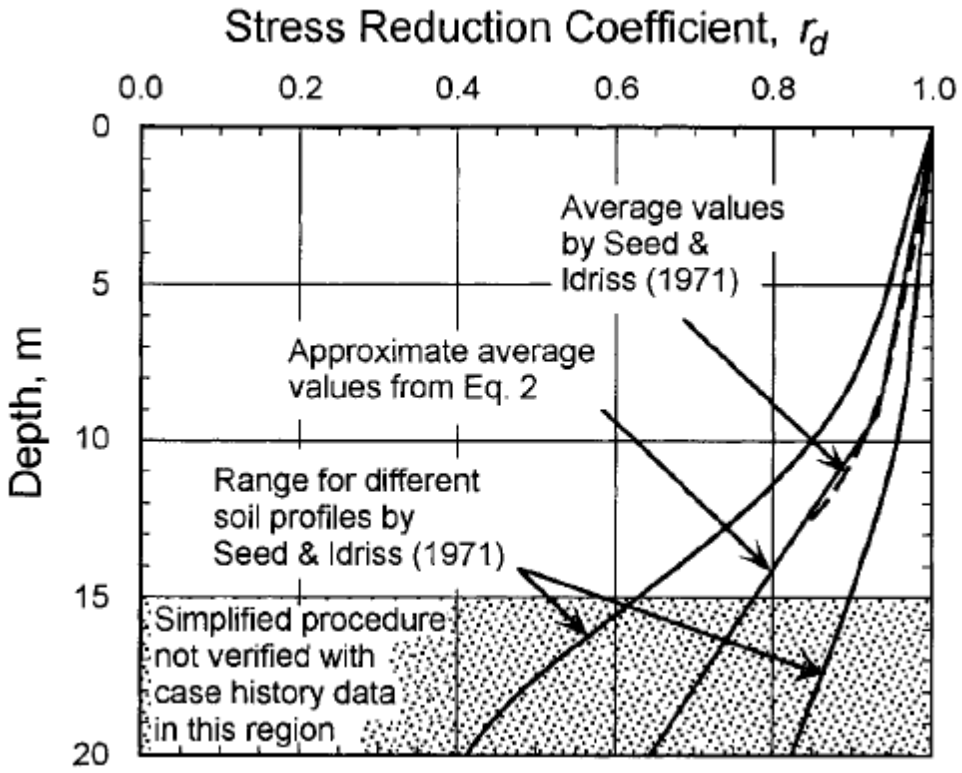

Figure 10. The reduction factors for different depths developed by Seed and Idriss after Youd et al. (2001).

In most cases, CRR is estimated based on in-situ measurements such as shear wave velocity (V_s) SPT $(N_1)_{60}$ or CPT cone tip resistance to avoid the difficulties related to sampling and laboratory testing. In most cases, SPT and CPT data is preferred due to the availability of more extensive databases and past experience. Youd et al. (2001) proposed equations for both SPT and CPT measurements. They presented a modified version of the $(N_1)_{60}$ versus CRR plot from Seed et al. (1985) for clean sands and sands with different fines content. They noted an increase of CRR with increased fines content. Besides the correction for fines content, SPT correction factors should be applied as well.

Youd et al. noted that the CPT results are generally more consistent and repeatable than results from other penetration tests. Moreover, the continuous profile provides a more detailed description of soil layers compared to the other methods. Because of this stratigraphic capability, the CPT is particularly considered to be suited for generating soil profiles for liquefaction analyses. Robertson and Wride developed a plot based on the data compiled from Stark and Olson (1995) and Suzuki et al. (1995) demonstrating the calculated cyclic resistance ratio as a function of normalized and corrected and CPT tip resistance (q_{c1N}). These were taken from sites where surface manifestation of liquefaction was or was not observed. Even though based on the case histories from the 1989 Loma Prieta earthquake, Idriss recommended that base curve should be shifted to the right by 10 to 15 percent, the majority of the researchers found this to be too conservative. Robertson and Wride proposed the equation of their suggested plot for magnitude of 7.5. Besides that, corrections for normalizing the CPT measurements should be considered.

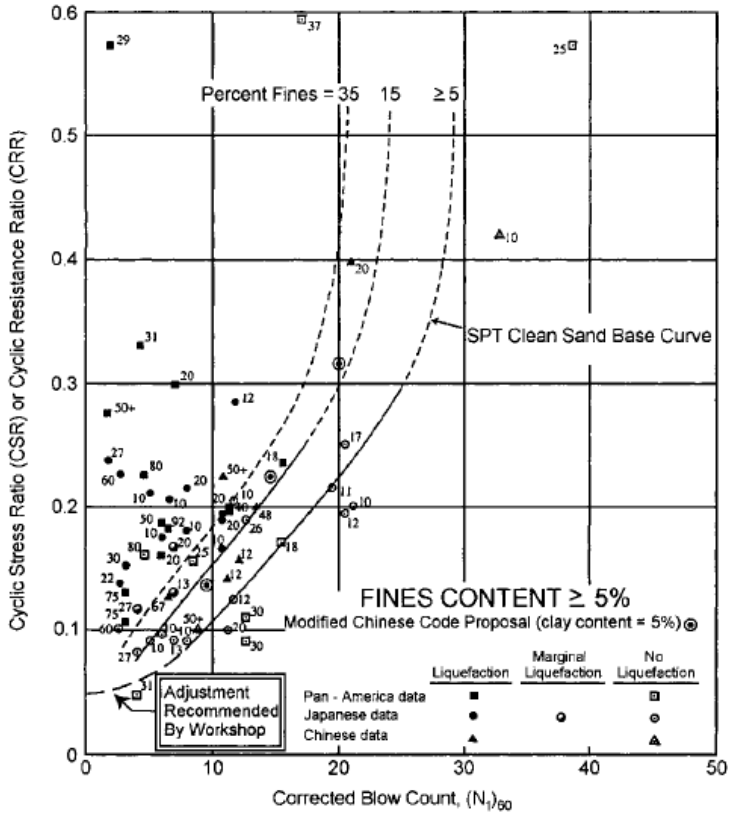

Figure 11. SPT clean-sand base curve for magnitude 7.5 earthquakes with data from liquefaction case histories after Youd et al. (2001)

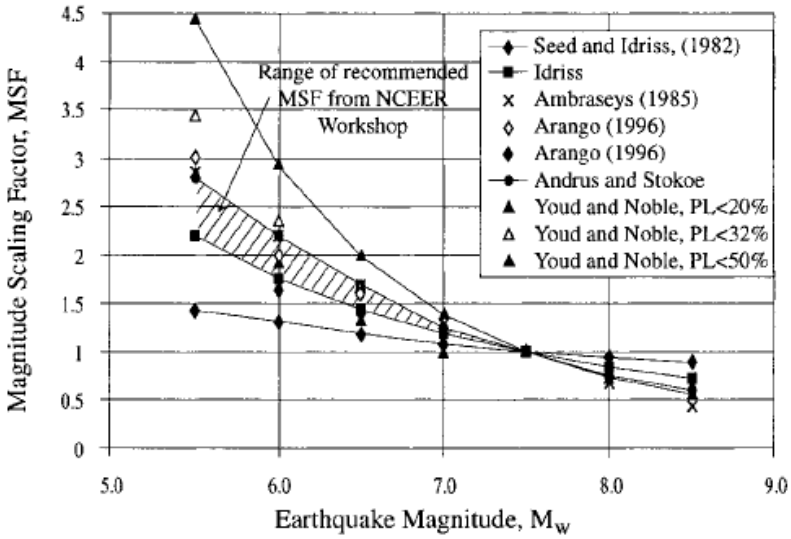

Figure 12. Magnitude scaling factors derived by various investigators after Youd et al. (2001)

As mentioned earlier, CRR curves for clean sands and sands with fines were presented for earthquakes with M = 7.5. In order to adjust the base curves for different magnitudes, Seed and Idriss (1982) introduced magnitude scaling factors (MSF) to scale the base resistance curves upward or downward, depending on the earthquake magnitude. The final form of the equation to obtain the factor of safety against liquefaction should be written in terms of CRR, CSR and MSF. MSF can be obtained from the work of several researchers (Figure 12).

$FS = \frac{CRR_{7.5}}{CSR} MSF$ Equation 4.

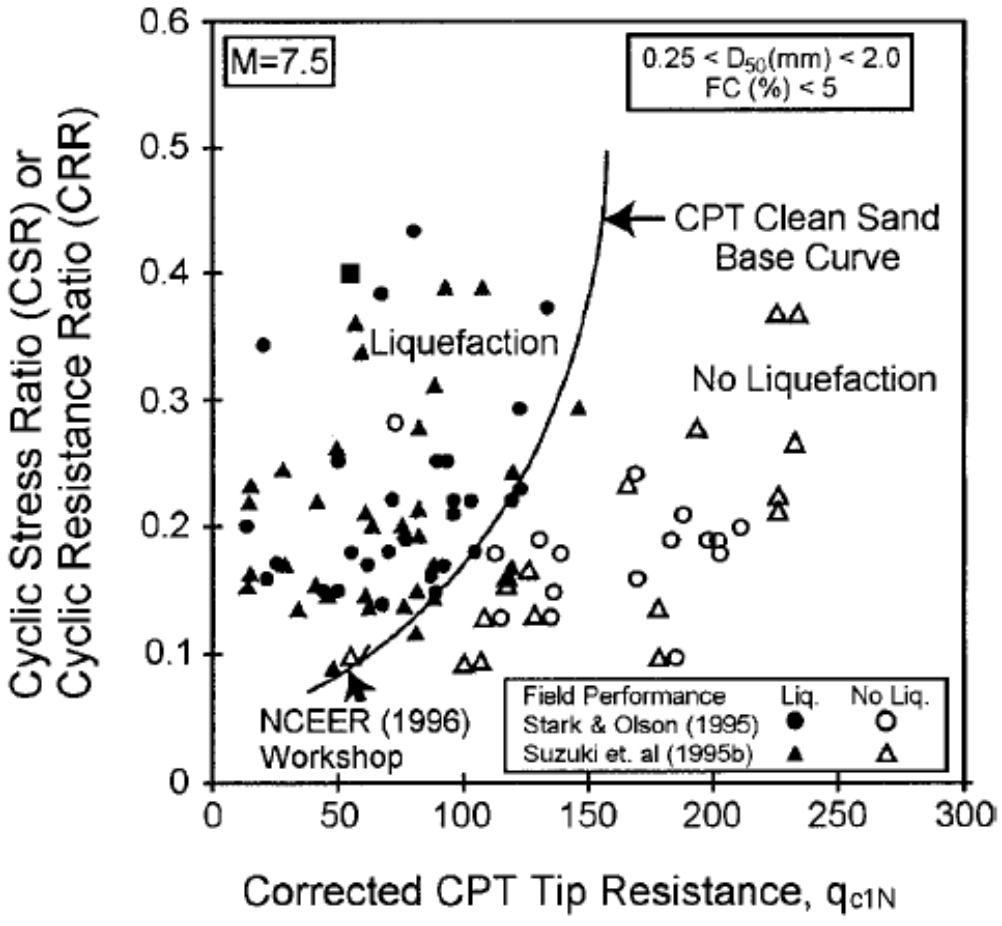

Figure 13. Curve recommended for calculation of CRR from CPT data along with empirical liquefaction data from compiled case histories after Youd et al. (2001)

More recently, different researchers have introduced the probabilistic-based assessment of liquefaction. Cetin et al. described the probabilistic framework for both liquefaction assessment and volumetric strain prediction. They conducted a series of stress-controlled cyclic triaxial and simple shear tests on reconstituted sand samples and included additional data have been gathered from previous efforts in their work. Based on their high-quality database, they were able to present equations and plots to estimate the volumetric strain as a function of $N_{1,60,cs}$ and $CSR_{ss,20,1D,1atm}$. The correction factors applied to CSR are K_{md} (to convert multidirectionally applied CSR from the field to the value of a unidirectionally applied in laboratory tests), K_{σ} (to account for the nonlinear increase in cyclic resistance to shear stresses with increasing confining effective stresses) and K_{MW} (to address for earthquake shaking with magnitude other than 7.5).They also used their probabilistic method to evaluate the earthquake-induced free-field settlement in 49 well-documented case histories.

$$CSR_{\mathrm{ss,20,1D,1atm}} = \frac{CSR_{field}}{K_{md}K_{MW}K_{\sigma}} \qquad \text{Equation 5.}$$

They also incorporated the equations introduced by Idriss and Boulanger (2004) to convert $N_{1,60,cs}$ or $q_{c,1}$ to relative density (D_r):

$$N_{1,60,\mathrm{CS}} = 0.0046 d_r^2 \qquad \text{Equation 6.}$$

$$\frac{q_{c,1}}{P_a} = \left(\frac{D_r + 106.3}{47.8}\right)^{3.788} \qquad \text{Equation 7.}$$

Cetin et al. (2009) illustrated the probabilistic aspect of their corrections related to performance-based assessment context in three cases. They plotted maximum shear strain and post-cyclic volumetric strain against $N_{1,60,cs}$ and $CSR_{ss,20,1D,1atm.}$

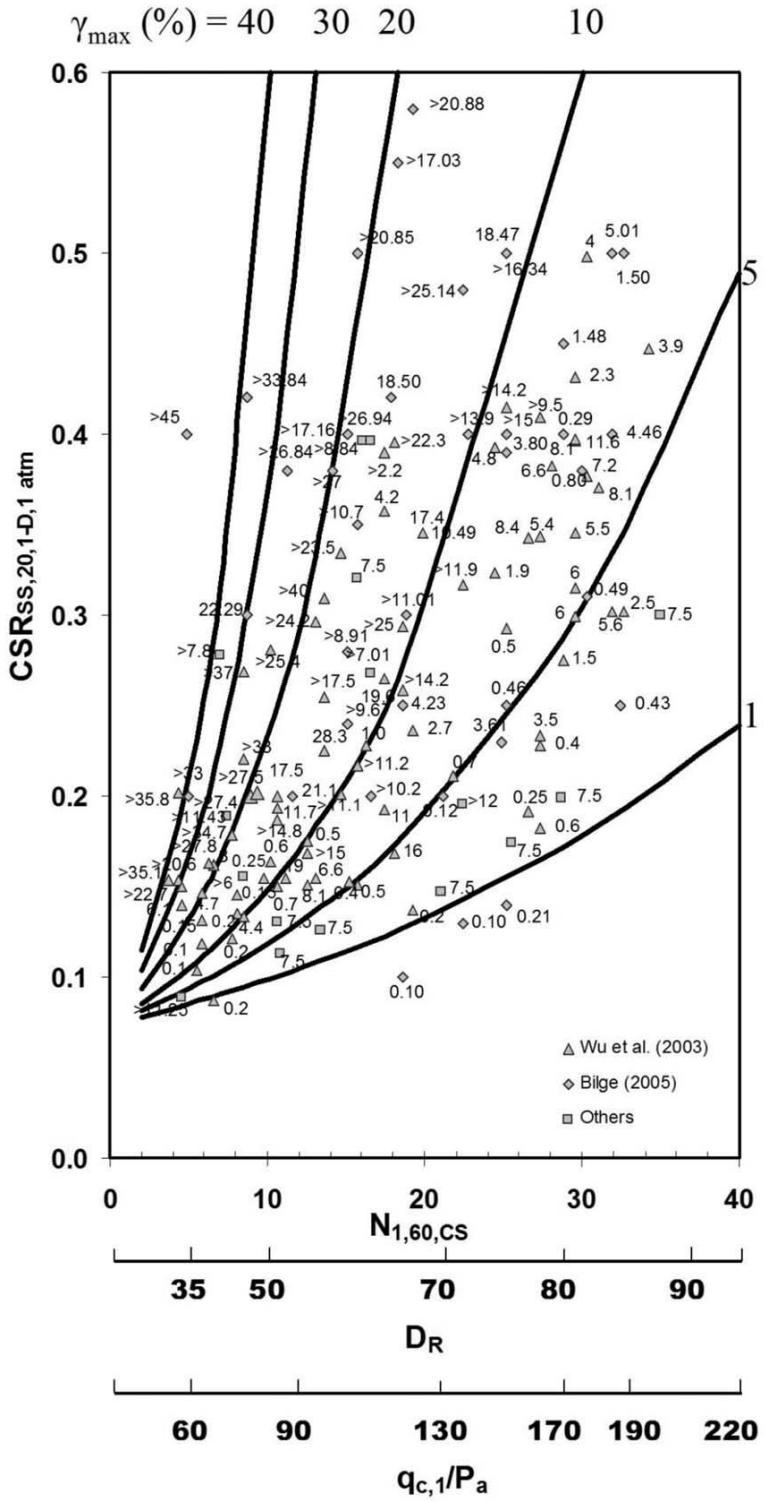

Figure 14. Recommended maximum double amplitude shear strain boundary curves after Cetin et al. (2009)

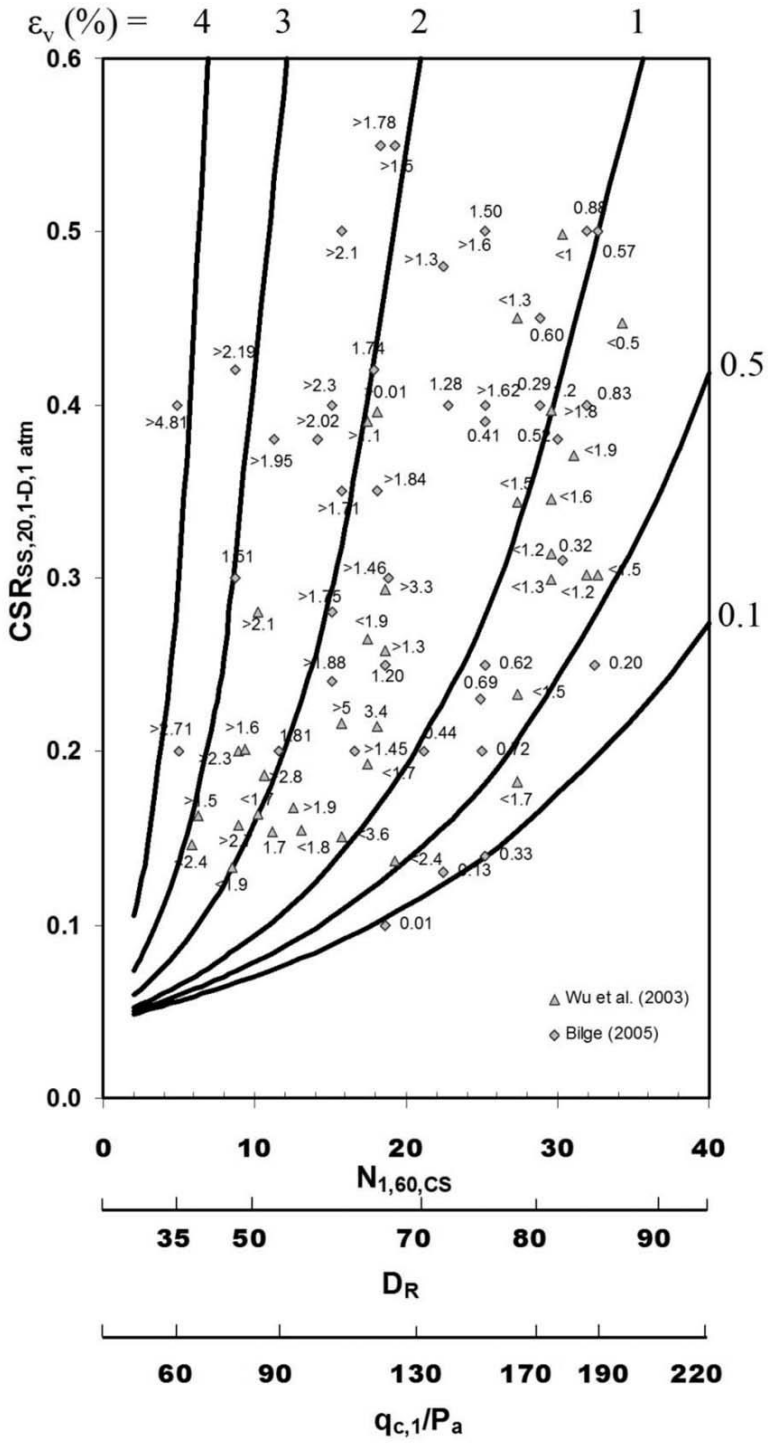

Figure 15. Recommended post-cyclic volumetric strain boundary curves after Cetin et al. (2009)

Idriss and Boulanger (2004) proposed their semi-empirical procedures for assessing the liquefaction potential of saturated cohesionless soils during earthquakes. They revisited and revised the stress reduction factor, magnitude scaling factor and the corrections previously proposed for CPT and SPT measurements, including overburden correction factor K_σ for cyclic stress ratios and overburden correction factor C_N for penetration resistance. They also presented modified versions the liquefaction potential curve and evaluated their method using SPT and CPT case histories. Idriss and Boulanger also proposed the liquefaction potential curves corrected for cohesionless soils with fines content.

They suggested that a reliable liquefaction assessment depends directly on the quality of the site characterization and the quality of the in-situ and laboratory measurements.

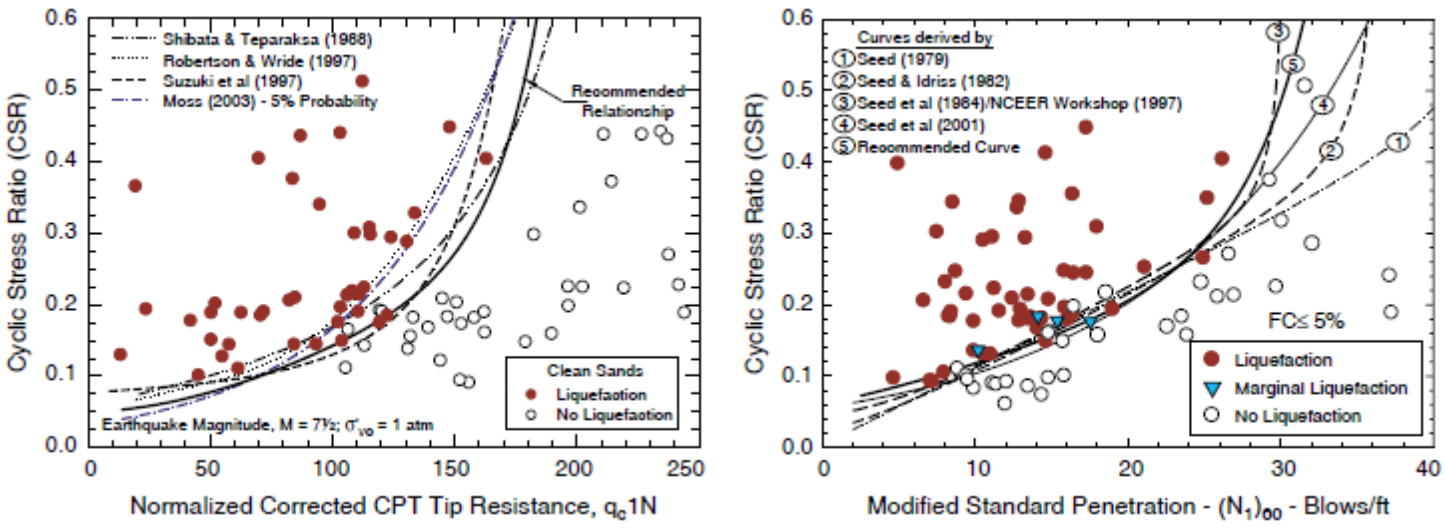

(a) (b)

Figure 16. Curves (a) relating CRR to SPT data for clean sands the recommended curve for M = $7\frac{1}{2}$ and σ'_{v0} = 1atm and (b) relating CRR to CPT data after Idriss and Boulanger (2004)

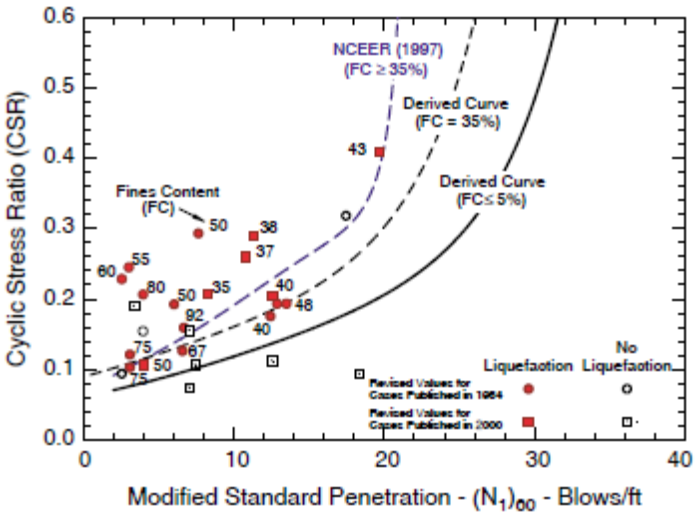

Figure 17. SPT case histories for cohesionless soils with FC≥35% and the NCEER Workshop curve and the recommended curves for both clean sand and for FC = 35% for M = $7_{1/2}$ and σ'_{v0} = 1atm after Idriss and Boulanger (2004)

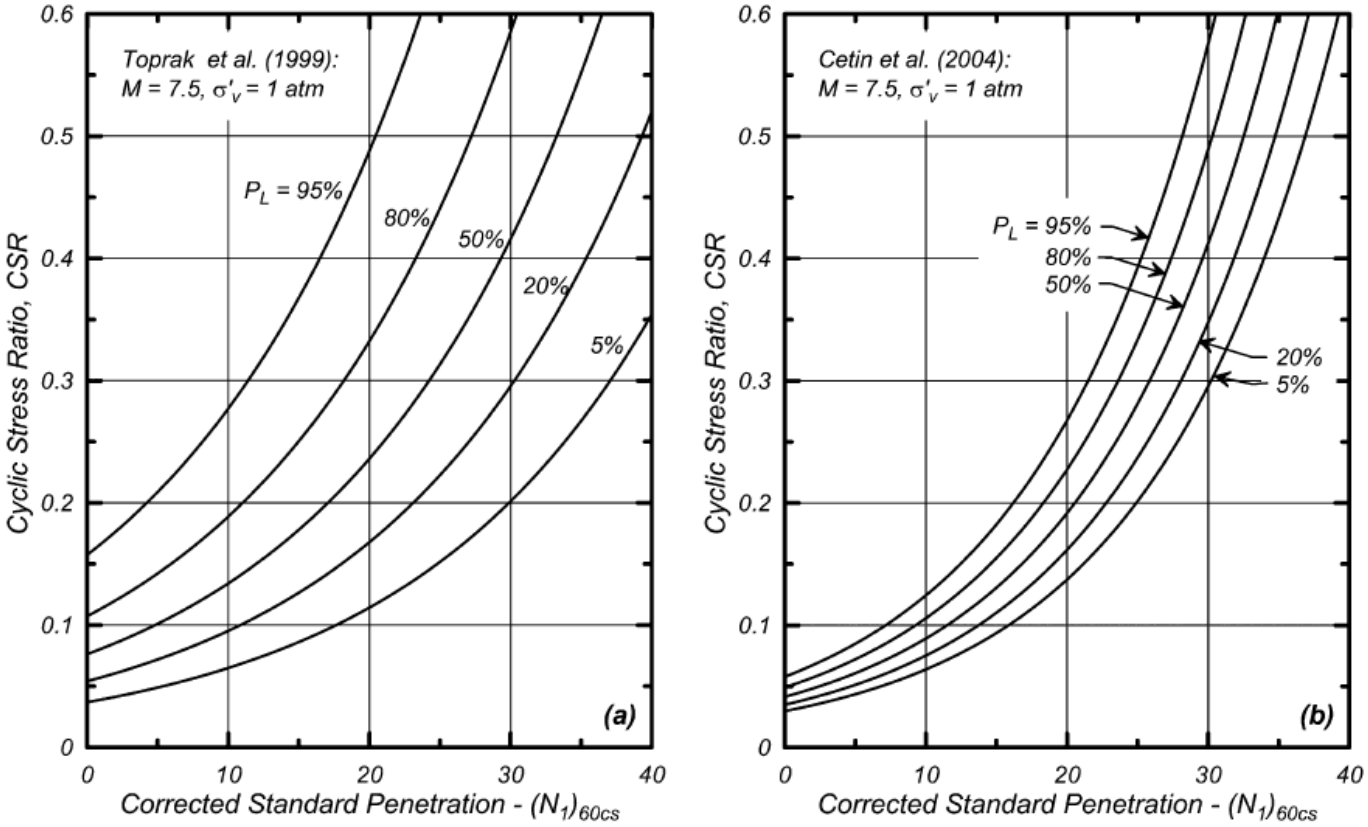

Figure 18. SPT-based probabilistic correlations for sands after Idriss and Boulanger (2008)

Later, Idriss and Boulanger (2012) published a probabilistic version of their previous liquefaction potential curves using an updated case history database based on the fact that previous works by Torpak et al. (1999) and Cetin et al. (2004) have already introduced different curves for various probabilities of liquefaction ($5\% \leq P_L \leq 95\%$) as shown in Figure 18. In most liquefaction case histories, the amount of information needed to quantify the sources of uncertainty is inadequate. As a result, a number of generalized assumptions and approximations concerning prevailing sources of uncertainty and their scatterings across the case history database are necessary for the probabilistic approach. In order to calculate CSR, they applied the MSF and K correction factors besides r_d (Equation 8). Additionally, they utilized the equation from their previous work (2008) to calculate CRR as a function of $(N_1)_{60cs}$ (Equation 10).

$$CSR_M = 0.65 \frac{\sigma_v}{\sigma'_v} \frac{a_{max}}{g} r_d \frac{1}{MSF} \frac{1}{K_\sigma} \qquad \text{Equation 8.}$$

$$(N_1)_{60cs} = (N_1)_{60} + \Delta(N_1)_{60} \qquad \text{Equation 9.}$$

$$CRR_{M=7.5,\sigma'_v=1\ atm} = \exp\{\frac{(N_1)_{60cs}}{14.1} + \left[\frac{(N_1)_{60cs}}{126}\right]^2 - \left[\frac{(N_1)_{60cs}}{23.6}\right]^3 + \left[\frac{(N_1)_{60cs}}{25.4}\right]^4 - 2.67 + \varepsilon\}$$

Equation 10.

They suggested a likelihood function as the product of the probabilities of the specific case histories, assuming that they are statistically independent and calculated the probability of liquefaction. The final equation for probability of liquefaction is a function of $(N_1)_{60cs}$ as well as $CSR_{M=7.5,\sigma'v=1\ atm}$

$$P_L = \Phi\{-\frac{\frac{(N_1)_{60cs}}{14.1} + \left[\frac{(N_1)_{60cs}}{126}\right]^2 - \left[\frac{(N_1)_{60cs}}{23.6}\right]^3 + \left[\frac{(N_1)_{60cs}}{25.4}\right]^4 - 2.67 - \ln(CSR_{M=7.5,\sigma'_v=1\ atm})}{\sigma_{\ln(R)}}\}$$

Equation 11.

They plotted the curves for different probabilities of liquefaction for probabilities of liquefaction of 15, 50, and 85% (Figure 19).

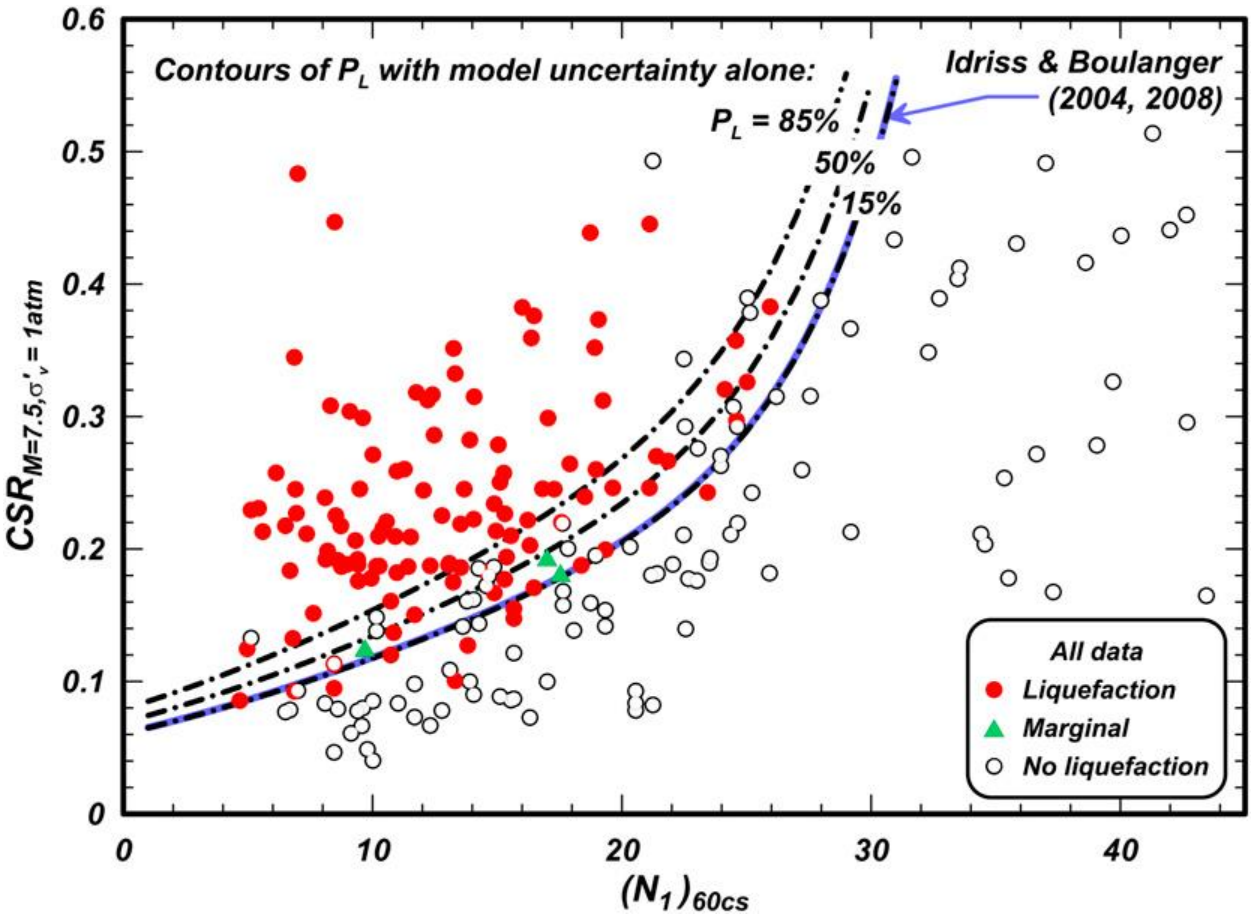

Figure 19. Liquefaction potential curves for different probabilities of liquefaction after Idriss and Boulanger (2012)

Idriss and Boulanger also showed that their previous deterministic liquefaction triggering curve is corresponding to P_L = 15% based on the relationship presented in their paper and considering the model uncertainty. They also compared their triggering relationship to the one suggested by Tokimatsu and Yoshimi (1983) based on frozen sampling test data. It was obvious that both methods are largely in good agreement for cases with $(N_1)_{60cs} \leq 15$. On the other hand, for values larger than 15, Tokimatsu and Yoshimi's curve tend to underestimate the liquefaction resistance of the soil.

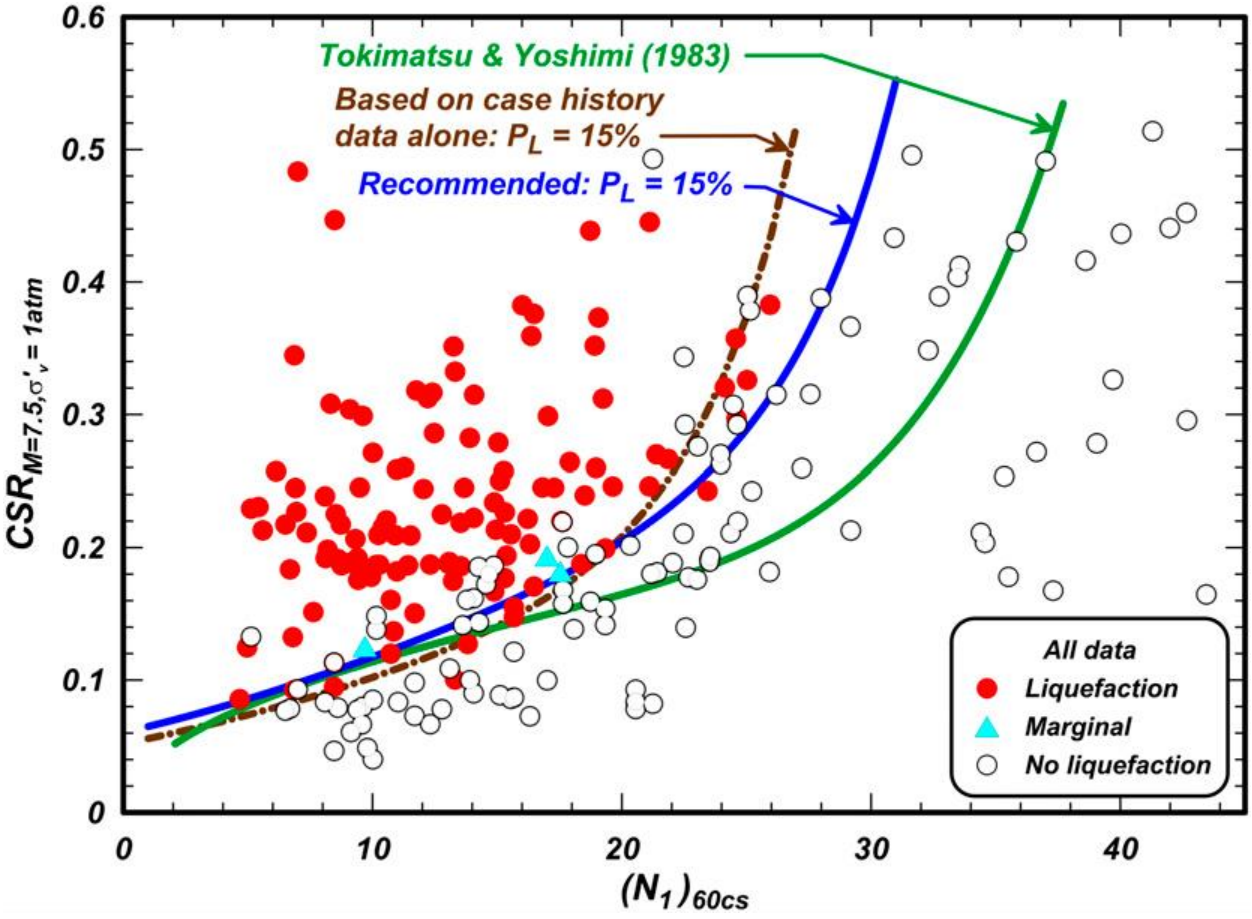

Figure 20. Comparison of liquefaction potential curves suggested by Idriss and Boulanger (2010) to Tokimatsu and Yoshimi (1983) after Idriss and Boulanger (2012)

Chapter 3: Incremental volumetric strain ($\Delta\varepsilon_v$) model

A simple two-parameter incremental shear-volume coupling model was suggested by Byrne which gives estimations that are in good agreement with data collected from the laboratory tests under uniform cycles of loading. Tests were undertaken on dry sand for a wide range of shear strain levels and relative densities. This model is based on the fact that grain slip-induced incremental permanent volumetric strain ($\Delta\varepsilon_v$) by a shear strain cycle can be expressed in terms of the shear strain amplitude, γ as:

$$\frac{\Delta\varepsilon_v}{\gamma} = C_1.EXP(-C_2(\varepsilon_v/\gamma)) \quad \text{Equation 12.}$$

In this equation, ε_v is the accumulated volumetric strain, C_1 controls the amount of volume change, while C_2 controls the shape of the accumulated volume change with the number of cycles. Here both γ and ε_v can be either in percent or in fraction. Martin et al studied the characteristic shapes of the development of volumetric strain with the number of cycles and found that it is similar for all relative densities. C_1 and C_2 can be obtained by fitting the equation to the laboratory-measured accumulated volumetric strain values reported by Tokimatsu and Seed for dry sands with different relative densities. The best-fit values of C_1 and C_2 were calculated for different relative densities and are presented in Table 2.

It can be observed that for these optimized values:

$$C_2.C_1 = 0.403 \quad \text{Equation 13.}$$

A simple script was developed to calculate the ε_v in a dry sandy element under uniform sinusoidal cyclic loads for different relative densities, using Byrne's equation.

Table 2. Optimized C_1 and C_2 values for the two-parameter incremental shear-volume coupling model

D_r (%)	C_1	C_2
35	0.97	0.415
45	0.6	0.672
55	0.34	1.185
60	0.27	1.493
75	0.16	2.518
80	0.132	3.05
90	0.078	5.17

As presented in Figure 21, the computed volumetric strain accumulation history over the cycles is in good agreement with the values reported by Tokimatsu and Seed (1987) for different amplitudes of shear strain. It can be observed that the ε_v increases with the level of shear strain applied, and for a given level of shear strain, the rate of accumulation of ε_v reduces with number of cycles. Martin et al. (1975) based on their simple shear test data also showed similar characteristics.

Equation 12 should be modified to determine the volumetric strain caused by a random strain history by considering volumetric strain associated with 0.5 cycle, which can be calculated as:

$$(\Delta\varepsilon_v)_{\frac{1}{2}Cycle} = 0.5.\gamma.C_1.EXP(-C_2(\varepsilon_v/\gamma)) \quad \text{Equation 14.}$$

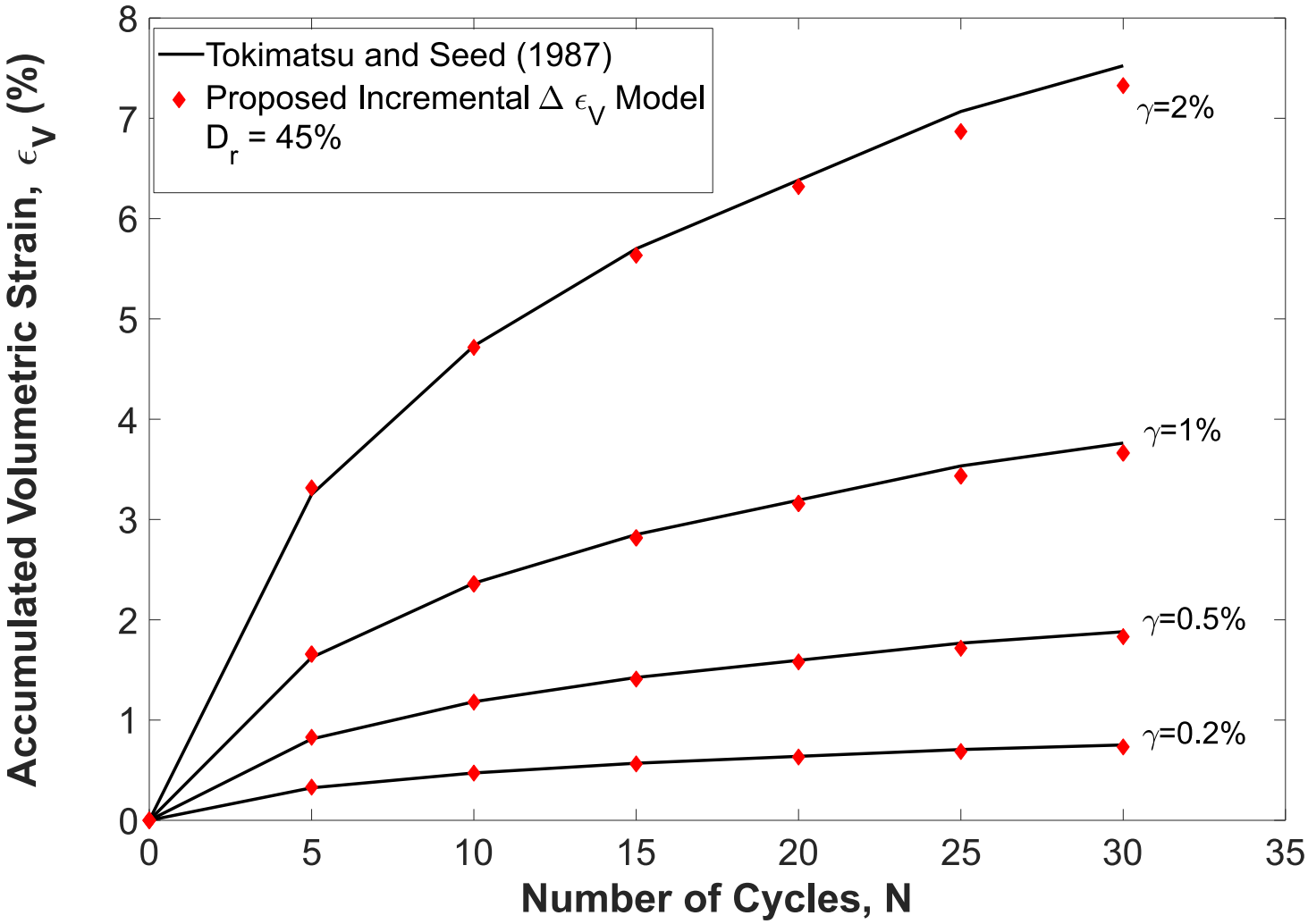

Figure 21. Accumulated volumetric strains from sinusoidal cyclic loads for dry sand with D_r = 45% under different shear strain amplitudes

The application of this equation for a random strain history shown in Figure 22 is presented below. It is assumed that the volumetric strains occur only during the unloading phases. In this particular shear strain history, AB, CD, EF, GH, and IJ are unloading sequences. The unloading sequence AB does not represent a full 0.5 cycle. The peak shear strain (amplitude) at A (γ_A) dictates the volumetric strain, $(\boldsymbol{\Delta\varepsilon_v})_{AB}$, and this is obtained by modifying $\boldsymbol{\Delta\varepsilon_v}$ given by Equation 14 using the factor γ_B/γ_A. Subsequently, for the unloading sequence CD, the shear strain peak γ_C is used. The

volumetric strain will accumulate until the unloading shear strain history intersects the time axis. There is no need to modify the Equation 14 for this sequence. Similarly, for the unloading sequence EF, the shear strain amplitude γ_C will be used and no modification is applied. The unloading sequences GH and IJ will be based on shear strain amplitudes γ_G and γ_I, respectively with no modifications.

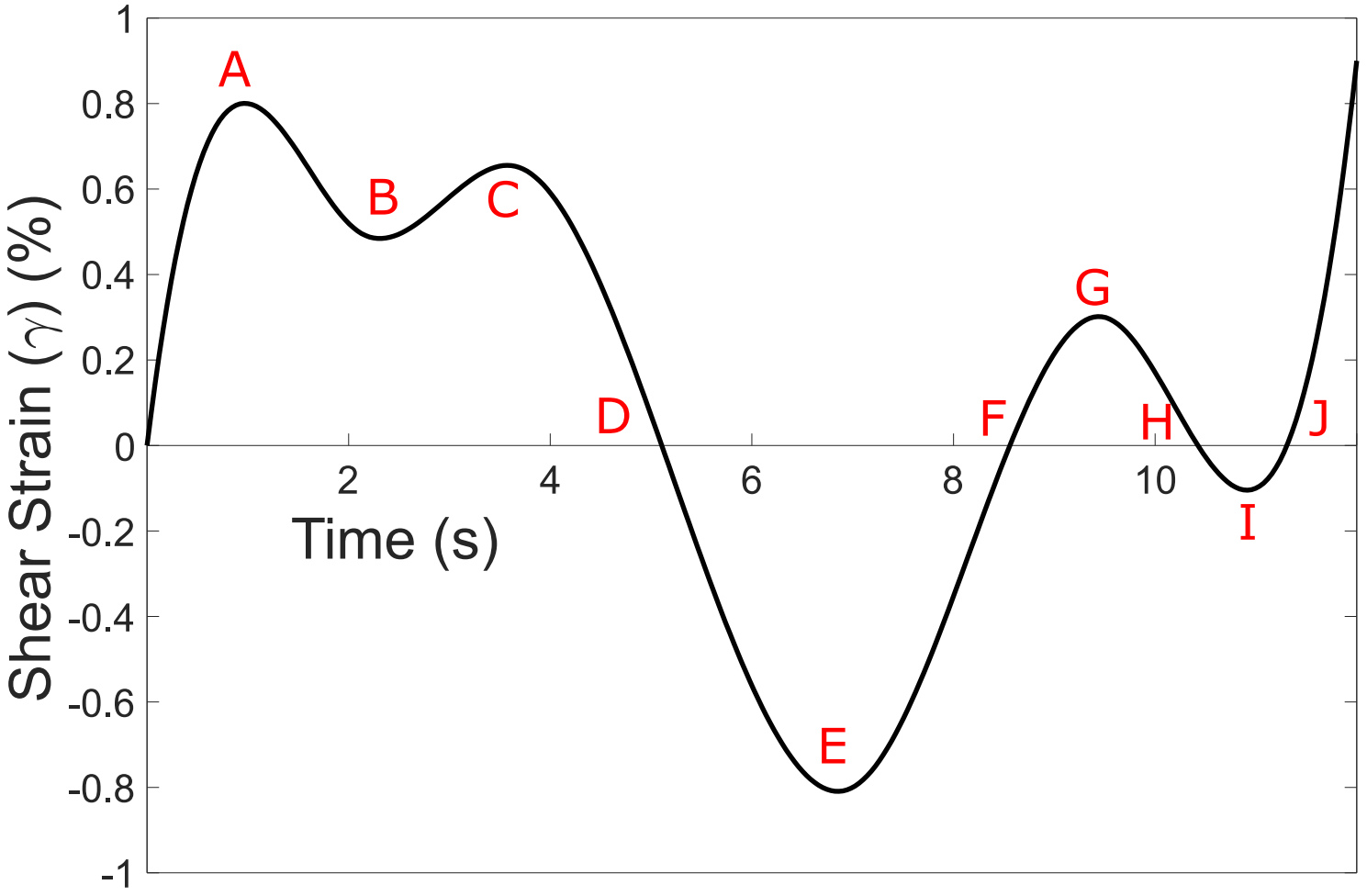

Figure 22. A random shear strain history with loading and unloading sequences

Chapter 4: Modeling single element using DEEPSOIL

DEEPSOIL is a one-dimensional layered soil response analysis platform with options for both equivalent linear and nonlinear analyses. DEEPSOIL analysis treats the entire soil deposits as a continuum that is made of many sublayers and the soil response is evaluated based on boundary (base excitation and surface) and layer interface conditions (deformation and shear stresses). The properties of the soil layers are nonlinear and stress-dependent; such a physics-based analysis allows for high fidelity modelling which is essential to capture the layered soil nonlinear response from propagating waves with high frequencies (excess of 10 Hz).

Under nonlinear mode, the solutions for wave propagation equation are obtained in time-domain with considerations given to hysteretic soil behavior (frequency-independent damping formulation), and seismically-induced excess porewater pressure (u_{ex}) generation and dissipation. The porewater pressure generation models allow for an effective stress-based analysis, where reduction is shear modulus and shear strength (softening) during the shaking can be considered. DEEPSOIL, which is a popular user-friendly platform available for free download, can provide the shear strain history of any layer needed for calculating the volumetric-induced settlement during the seismic shaking. Previous versions of DEEPSOIL had the option of evaluating the dynamic response of a single soil element, however, the shear strain histories were not available for export.

In order to simulate a single element using DEEPSOIL, a sandy layer with a thickness of 10 cm was considered. This thickness is within the suggested range for cyclic direct simple shear samples. In DEEPSOIL, the confining pressure in a particular layer depends on the overburden pressure created by the upper layers. In order to assign a vertical stress of 100 kPa to the element, a thin

layer (2 cm) with relatively large unit weight and shear modulus similar to steel was assigned to the top of the element (Figure 23).

Among the different dynamic soil properties models available on DEEPSOIL platform, a modified version of the hyperbolic MKZ model (Kondner and Zelasko) was chosen as the soil model for the proposed element. MKZ model requires input parameters that can easily be obtained by a curve fitting procedure included in DEEPSOIL. Widely-used mean strain-dependent dynamic soil properties curves such as shear modulus ratio (G/G_{max}) and damping ratio (D) reported by Seed and Idriss were specified as input parameters to DEEPSOIL. DEEPSOIL fits the MKZ model parameters to the specified G/G_{max}-γ and damping ratio-γ reference curves, as shown in Figure 24. Though damping in soil is due to its hysteretic behavior (strain-dependent), laboratory measurements have indicated that a small amount of damping (around 1.5%) exists at very low strain levels. This is included in DEEPSOIL using Rayleigh damping formulation.

Another input parameter required by DEEPSOIL, shear wave velocity (V_s), was calculated according to the following equations. Seed and Idriss (1970) proposed the equation to determine the maximum shear modulus (G_{max} in kPa):

$$G_{max} = 218.8\, K_{2\,max}\sqrt{\sigma'_m} \quad \text{Equation 15.}$$

$K_{2\,max}$ is the empirical soil modulus coefficient which depends on D_r, and σ'_m is the mean effective stress (kPa). These parameters can be obtained as:

$$K_{2\,max} = 16 + 0.6\, D_r \quad \text{Equation 16.}$$

$$\sigma'_m = \sigma'_0 \frac{1+2K_0}{3} \quad \text{Equation 17.}$$

where K_0 is the lateral earth pressure coefficient at rest and it was assumed to be 0.45. Unit weight of the soil was assumed between 17.3 (kN/m^3) and 19.5 (kN/m^3) depending on the relative density (DM 7.01). After estimating G_{max}, the shear wave velocity can be calculated using:

$$G_{max} = \rho V_s^2 \qquad \text{Equation 18.}$$

where, ρ is the density of the soil. It should be noted that to maintain the 100 kPa effective stress in the middle of the soil layer, the unit weight of the steel layer varies as well.

The results of the DEEPSOIL analysis presented in Figure 26 show that when a sinusoidal base motion is applied to the sandy layer, the response is steady-state sinusoidal because of the stiff nature of the system (thin soil and steel layer) being considered. The results show that the thin top "steel" layer has a negligble effect on the response, reproducing Sinuisoidal response similar to the input motion within the soil while inducing the needed shear stress amplitude in the soil element.

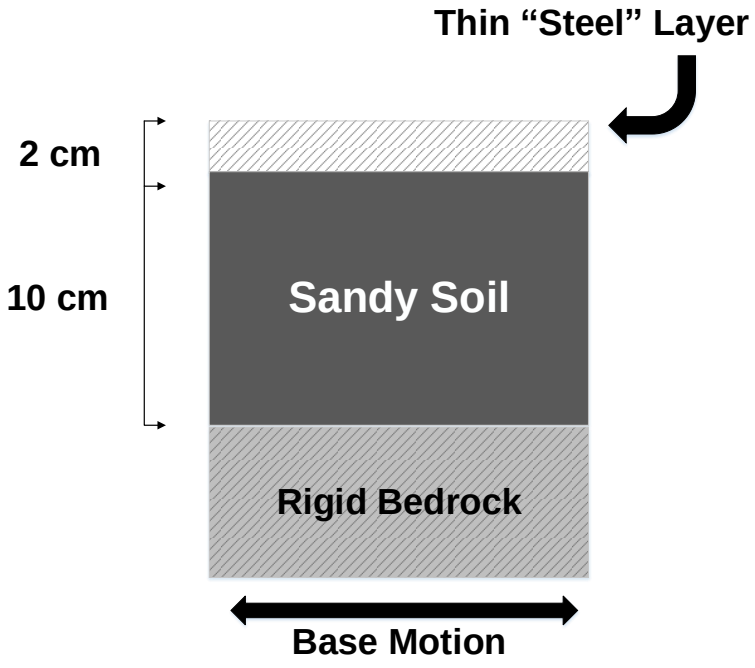

Figure 23. The proposed DEEPSOIL element with soil and steel layers

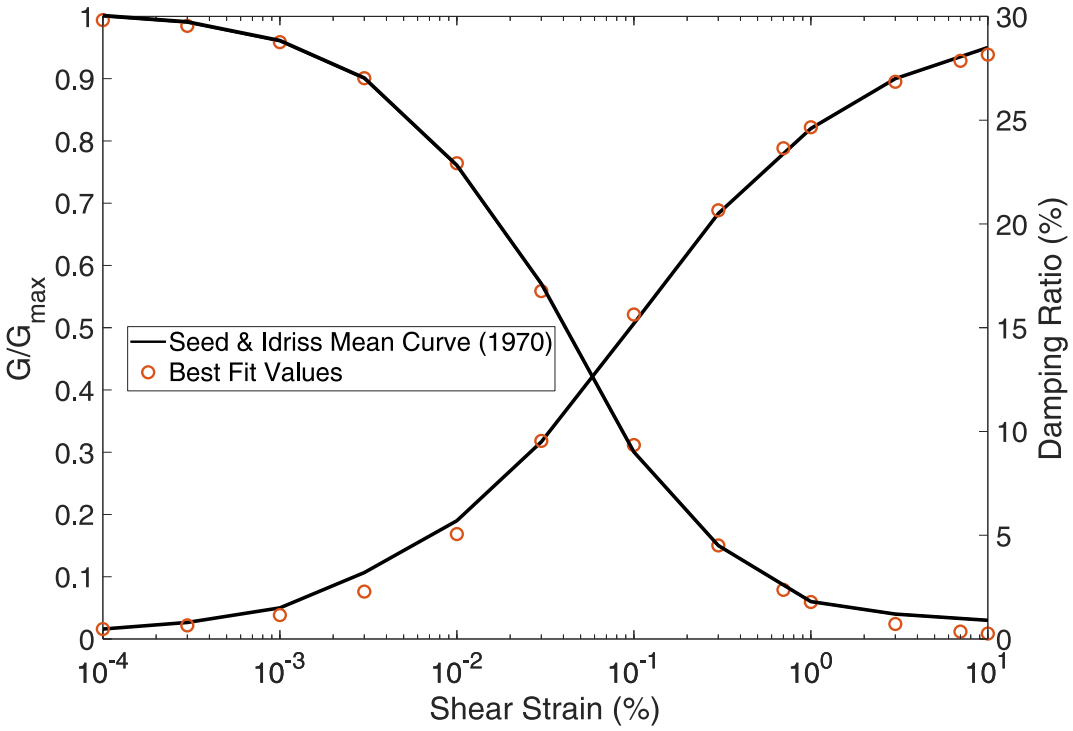

Figure 24. Result of fitting the MKZ model to Seed & Idriss (1970) mean curves for the proposed DEEPSOIL element (D_r = 55%)

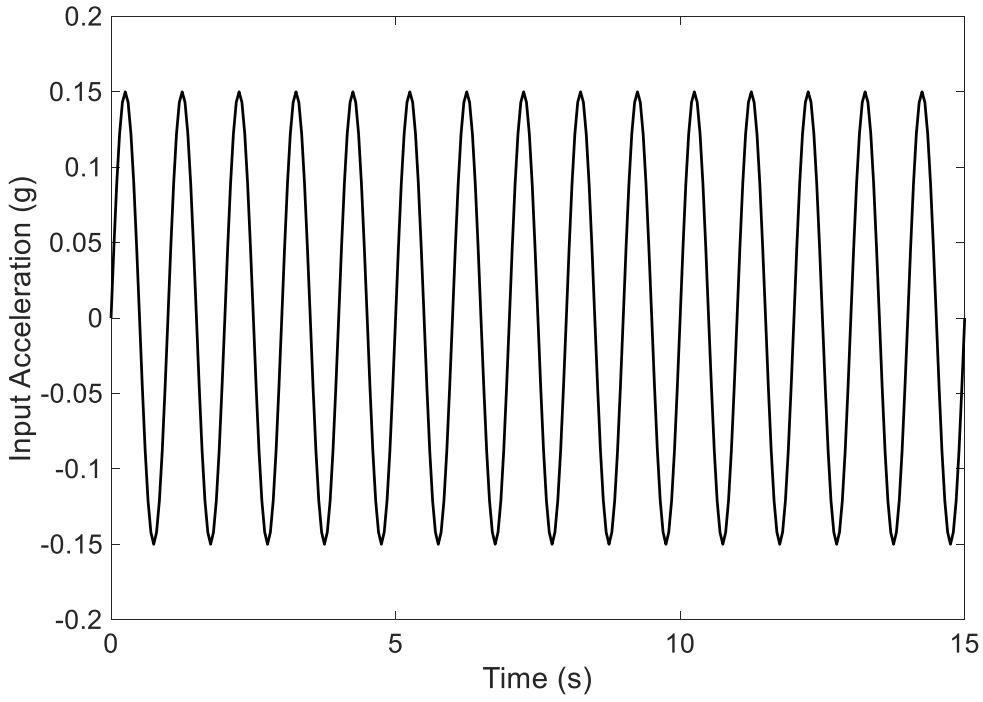

Figure 25. Sinusoidal input base acceleration for the DEEPSOIL element

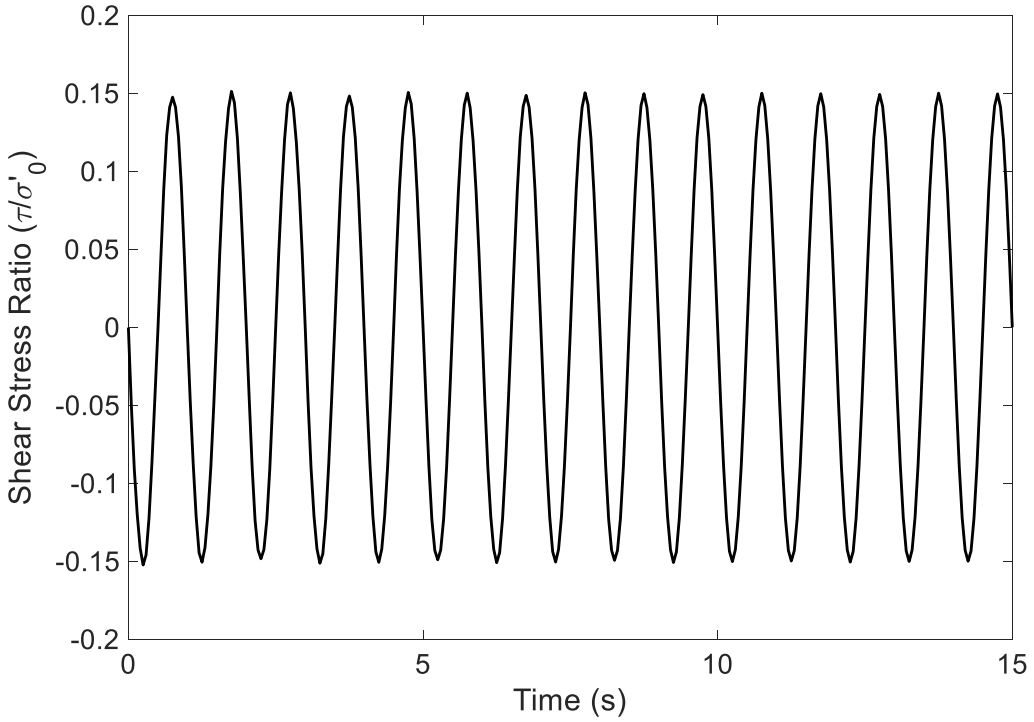
Shear Stress Ratio (τ/σ'_0)
0.2
0.15
0.1
0.05
0
-0.05
-0.1
-0.15
-0.2
0
5
10
15
Time (s)

(a)

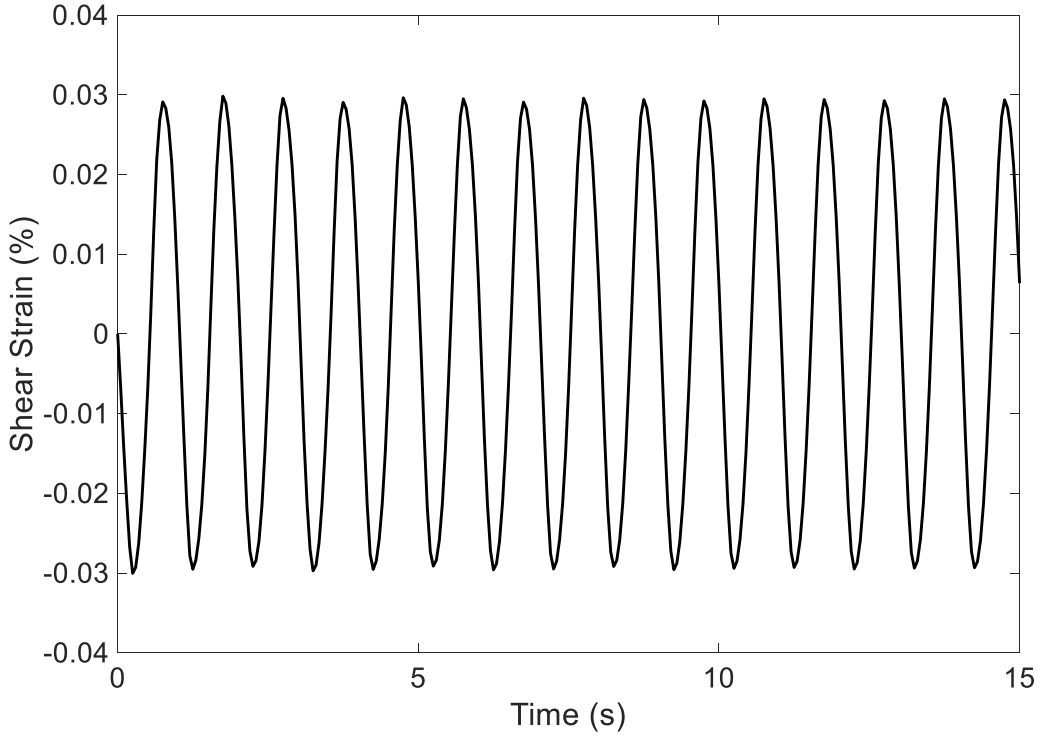
Shear Strain (%)
0.04
0.03
0.02
0.01
0
-0.01
-0.02
-0.03
-0.04
0
5
10
15
Time (s)

(b)

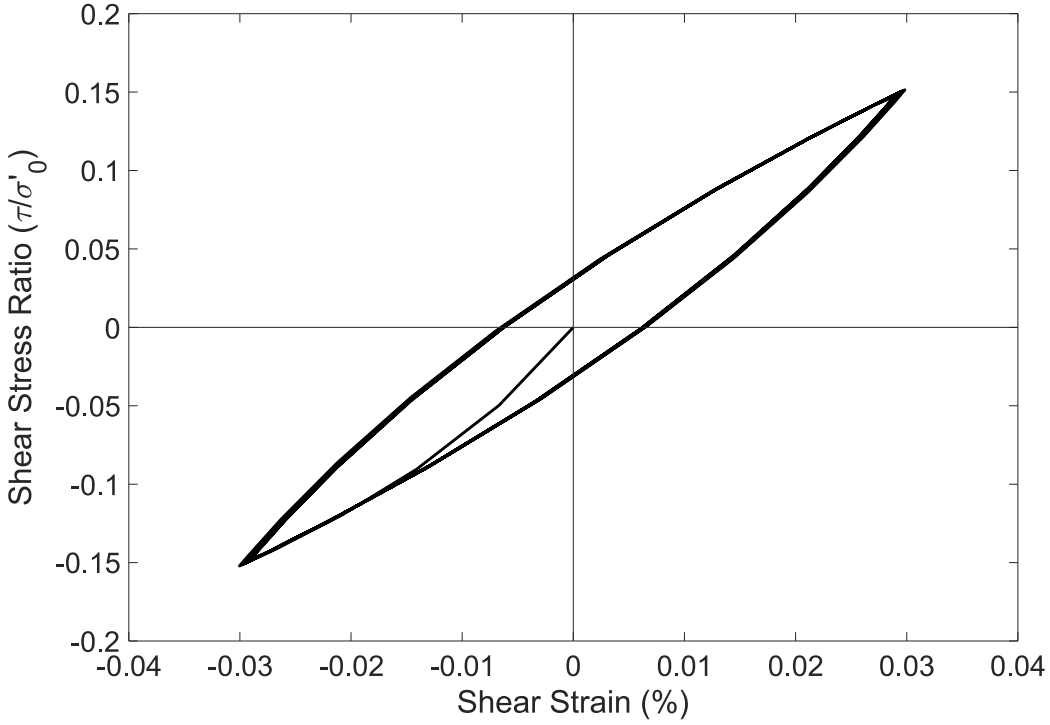

(c)

Figure 26. Computed responses of (a) shear stress ratio, (b) shear strain, and (c) hysteresis loops for the proposed DEEPSOIL element (D_r = 55%, Cyclic Stress Ratio = 0.15)

Many recently proposed methods to estimate the post-liquefaction settlement have utilized advanced constitutive models such as PM4 Sand and PDMY02 and they have been incorporated into programs such as FLAC 3D and OpenSees. Even though these advanced models allow considerable flexibility and generality in modelling dynamic response, using them requires many more parameters than equivalent linear analysis models such as SHAKE or the nonlinear effective stress-based models incorporated into DEEPSOIL. Obtaining soil parameters for advanced constitutive models is difficult in most cases as they differ from one constitutive model to another, and their values can vary depending on the type of test used to estimate them. In addition, there is no comprehensive database of values for those soil parameters from many sources so that

representative values can be selected with confidence by practicing engineers and researchers. The fact that the characteristic dynamic behavior (G/Gmax-γ and D-γ plots) of a single element could be captured using a simpler proposed model, offers a considerable practical advantage over the more complex models.

Chapter 5: Calibration of porewater pressure model

In order to successfully model a softening single element (during seismic excitation) in DEEPSOIL, the inclusion of excess porewater pressure is needed. Five different porewater pressure generation models are available in DEEPSOIL. Among these models, the Generalized Model, which is based on works of Berrill and Davis and Green et al. was chosen due to this energy-based model's simplicity and ability to model both clean sand and soils with fines content. The model uses the general functional form presented originally by Berrill and Davis and later modified by Green et al., known commonly as the GMP model. The GMP model is a special case of the more general energy-based model proposed by Berrill and Davis. DEEPSOIL uses the following equation to calculate the excess porewater pressure (Generalized GMP Model):

$$r_u = \alpha . {w_s}^{\beta} \qquad \text{Equation 19.}$$

where α is the curve fitting coefficient, β is the curve fitting parameter, and w_s is the normalized dissipated energy per unit volume of soil. Another input is ν, which is the degradation parameter. The degradation parameter was introduced by Matasovic and Vucetic and DEEPSOIL uses this formulation. The input parameters of the Generalized GMP Model were calibrated against the liquefaction potential curves of different relative densities. Numerous liquefaction potential curves have been introduced in the literature. The work of Youd et al. based on the liquefaction resistance ratio (CRR) has been one of the widely used in practice. More recently, the performance-based

probabilistic approach has been the framework for newer liquefaction assessment curves. Cetin et al. proposed a SPT-based method with inclusion of the probability of liquefaction (P_L). Boulanger and Idriss developed similar liquefaction-triggering curves for different probabilities of liquefaction. The initial curve starting at P_L = 15% had been developed on the basis of their previous deterministic liquefaction-assessment work. The CRR value corresponding to sands of various SPT values (corresponding to different D_r values) were developed based on field observations of liquefaction from earthquakes with M_w of about 7.5 (15 cycles). It is possible to use these CRR values combined with Magnitude Scaling Factors (MSFs) and the associated number of cycles of loading of other earthquakes to arrive at field-based liquefaction curves as a function of D_r. These curves have been chosen as the benchmark for the calibration of the porewater pressure model. The final calibrated values of the Generalized GMP Model parameters are presented in Table 6. The relative densities shown in Table 3 have been chosen to cover the typical values used in most studies and also include the values used by Tokimatsu and Seed in their work to evaluate the settlement in clean sands.

The single element DEEPSOIL results and the liquefaction resistance curves associated with P_L = 15% for three different relative densities are presented in Figure 27. It is important to note that the liquefaction criterion for the computed DEEPSOIL response has been either porewater pressure ratio (r_u) equal to 0.99 or shear strain (γ) equal or larger than 3.5%. These limiting values were selected by Ishihara and Yoshimine in their evaluation of settlement in sand deposits using the direct simple shear device.

Table 3. Initial DEEPSOIL input values for different soil conditions

Model	Layer	Thickness (m)	Unit Weight (kN/m^3) *	V_s (m/s)
D_r = 35%	Steel	0.02	4977.425	395.34
	Soil	0.1	18.84	183.16
D_r = 45%	Steel	0.02	4976.075	395.39
	Soil	0.1	19.38	194.66
D_r = 55%	Steel	0.02	4974.7	395.45
	Soil	0.1	19.93	204.94
D_r = 60%	Steel	0.02	4974.025	395.47
	Soil	0.1	20.2	209.69
D_r = 75%	Steel	0.02	4971.975	395.55
	Soil	0.1	21.02	222.65
D_r = 80%	Steel	0.02	4971.3	395.58
	Soil	0.1	21.29	226.6
D_r = 90%	Steel	0.02	4969.925	395.64
	Soil	0.1	21.84	236.98

*Unit weights vary such that the effective vertical stress in the middle of the soil layer is 100 kPa

Table 4. DEEPSOIL soil model input values for different layers

Layer	Soil Model	D_{min} (%)	Ref. Strain (%)	Reference Stress (MPa)	β	s	b	d
Soil	MKZ	0.371	0.066	0.18	1.545	0.855	0	0

Table 5. DEEPSOIL curve fitting input values for different layers

Layer	Reduction Factor Formulation	P1	P2	P3
Soil	MRDF-UIUC	0.992	0.386	1.35

Table 6. Best-fit values of the Generalized GMP Model parameters calibrated to Boulanger & Idriss P_L = 15% curve

D_r (%)	α	β	ν
35	0.739	0.3	0.33
45	0.654	0.3	0.324
55	0.569	0.3	0.39
60	0.68	0.3	0.5
75	0.403	0.3	0.71
80	0.364	0.3	1.6
90	0.29	0.3	0.98

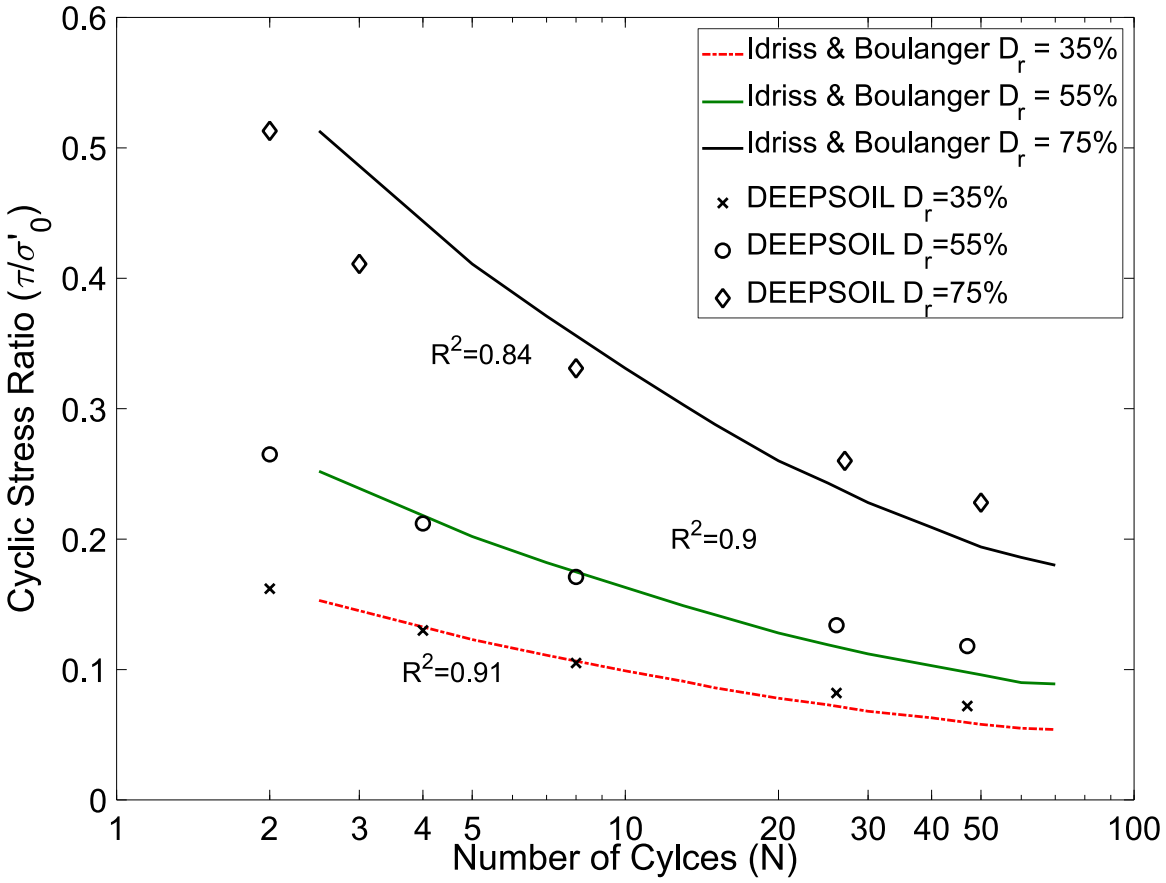

Figure 27. Comparison between the P_L = 15% Idriss and Boulanger liquefaction potential curves and the results from the DEEPSOIL element using the best-fit values

The porewater pressure generation rate through cycles of loading up to liquefaction (N_L) has been discussed by several investigators. Researchers including Lee and Albaisa (1974), Seed et al. (1976), and Iwasaki et al (1984) studied the relationship between porewater pressure and the normalized number of cycles (N/N_L) and suggested ranges for the rate of porewater pressure build-up based on laboratory tests. The porewater pressure generation rate, generated in the element modeled with DEEPSOIL was compared with the ranges reported by Seed et al (1976) and Lee and Albasia (1974). Figure 28 shows that the proposed DEEPSOIL element's behavior for the

stress ratios needed to liquefy the element in N_L=10 cycles. It can be observed that the behavior of this element falls within the ranges previously proposed.

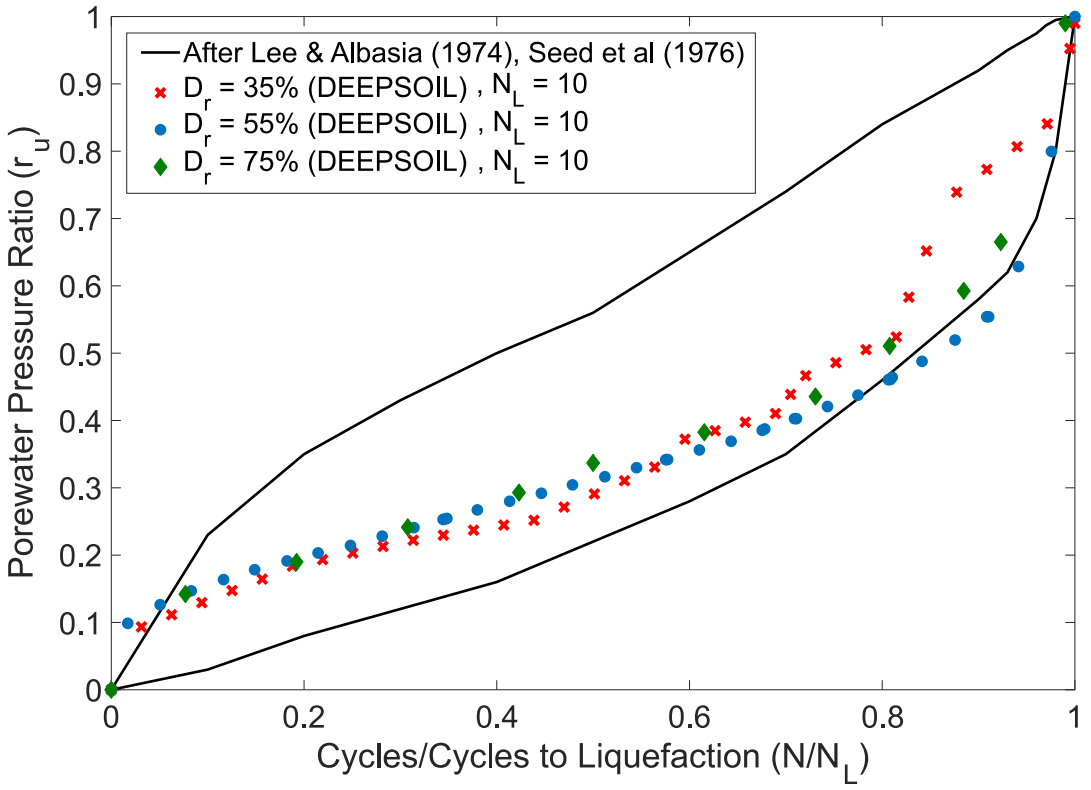

Figure 28 Comparison of the porewater pressure generation rate of DEEPSOIL soil element and the range suggested by Seed et al. and Lee and Albasia

The effect of porewater pressure generation can be seen on the softening cyclic response of the saturated element (Figure 28). While the porewater pressure builds up through the cycles, the shear strain increases, hysteresis loops become more inclined (softer behavior) and the shear stress history is no more a sinusoidal function of time. This process continues until either of the aforementioned liquefaction criterion (in this case γ = 3.5% was reached before r_u = 0.99) is reached. The strain-softening behavior presented in Figures 29a and 29c is in good agreement with

the laboratory investigations, where developing liquefaction conditions have been reported. At the same time, acceleration response above liquefied soil layers in field observations have also revealed the similar behavior seen in Figure 9b.

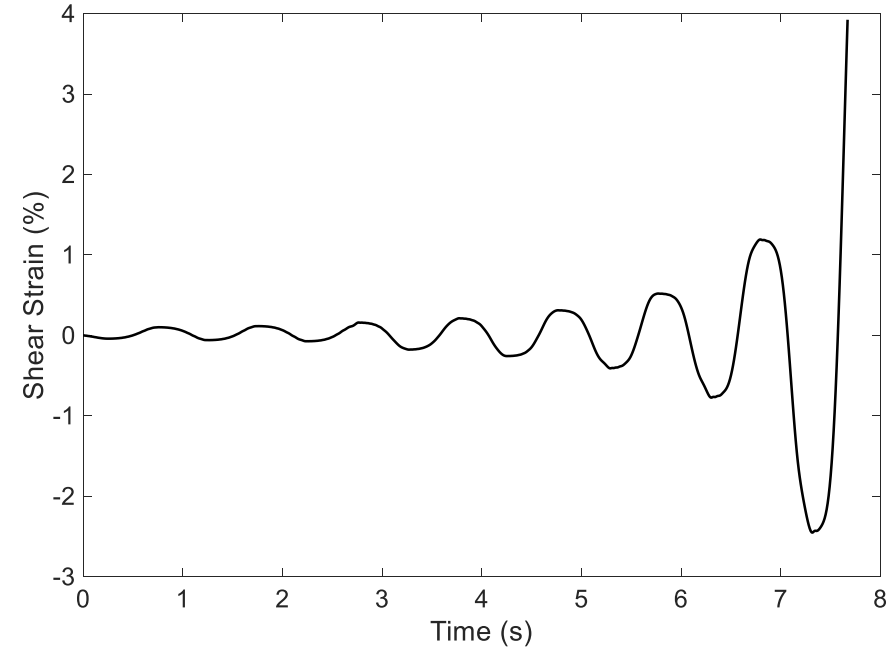

(a)

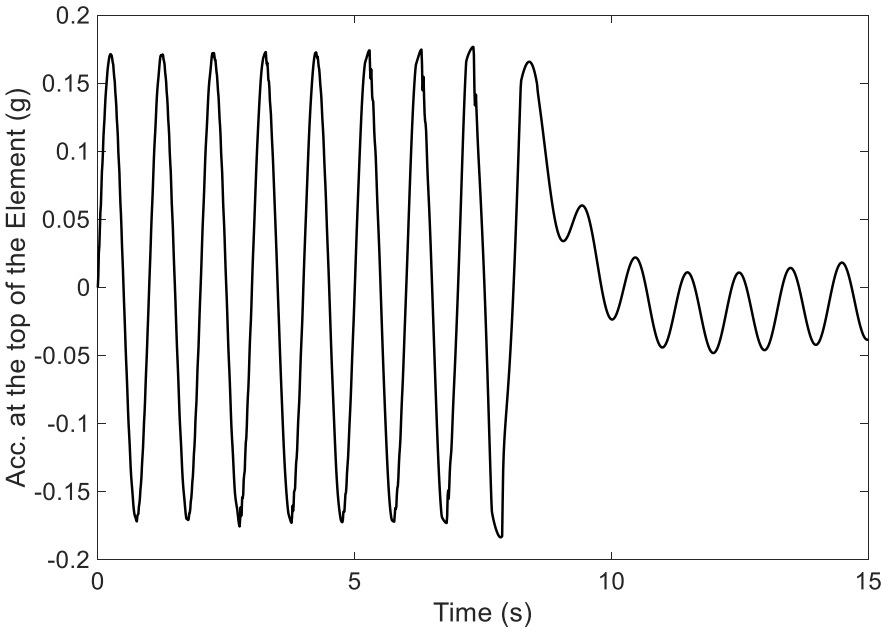

(b)

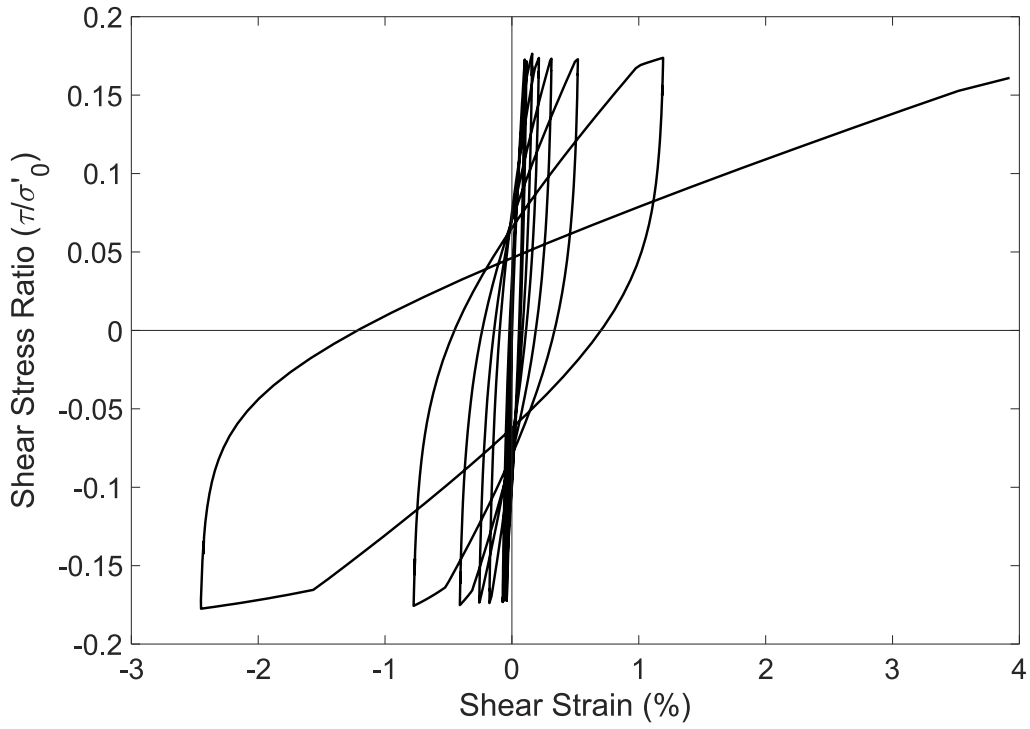

Figure 29. Computed responses of (a) shear strain, (b) acceleration, and (c) hysteresis loops for the proposed DEEPSOIL element (D_r = 55%, Cyclic Stress Ratio = 0.179)

A similar procedure can be used to calibrate the proposed soil element to match with liquefaction potential curves with different probabilities of liquefaction (P_L) as suggested by Boulanger and Idriss. This can be readily incorporated in the performance-based engineering (PBE) design methodology. PBE requires consideration of a number of plausible scenarios that entail multi-ensemble simulations of earthquakes of different hazard levels to quantify the uncertainty (Fragility Determination) in seismic performance. The different hazard levels can represent field cases of combined instances of developing liquefaction and post-liquefaction in some or all individual soil layers present in the deposit.

A MATLAB code was developed and used to calculate the ε_v for a saturated soil element with excess porewater pressure. Figure 30 shows the volumetric strain time history before and after the liquefaction. In this plot, the volumetric strain was calculated only up to the level when the cumulative value reaches the terminal value proposed by Ishihara and Yoshimine (1992) from their simple shear tests conducted on clean sands. The proposed method shows that the ε_v history progressively increased as the excitation continued, followed by a significant surge after the liquefaction at N_L = 8 cycles. As noted in chapter 2, because of uncertainty in ε_v estimation after the liquefaction due to the fact that the results rely on the field and laboratory measurements, the volumetric strain history was capped once the terminal ε_v value was reached.

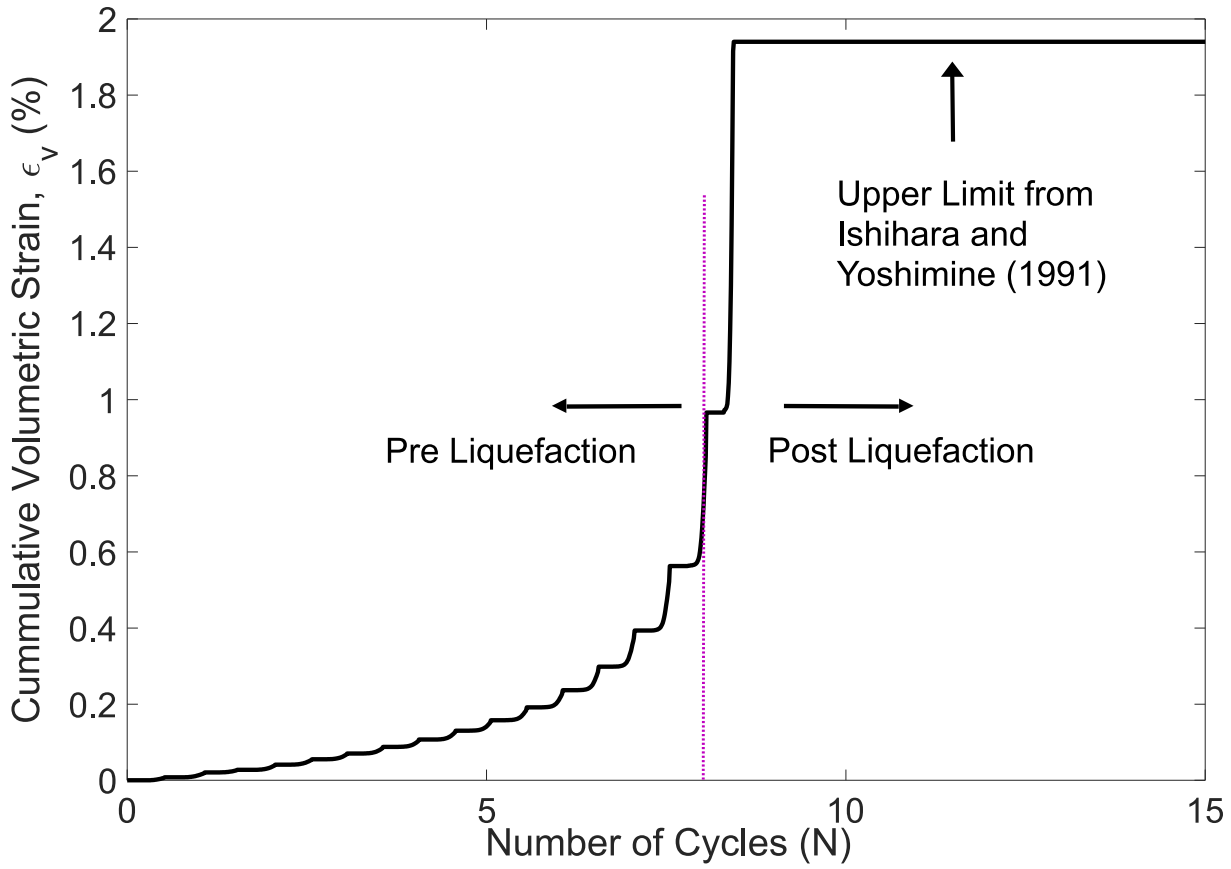

Figure 30 Volumetric strain from sinusoidal cyclic loads for a saturated element during the process of liquefaction (D_r = 75%, Cyclic Stress Ratio = 0.331)

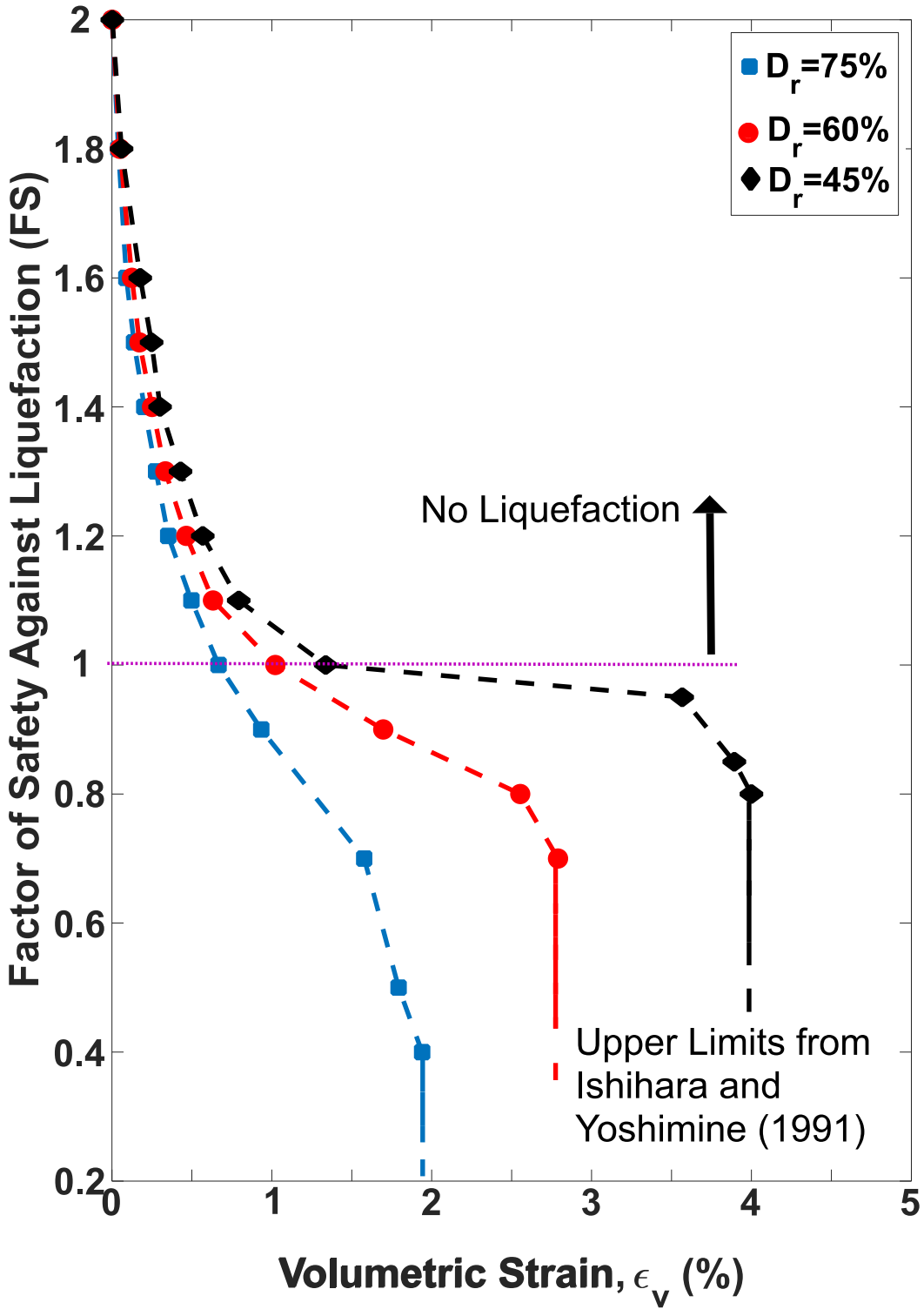

Figure 31. Volumetric strain from sinusoidal cyclic loads for a saturated element versus factor of safety against liquefaction, $N_L = 10$

Figure 31 presents the volumetric strain versus the factor of safety against liquefaction (FS) for soils with different relative densities. The FS is calculated as a ratio of CRR (N_L = 10 cycles from Figure 27) and the applied cyclic stress ratio. It can be observed that this plot is similar to curves proposed by Ishihara and Yoshimine (1992) to estimate the post-liquefaction volumetric strain of clean sands. Ishihara and Yoshimine surmised their curves as a function of FS based on the data gathered from their simple shear tests that investigated post-liquefaction behavior. Unlike their work, the proposed method is able to obtain the volumetric settlement history under developing liquefaction conditions as well. It should be mentioned that a cut off for the calculation of the volumetric strain was selected based on the values suggested by Ishihara and Yoshimine (1992) for post-liquefaction state.

Chapter 6 Volumetric-induced settlement calculation

The calibrated DEEPSOIL soil element models were used to evaluate the response shear strain histories needed to calculate the total volumetric strain in a layered soil profile. The vertical volumetric strain (ε_{vi}) is calculated for each layer based on its shear strain history and then is integrated with depth to estimate the total free-field settlement ($D_{Surface}$) due to the ground motion. For a profile with n layers or sublayers, it can be calculated as:

$$D_{Surface} = \sum_{i=1}^{n} h_i \,.\, \epsilon_{vi} \qquad \text{Equation 20.}$$

where h_i is the thickness of each layer. A MATLAB code was developed to evaluate the surface settlement history based in the volumetric strain histories of soil layers (or the sublayers). In order to get more realistic results, it is recommended to divide the soil layers into thin sublayers in the DEEPSOIL analysis. The sublayer thickness should be small enough to model high- frequency waves that travel with short wave lengths, calculated to be 0.7 meters. It is was decided to limit

the thickness of the sublayers to 0.5 meters. In addition, in order to capture the sensitivity of the total settlement to the deformation of liquefied layers, the saturated soil layer was divided into sublayers with a thickness of 0.25 meters.

Chapter 7: Evaluation of the proposed model: Case histories

Several earthquake-induced settlement measurements have been made at many sites during the past earthquakes. Some of these sites have well-documented SPT or CPT measurements. These measurements could be used to generate the DEEPSOIL site profile and perform the response analysis to create the shear strain history needed to calculate the volumetric strain in each layer. Among the case histories available, three were chosen to assess the predictability of proposed method due to the high quality of CPT/SPT measurements and well-documentation of settlement. The base excitations were chosen based on the nearest outcrop acceleration records to the sites as selected by other researchers who undertook investigation of free-field settlement.

Only the strongest horizontal acceleration time histories were used. If needed, the other horizontal component of the excitation could be considered independently using the proposed approach. It should be noted that since the role of other two acceleration components were not incorporated in the calculations, the evaluations presented below should be seen as lower estimates. It should be noted that even though the proposed method has been developed for cases with or without liquefaction, in all the case histories studied, liquefaction occurred at least in a partial manner.

7.1. 1989 Loma Prieta earthquake

Immediately after the 1989 Loma Prieta earthquake, USGS inspected the damages caused in the Marina District in the northern part of San Francisco. Both liquefaction and amplification of

ground motion were recognized in the Marina District, which caused severe damages to structures and lifelines. Even though most of the liquefaction-induced damage in the Marina District was in the loose artificial deposits (reclaimed area), it was also observed in the areas formed by natural sand deposits. A series of comprehensive in-situ subsurface site investigations in the Marina District, including CPT and SPT measurements, were carried out by USGS. The locations of these measurements are indicated in Figure 32. Investigations showed that the area mainly consisted of three major layers: Holocene Bay Mud, natural sand and hydraulic fill (artificial sand deposits) [34]. In section A of the area, including M1, M2, and M3 points, the top 8 meters of the soil deposit consisted of natural beach sand sitting on top of the bay mud. On the other hand, in the points closer to section B, which are M4, M5, C4, C7, C8, C10, and C15, the top layer mostly consisted of hydraulically filled sand and silty sand on top of the bay mud. These un-compacted deposits caused relatively larger settlements in this section of the Marina District. Point M6 is located within section C, which mostly consisted of dune sands, with no bay mud below.

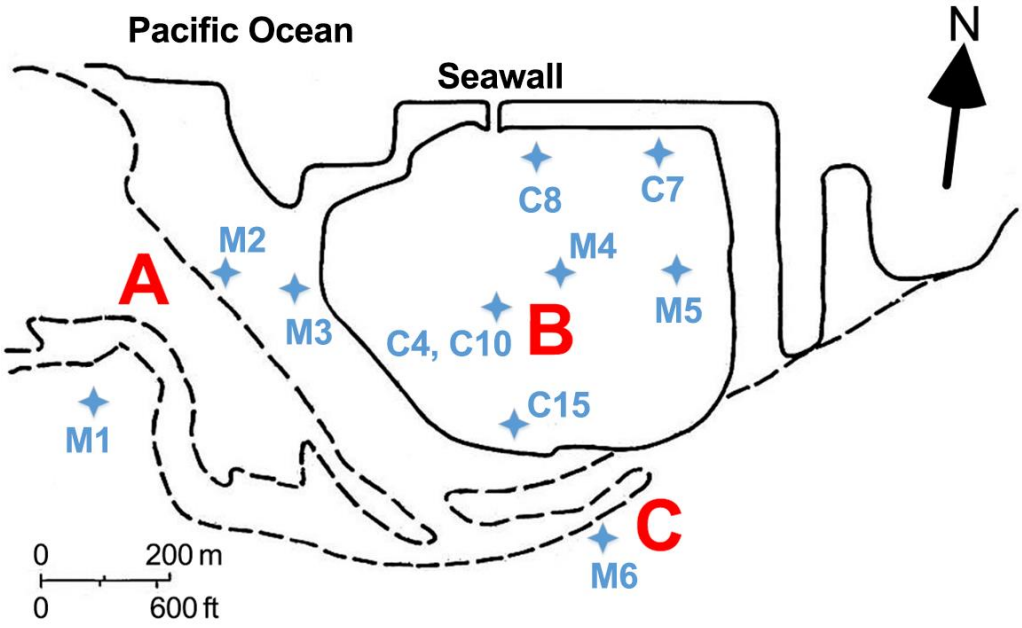

Figure 32. Plan view of Marina District and the locations of SPT and CPT measurements

When determining the input parameters for the DEEPSOIL model, a critically important parameter is the relative density. For points M1, M2, M3, M4, M5, and M6, the CPT measurements were used. In layers with fine content, the procedure proposed by Robertson and Wride (1998) was used to calculate the equivalent q_c for clean sand. The relative density was calculated according to $(q_{c1N})_{cs}$ using Equation 21. For points C4, C7, C8, C10, and C15, SPT values were used to determine relative density according to Equation 22.

$$q_{c1N} = 0.9\left(\frac{\frac{D_r}{100}+1.063}{0.465}\right)^{3.788} \qquad \text{Equation 21.}$$

$$D_r = \sqrt{N_{1,60}/46} \qquad \text{Equation 22.}$$

After calculating the relative density, shear wave velocity was calculated according to the Equation 15 – Equation 18. Another input parameter, effective stress, was obtained according to the unit weight of each sublayer, which was assumed between 14 and 17 (kN/m^3) according to the relative density and the soil type. The other major inputs needed for the DEEPSOIL profile are: 1) depths to the water table, which ranged from 2.3 to 5.5 meters [Bennett (1990) and O'Rourke et al. (1991)], 2) porewater pressure parameters (from Table. 2) selected based on the relative density, and 3) the ground motion. In the Marina District, no accelerometers were located to record the ground motions. The accelerogram used for this study was the main shock recorded at the closest rock outcrop (based on $V_{s,30}$ > 650 m/s), which was roughly 1 mile away from the site. The measured volumetric-induced ground settlements and the values calculated using the proposed method are presented in Table 17. The comparison shows a good agreement between these values. In order to appraise the accuracy of this model, the available estimates made by Zhang et al. (2008) are also presented for a number of locations.

Table 7. Main inputs for DEEPSOIL model of M1 site

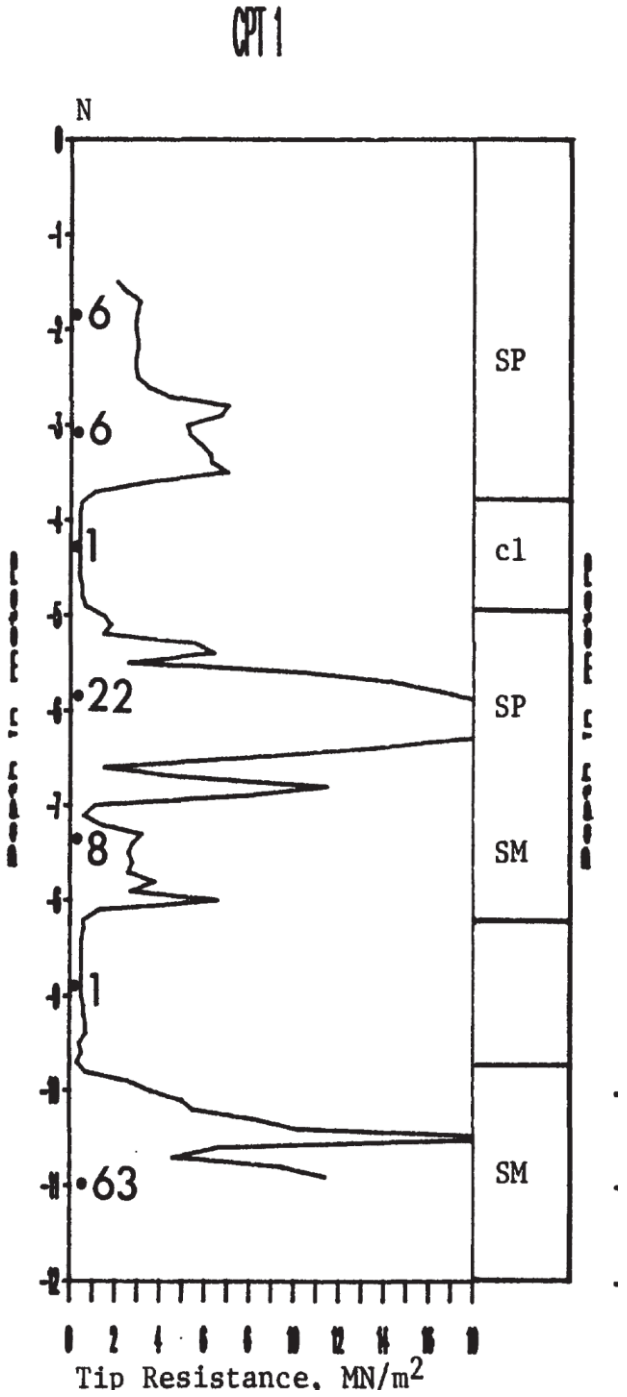

Main Inputs			PWP Model Inputs		
Depth (m)	Unit Weight (kN/m^3)	V_s (m/s)	α	β	ν
0.5	17	121.68	0.36	0.3	1.60
1	17	134.56	0.68		0.50
1.5	17	141.94	0.57		0.39
2	17	146.97	0.65		0.32
2.5	17	167.18	0.68		0.50
3	17	171.24	0.68		0.50
3.5	17	195.73	0.40		0.71
4	17	212.99	0.36		1.60
4.5	14	186.70	0.65		0.32
5	14	191.53	0.65		0.32
5.5	14	180.34	0.74		0.33
6	17	197.85	0.68		0.50
6.5	17	235.88	0.29		0.98
7	17	240.76	0.29		0.98
7.5	16.5	180.83	0.74		0.33
8	16.5	183.84	0.74		0.33
8.5	16.5	231.71	0.57		0.39
9	14	237.86	0.57		0.39
9.5	14	240.98	0.57		0.39
10	14	244.03	0.57		0.39
10.5	16.5	205.94	0.65		0.32
11	16.5	270.46	0.29		0.98
11.5	16.5	273.69	0.29		0.98
12	16.5	276.81	0.29		0.98

Figure 33. CPT measurements for M1 site by Bennett (1990)

Table 8. Main inputs for DEEPSOIL model of M2 site

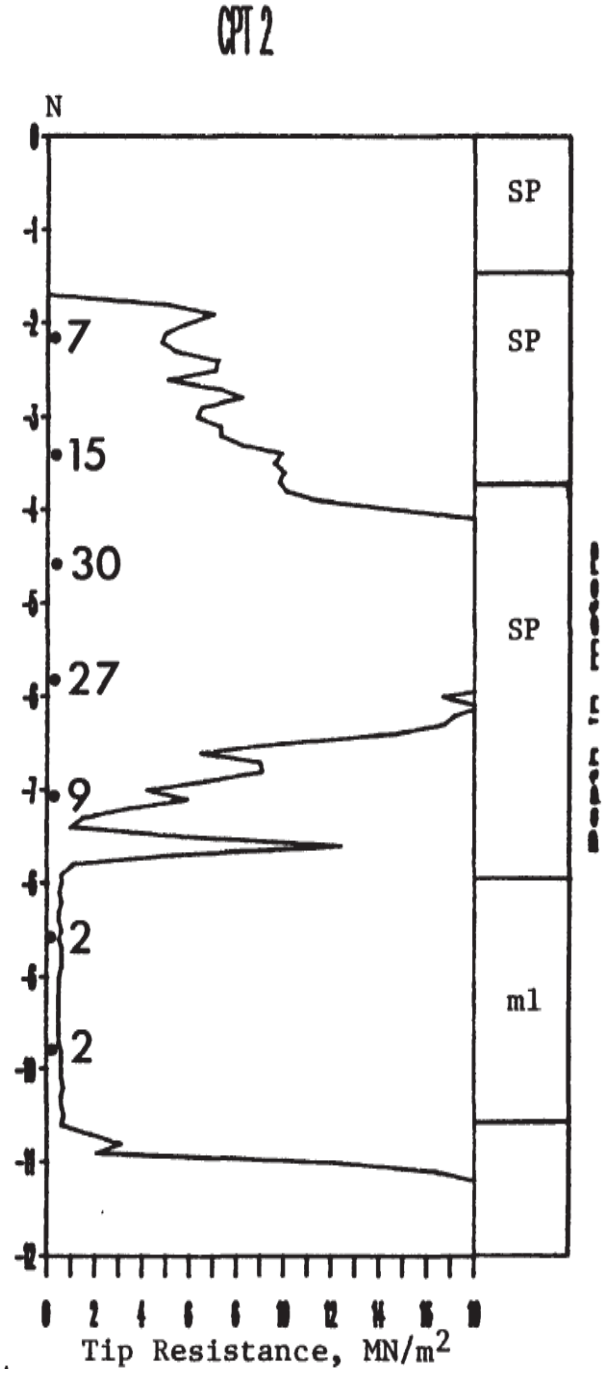

Main Inputs			PWP Model Inputs		
Dept (m)	Unit Weight (kN/m^3)	V_s (m/s)	α	β	ν
0.5	17	127.50	0.29	0.3	0.98
1	17	151.63	0.29		0.98
1.5	17	167.80	0.29		0.98
2	17	180.32	0.29		0.98
2.5	17	190.66	0.29		0.98
3	17	199.55	0.29		0.98
3.5	17	207.39	0.29		0.98
4	17	214.43	0.29		0.98
4.5	17	220.84	0.29		0.98
5	17	226.74	0.29		0.98
5.5	17	232.20	0.29		0.98
6	17	237.31	0.29		0.98
6.5	17	242.11	0.29		0.98
7	17	246.63	0.29		0.98
7.5	17	218.05	0.569		0.39
8	17	219.91	0.569		0.39
8.5	14	240.60	0.569		0.39
9	14	243.66	0.569		0.39
9.5	14	246.65	0.569		0.39
10	14	249.57	0.569		0.39
10.5	14	252.43	0.569		0.39
11	14	255.22	0.569		0.39
11.5	14	297.12	0.29		0.98
12	17	272.94	0.29		0.98

Figure 34. CPT measurements for M2 site by Bennett (1990)

Table 9. Main inputs for DEEPSOIL model of M3 site

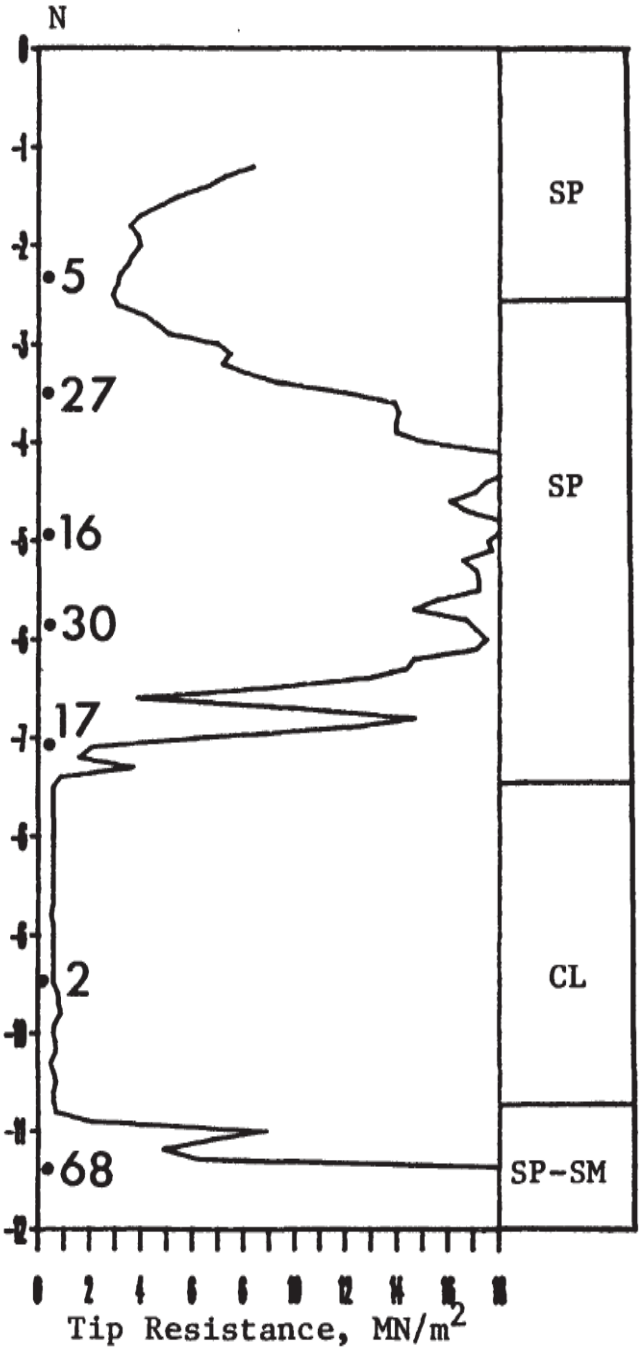

Main Inputs			PWP Model Inputs		
Dept (m)	Unit Weight (kN/m^3)	V_s (m/s)	α	β	ν
0.5	17	121.68	0.36	0.3	1.60
1	17	134.56	0.68		0.50
1.5	17	141.94	0.57		0.39
2	17	146.97	0.65		0.32
2.5	17	167.18	0.68		0.50
3	17	171.24	0.68		0.50
3.5	17	195.73	0.40		0.71
4	17	212.99	0.36		1.60
4.5	14	186.70	0.65		0.32
5	14	191.53	0.65		0.32
5.5	14	180.34	0.74		0.33
6	17	197.85	0.68		0.50
6.5	17	235.88	0.29		0.98
7	17	240.76	0.29		0.98
7.5	16.5	180.83	0.74		0.33
8	16.5	183.84	0.74		0.33
8.5	16.5	231.71	0.57		0.39
9	14	237.86	0.57		0.39
9.5	14	240.98	0.57		0.39
10	14	244.03	0.57		0.39
10.5	16.5	205.94	0.65		0.32
11	16.5	270.46	0.29		0.98
11.5	16.5	273.69	0.29		0.98
12	16.5	276.81	0.29		0.98

Figure 35. CPT measurements for M3 site by Bennett (1990)

Table 10. Main inputs for DEEPSOIL model of M4 site

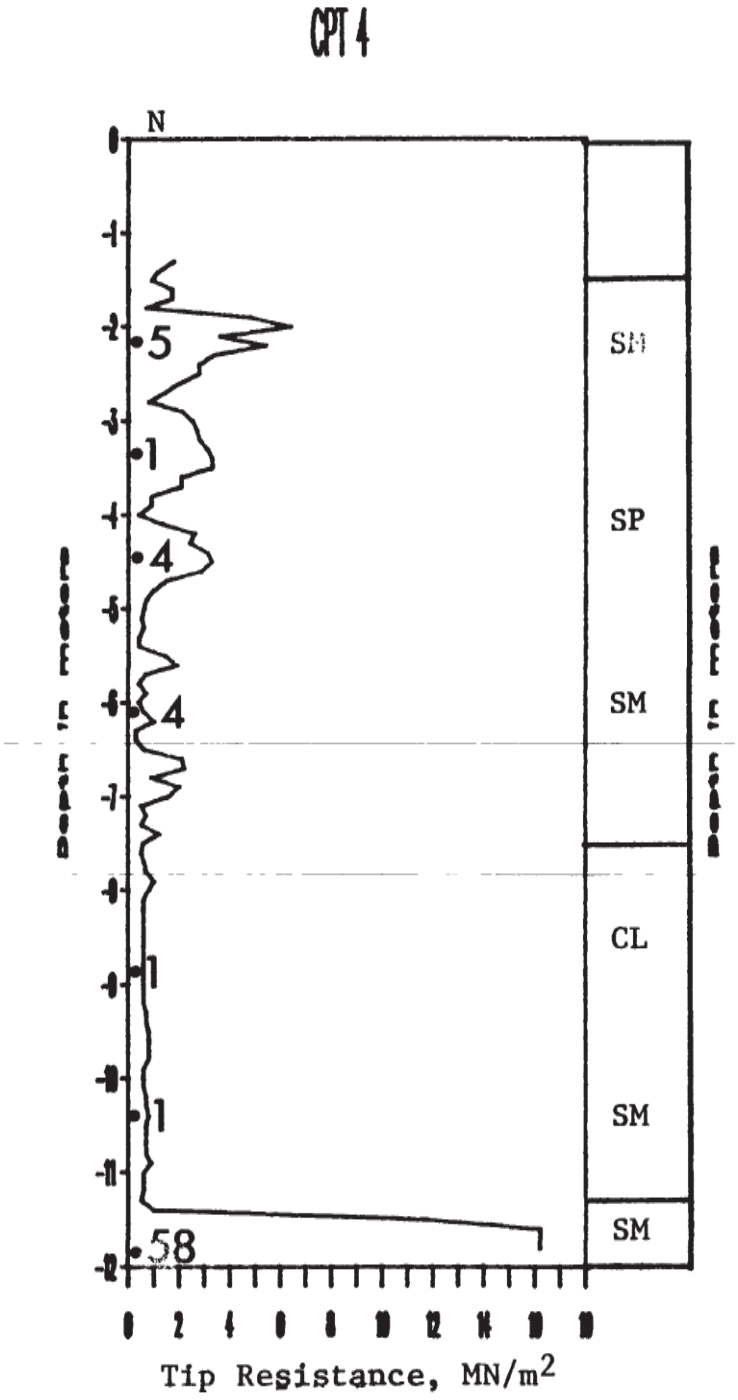

Main Inputs			PWP Model Inputs		
Dept (m)	Unit Weight (kN/m^3)	V_s (m/s)	α	β	ν
0.5	16.5	104.57	0.57	0.3	0.39
1	16.5	112.47	0.74		0.33
1.5	16.5	121.56	0.74		0.33
2	16.5	130.62	0.74		0.33
2.5	16.5	189.98	0.29		0.98
3	16.5	172.15	0.68		0.50
3.5	16.5	167.54	0.65		0.32
4	16.5	178.56	0.57		0.39
4.5	17	168.30	0.65		0.32
5	17	204.49	0.68		0.50
5.5	17	166.58	0.74		0.33
6	16.5	172.73	0.74		0.33
6.5	16.5	176.16	0.74		0.33
7	16.5	179.40	0.74		0.33
7.5	16.5	182.47	0.74		0.33
8	14	200.06	0.74		0.33
8.5	14	201.98	0.74		0.33
9	14	203.84	0.74		0.33
9.5	14	205.65	0.74		0.33
10	14	207.42	0.74		0.33
10.5	14	209.14	0.74		0.33
11	16.5	195.14	0.74		0.33
11.5	16.5	197.54	0.74		0.33
12	16.5	267.57	0.74		0.33

Figure 36. CPT measurements for M4 site by Bennett (1990)

Table 11. Main inputs for DEEPSOIL model of M6 site

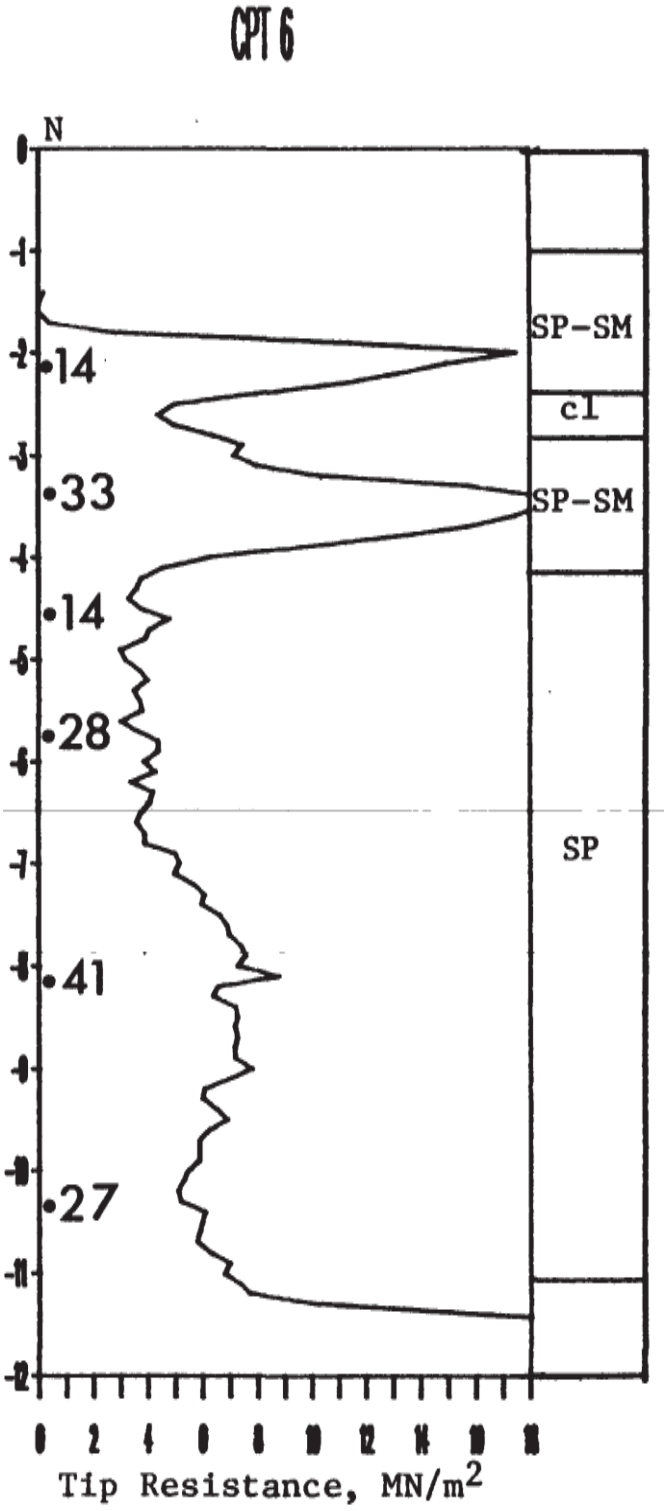

Main Inputs			PWP Model Inputs		
Dept (m)	Unit Weight (kN/m^3)	V_s (m/s)	α	β	ν
0.5	17	127.50	0.29	0.3	0.98
1	17	151.63	0.29		0.98
1.5	17	167.80	0.29		0.98
2	17	180.32	0.29		0.98
2.5	17	190.66	0.29		0.98
3	14	204.07	0.36		1.60
3.5	17	204.14	0.40		0.71
4	17	211.50	0.29		0.98
4.5	17	192.09	0.36		1.60
5	17	194.95	0.36		1.60
5.5	17	197.51	0.36		1.60
6	17	199.81	0.36		1.60
6.5	17	201.90	0.29		0.98
7	17	203.81	0.29		0.98
7.5	17	226.29	0.36		1.60
8	17	242.36	0.36		1.60
8.5	17	238.16	0.36		1.60
9	17	240.20	0.36		1.60
9.5	17	242.13	0.36		1.60
10	17	235.74	0.36		1.60
10.5	17	237.32	0.36		1.60
11	17	247.33	0.36		1.60
11.5	17	277.91	0.36		1.60
12	17	280.94	0.29		0.98

Figure 37. CPT measurements for M6 site by Bennett (1990)

Table 12. Main inputs for DEEPSOIL model of C4 site

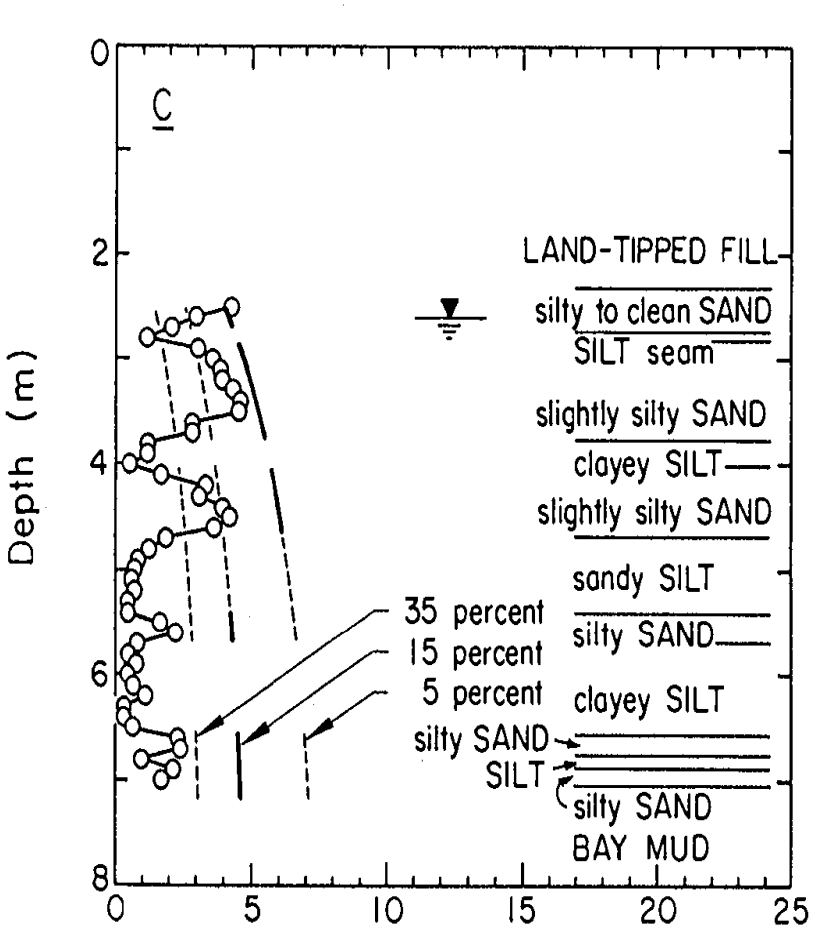

Main Inputs			PWP Model Inputs		
Dept (m)	Unit Weight (kN/m^3)	V_s (m/s)	α	β	ν
0.5	17	159.13	0.29	0.3	0.98
1	17	177.19	0.40		0.71
1.5	17	187.85	0.68		0.50
2	17	195.33	0.68		0.50
2.5	17	201.03	0.57		0.39
3	17	203.01	0.57		0.39
3.5	17	188.94	0.65		0.32
4	16.5	192.96	0.74		0.33
4.5	14	203.15	0.74		0.33
5	14	229.38	0.57		0.39
5.5	14	241.75	0.68		0.50
6	17	190.37	0.74		0.33
6.5	16.5	201.49	0.74		0.33
7	16.5	198.09	0.74		0.33
7.5	16.5	200.39	0.74		0.33
8	16.5	202.61	0.74		0.33
8.5	16.5	204.76	0.74		0.33

Figure 38. Normalized tip resistance for C4 site by Bennett (1990)

Table 13. Main inputs for DEEPSOIL model of C7 site

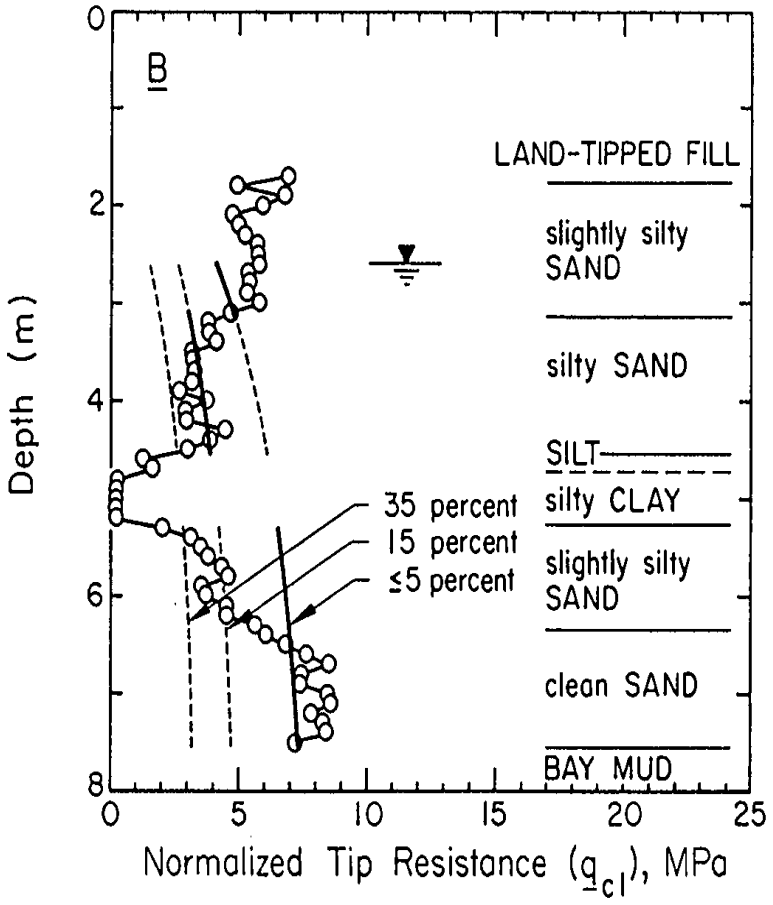

Main Inputs			PWP Model Inputs		
Dept (m)	Unit Weight (kN/m^3)	V_s (m/s)	α	β	ν
0.5	16.5	160.36	0.29	0.3	0.98
1	16.5	179.06	0.40		0.71
1.5	16.5	189.88	0.68		0.50
2	16.5	197.49	0.68		0.50
2.5	16.5	203.28	0.57		0.39
3	16.5	205.22	0.57		0.39
3.5	16.5	207.01	0.57		0.39
4	16.5	208.66	0.57		0.39
4.5	16.5	210.19	0.57		0.39
5	16.5	211.61	0.57		0.39
5.5	17	239.92	0.57		0.39
6	17	241.86	0.68		0.50
6.5	17	243.70	0.68		0.50
7	17	245.45	0.68		0.50
7.5	17	270.48	0.29		0.98
8	17	272.44	0.29		0.98
8.5	17	274.31	0.29		0.98

Figure 39. Normalized tip resistance for C7 site by Bennett (1990)

Table 14. Main inputs for DEEPSOIL model of C8 site

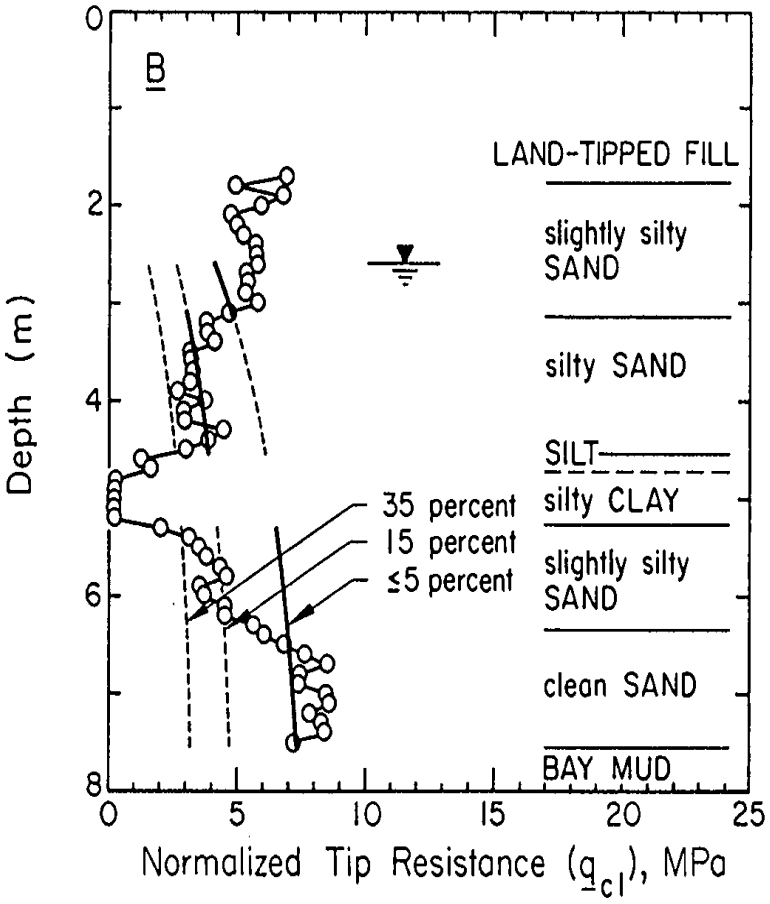

Main Inputs			PWP Model Inputs		
Dept (m)	Unit Weight (kN/m^3)	V_s (m/s)	α	B	ν
0.5	17	159.17	0.29	0.3	0.98
1	17	189.28	0.29		0.98
1.5	17	209.48	0.29		0.98
2	17	219.64	0.36		1.60
2.5	17	220.41	0.68		0.50
3	17	214.22	0.68		0.50
3.5	17	216.35	0.68		0.50
4	17	190.19	0.74		0.33
4.5	17	185.81	0.74		0.33
5	14	206.54	0.74		0.33
5.5	14	244.41	0.57		0.39
6	17	203.05	0.65		0.32
6.5	17	204.12	0.74		0.33
7	17	245.20	0.68		0.50
7.5	17	253.98	0.40		0.71
8	17	258.91	0.40		0.71
8.5	14	274.76	0.68		0.50

Figure 40. Normalized tip resistance for C8 site by Bennett (1990)

Table 15. Main inputs for DEEPSOIL model of C10 site

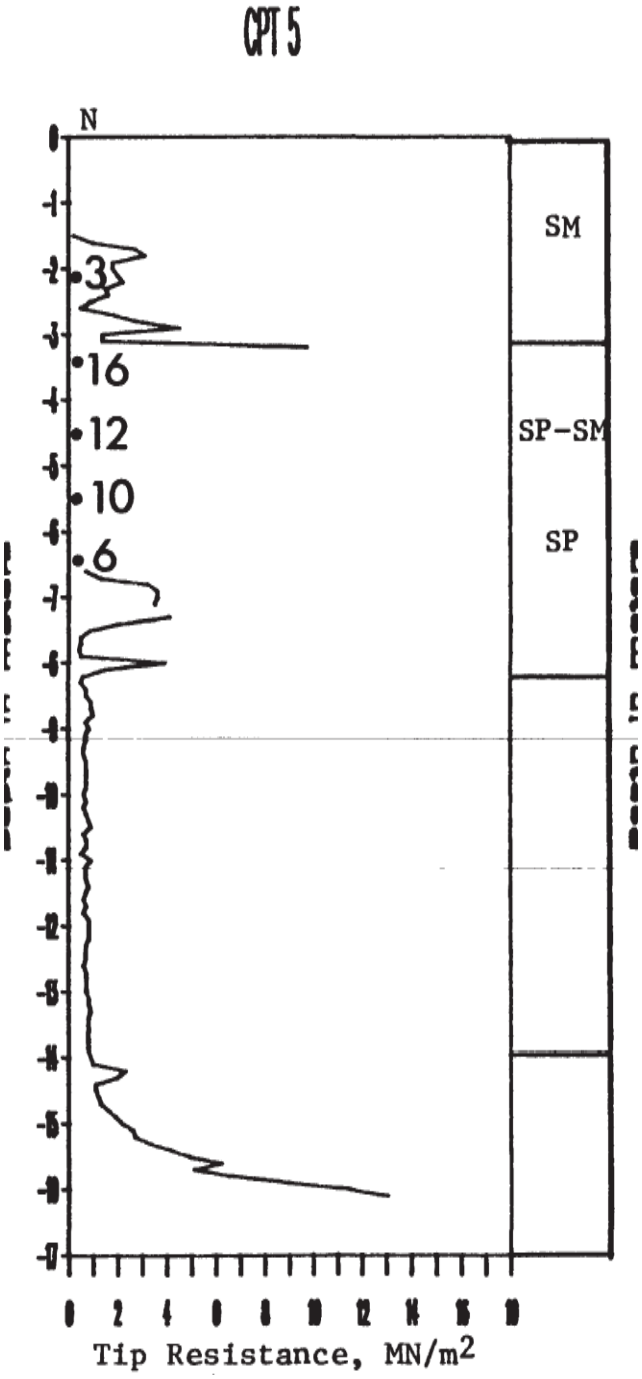

Main Inputs			PWP Model Inputs		
Dept (m)	Unit Weight (kN/m^3)	V_s (m/s)	α	β	ν
0.5	16.5	92.36	0.74	0.3	0.33
1	16.5	109.84	0.74		0.33
1.5	16.5	121.56	0.74		0.33
2	16.5	130.62	0.74		0.33
2.5	16.5	139.02	0.74		0.33
3	16.5	144.56	0.74		0.33
3.5	16.5	175.61	0.68		0.50
4	16.5	162.39	0.74		0.33
4.5	16.5	170.25	0.65		0.32
5	16.5	177.51	0.65		0.32
5.5	16.5	184.27	0.65		0.32
6	16.5	190.60	0.65		0.32
6.5	16.5	196.57	0.65		0.32
7	16.5	202.23	0.65		0.32
7.5	16.5	191.50	0.65		0.32
8	14	199.33	0.74		0.33
8.5	14	201.27	0.74		0.33
9	14	203.15	0.74		0.33
9.5	14	204.98	0.74		0.33
10	14	206.76	0.74		0.33
10.5	14	208.50	0.74		0.33
11	14	210.19	0.74		0.33
11.5	14	211.85	0.74		0.33
12	14	213.47	0.74		0.33

Figure 41. Tip resistance for C10 site by Bennett (1990)

Table 16. Main inputs for DEEPSOIL model of C15 site

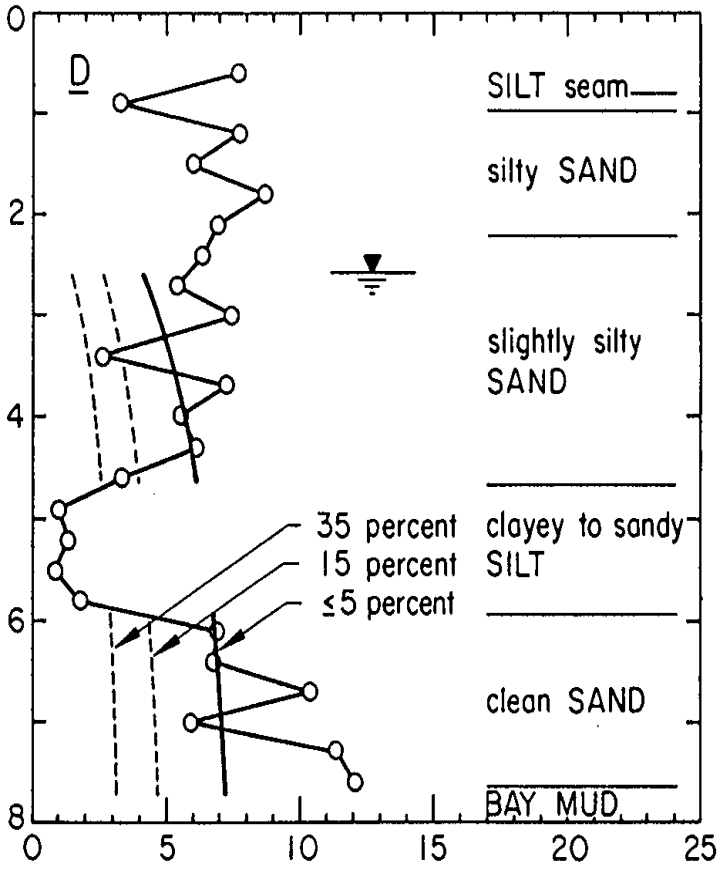

Main Inputs			PWP Model Inputs		
Dept (m)	Unit Weight (kN/m^3)	V_s (m/s)	α	β	ν
0.5	17	159.13	0.29		0.98
1	17	177.19	0.40		0.71
1.5	17	187.85	0.68		0.50
2	17	195.33	0.68		0.50
2.5	17	201.03	0.57		0.39
3	17	203.01	0.57		0.39
3.5	17	188.94	0.65		0.32
4	16.5	192.96	0.74		0.33
4.5	14	203.15	0.74	0.3	0.33
5	14	229.38	0.57		0.39
5.5	14	241.75	0.68		0.50
6	17	190.37	0.74		0.33
6.5	16.5	201.49	0.74		0.33
7	16.5	198.09	0.74		0.33
7.5	16.5	200.39	0.74		0.33
8	16.5	202.61	0.74		0.33
8.5	16.5	204.76	0.74		0.33

Figure 42. Tip resistance for C15 site by Bennett (1990)

Table 17. Comparison of the volumetric-induced settlements for different locations at the Marina District after the 1989 Loma Prieta Eartquake

Location	Depth to Water Table (m)	Measured Settlement (cm)	Calculated Settlement Using the Proposed Method (cm)	Calculated Settlement by Zhang et al. (cm)
M1	2.3	0-3.4	2.2	5.9
M2	2.7	0-3.4	1.1	1.9
M3	2.7	1.1	1.4	1.0
M4	2.4	9.6	8.7	11.2
M5	2.4	9.6	9.3	11.2
M6	5.5	0-1.6	0.8	2.3
C4	2.3	9.5	8.9	NA
C7	2.5	8.0	8.9	NA
C8	2.4	13.5	12.2	NA
C10	2.3	9.5	8.9	NA
C15	2.3	9.6	9.4	9.4

Zhang et al. (2008) showed that the settlements calculated by their CPT-based method for the Marina District are much closer to the measured values than those calculated using the SPT-based method suggested by O'Rourke et al. (1991), especially for the hydraulic fill zone where large

settlements occurred. The SPT-based method overestimated the settlements by up to a factor of two. Results presented in Table 17 show that the settlements calculated by the proposed method based on the incremental shear-volume coupling equation are closer to the measured values.

7.2. 1995 Kobe earthquake

Reclaimed islands were significantly damaged by extensive liquefaction after the 1995 Kobe earthquake. Port Island with an area of 436 hectares was constructed during the period from 1966 to 1980 by transporting soils from Suma, which mainly consisted of sands (around 55%) and gravels (40%) with some fines (around 5%) with an average relative density of 47%. This meant that the material used had high susceptibility for liquefaction. A soil profile at the site with a vertical array of V_s and SPT measurements was provided by Toki (1995) and used by Ishihara et al. (1996) to estimate the settlement using the SPT-based method proposed by Ishihara and Yoshimine (1992). Ishihara et al. based on field observations, estimated the total liquefaction-induced settlement to range from 30 to 60 cm. It should be noted that some amount of this measured settlement may be lateral spread-induced.

Later, Ziotopoilou and Boulanger (2015) used the same measurements to calculate the settlement using a modified version of the bounding surface plasticity constitutive model PM4Sand and arrived at an estimate of 41 cm, which was within the measured settlement range.

A DEEPSOIL profile was created to estimate the free-field settlement in the Port Island after the 1995 Kobe earthquake. A procedure similar to the Marina District case history was undertaken to calculate the D_r using Equation 17 and Equations 18 to 21 were used to calculate V_s when only SPT values were available. The porewater pressure parameters were chosen based on the relative density (Table 2). The input ground motion used for the model was the Kobe motion available on

DEEPSOIL database. The calculated settlement using the proposed method was 35 cm, which is within the measured range.

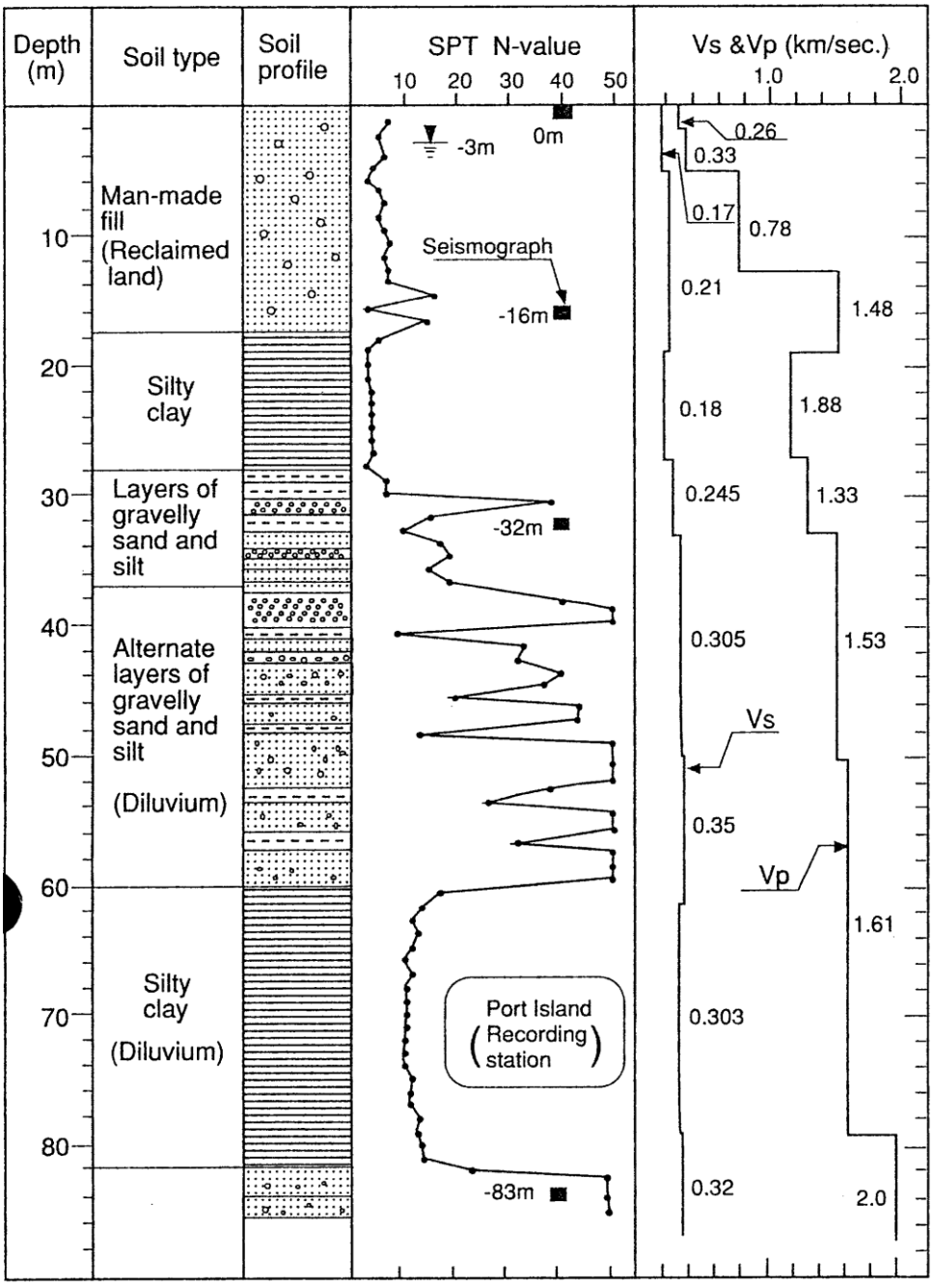

Figure 43. SPT measurements by Ishihara (1996)

Table 18. Main inputs for DEEPSOIL model of the Kobe site

Main Inputs			PWP Model Inputs		
Dept (m)	Unit Weight (kN/m^3)	V_s (m/s)	α	β	ν
2	16.5	170	0.65	0.3	0.32
4	16.5	170	0.65		0.32
6	16.5	210	0.65		0.32
8	16.5	210	0.65		0.32
10	16.5	210	0.65		0.32
12	16.5	210	0.65		0.32
14	16.5	210	0.68		0.50
16	16.5	210	0.68		0.50
18	16.5	210	0.65		0.32
20	14	180	0.65		0.32
22	14	180	0.65		0.32
24	14	180	0.65		0.32
26	14	180	0.65		0.32
28	17	245	0.65		0.32
30	17	245	0.29		0.98
32	17	245	0.74		0.33
34	17	305	0.40		0.71
36	17	305	0.40		0.71
38	17	305	0.29		0.98
40	17	305	0.74		0.33
42	17	305	0.29		0.98
44	17	305	0.29		0.98
46	17	305	0.29		0.98
48	17	305	0.29		0.98
50	17	350	0.29		0.98
52	17	350	0.29		0.98
54	17	350	0.29		0.98
56	17	350	0.29		0.98
58	17	350	0.29		0.98
60	17	350	0.68		0.50
62	14	303	0.68		0.50
64	14	303	0.68		0.50

66	14	303	0.68		0.50
68	14	303	0.68		0.50
70	14	303	0.68		0.50
72	14	303	0.68		0.50
74	14	303	0.68		0.50
76	14	303	0.68		0.50
78	14	320	0.68		0.50
80	14	320	0.68		0.50

7.3. 2011 Canterbury (Christchurch) earthquake

A series of earthquake sequences damaged the city of Christchurch in New Zealand in 2010 and 2011. The main causes of the devastating damage were from many contributing factors, including liquefaction-induced settlement. The city of Christchurch is located on the predominantly low-lying and low-gradient coastal portion of the Waimakariri River flood plain, constructed of sediments from various sources including the Waimakariri River, the Canterbury continental shelf and other sediments deposited through coastal processes. The area was characterized as marshy, poorly draining land. To make the land habitable, land drainage was improved during the mid-1870s. Due to the existence of a dense network of strong motion stations, detailed subsurface investigations, and documentation of liquefaction induced settlements, these earthquakes added numerous well-documented case histories to the available database. GEER reports classified the ejected material as silty sands and fine sands. Many of the case histories were recorded in the areas occupied by structures and buildings within the city. A series of 6 high-quality case histories from the 2011 earthquake with SPT and CPT measurements and laboratory index tests were presented by Bastani. The locations of these measurements are presented in Figure 44. Five of these case histories were located within central business district, while the sixth site was located in the Ferrymead area. At least four CPT tests and one or two SPT tests were performed at each site.

Bastani used several SPT and CPT-based methods to estimate the liquefaction induced settlement at these sites.

A DEEPSOIL profile was created to estimate the liquefaction induced settlement in each of these sites according to the available CPT and SPT measurements. The procedures used to determine the input parameters and create the profile were similar to the previous examples presented in this paper. Table 25 compares the results from the proposed method, measured settlements and estimates made by different methods from Bastani. The settlements calculated using the proposed method are in good agreement with the range of measurements at each of the sites.

Figure 44. Location of CPT logs based on Bastani (2012)

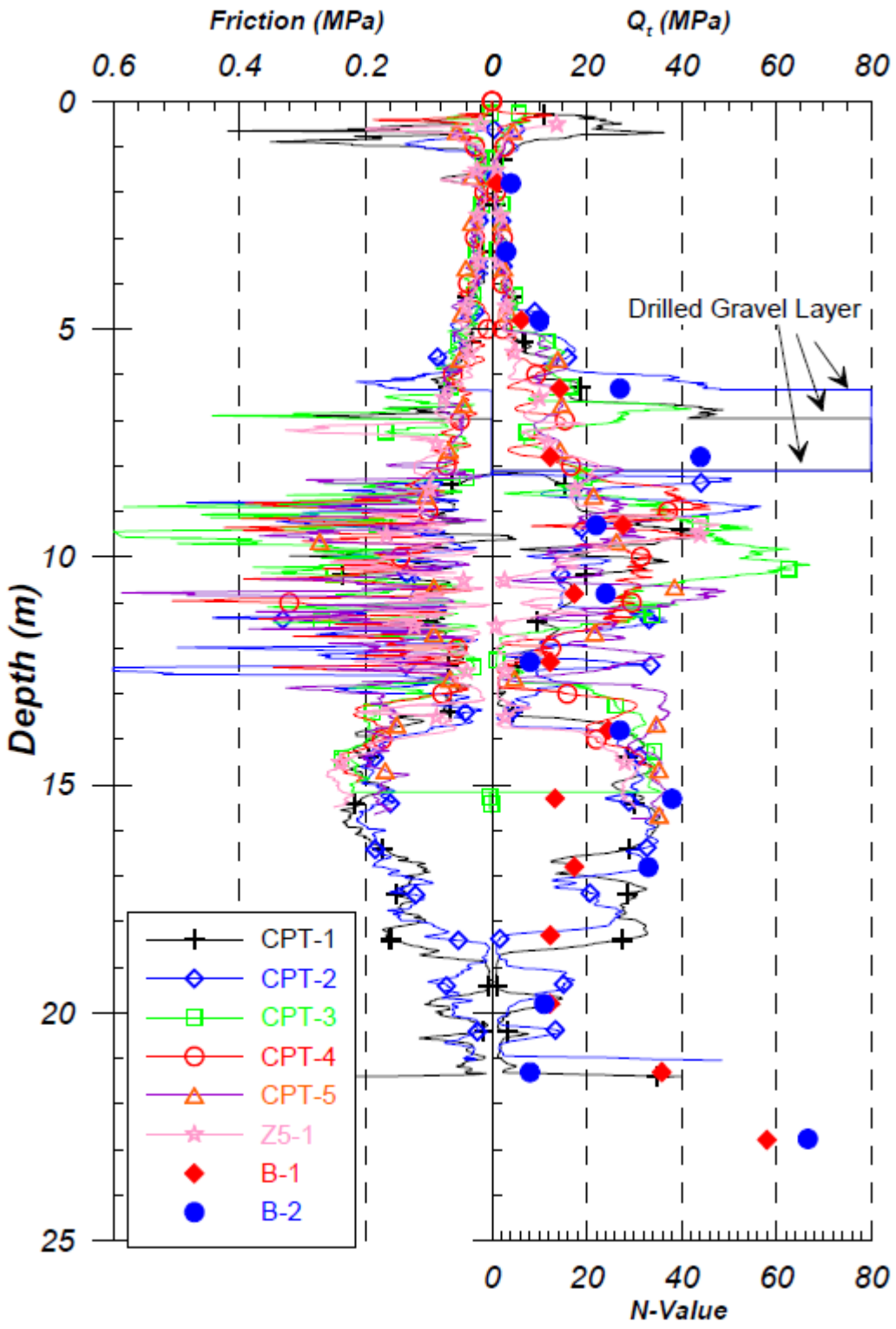

Figure 45. CPT measurements for Site 1 by Bastani (2012)

Table 19. Main inputs for DEEPSOIL model of Site 1

Main Inputs			PWP Model Inputs		
Dept (m)	Unit Weight (kN/m^3)	V_s (m/s)	α	B	ν
2	17	118.31	0.74	0.3	0.33
3.5	17	140.70	0.74		0.33
5	17	173.59	0.57		0.39
6.5	17	224.56	0.29		0.98
8	17	260.78	0.29		0.98
9.5	17	231.35	0.36		1.60
11	17	241.38	0.36		1.60
12.5	17	200.96	0.65		0.32
14	17	258.39	0.29		0.98
15.5	17	274.77	0.29		0.98
17	17	272.63	0.29		0.98
20	17	224.58	0.57		0.39
21.5	17	215.82	0.65		0.32
23	17	273.41	0.29		0.98

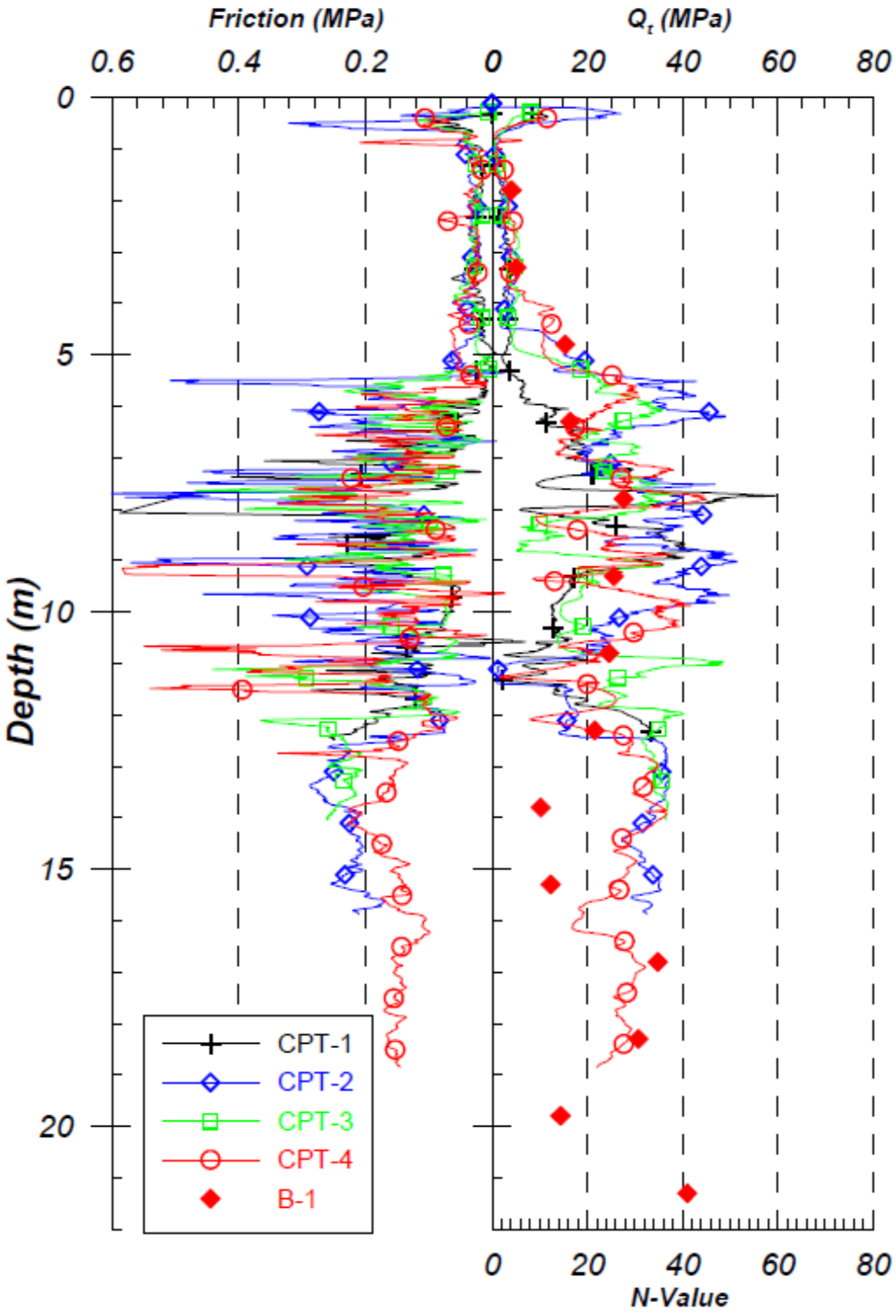

Figure 46. CPT measurements for Site 2 by Bastani (2012)

Table 20. Main inputs for DEEPSOIL model of Site 2

Main Inputs			PWP Model Inputs		
Dept (m)	Unit Weight (kN/m^3)	V_s (m/s)	α	β	ν
2	17	118.31	0.74	0.3	0.33
3.5	17	140.70	0.74		0.33
5.5	17	186.15	0.68		0.50
7.5	17	204.57	0.68		0.50
9	17	237.44	0.36		1.60
11	17	236.99	0.36		1.60
12.5	17	241.38	0.36		1.60
14	17	237.62	0.40		0.71
15.5	17	211.79	0.57		0.39
17	17	215.00	0.57		0.39
19	17	274.19	0.29		0.98
20.5	17	269.63	0.29		0.98
22.5	17	237.13	0.68		0.50
24	17	292.55	0.29		0.98

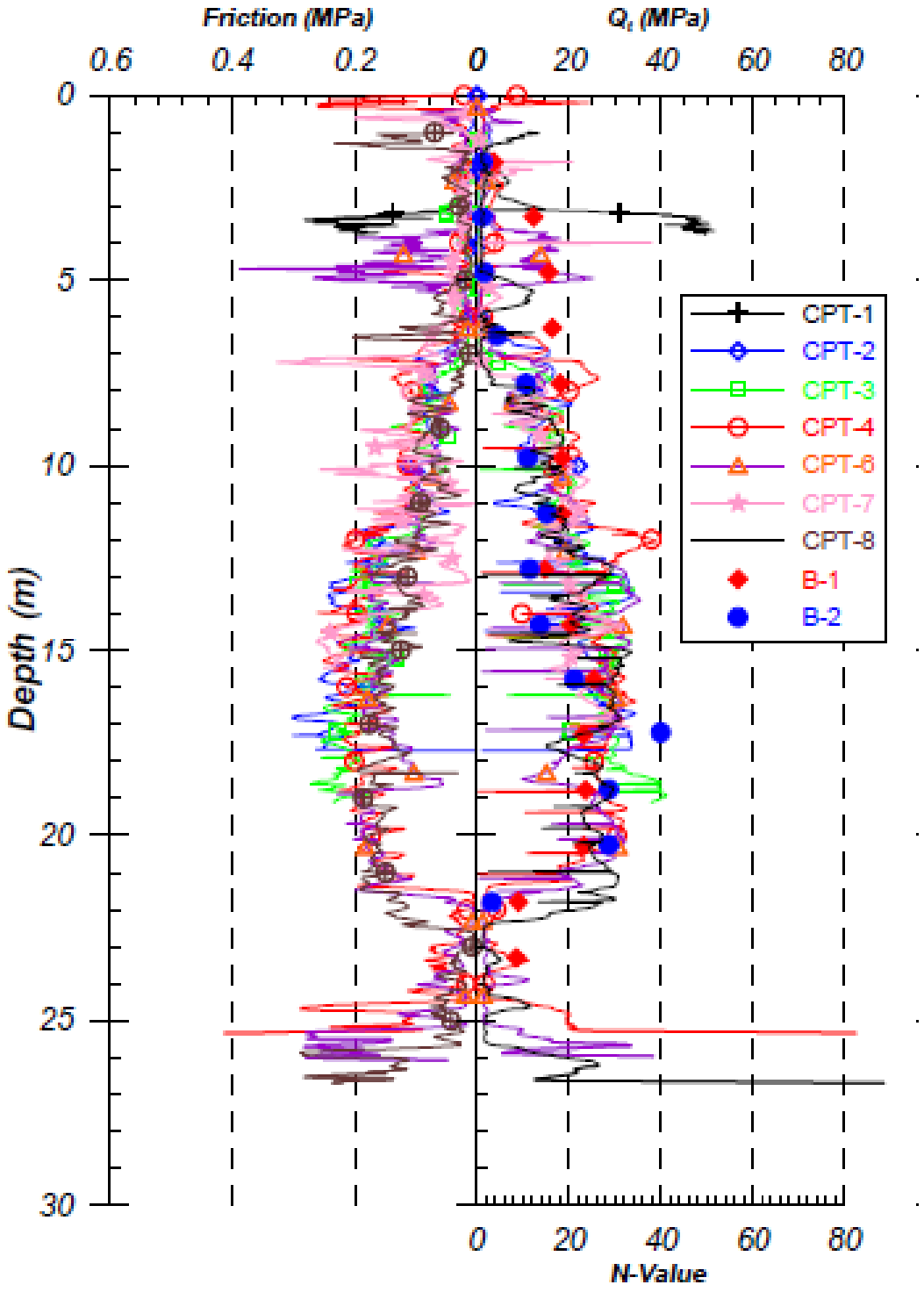

Figure 47. CPT measurements for Site 3 by Bastani (2012)

Table 21. Main inputs for DEEPSOIL model of Site 3

Main Inputs			PWP Model Inputs		
Dept (m)	Unit Weight (kN/m^3)	V_s (m/s)	α	β	ν
1.5	17	115.72	0.74	0.3	0.33
3	17	137.62	0.74		0.33
5.5	17	152.30	0.74		0.33
6.5	17	192.38	0.57		0.39
8	17	203.42	0.57		0.39
9.5	17	218.24	0.68		0.50
10.5	17	211.33	0.57		0.39
12	17	226.10	0.68		0.50
13.5	17	247.57	0.29		0.98
14.2	17	277.60	0.29		0.98
15.5	17	266.04	0.29		0.98
17	17	269.63	0.29		0.98
18.2	17	200.79	0.74		0.33
24	17	292.55	0.29		0.98

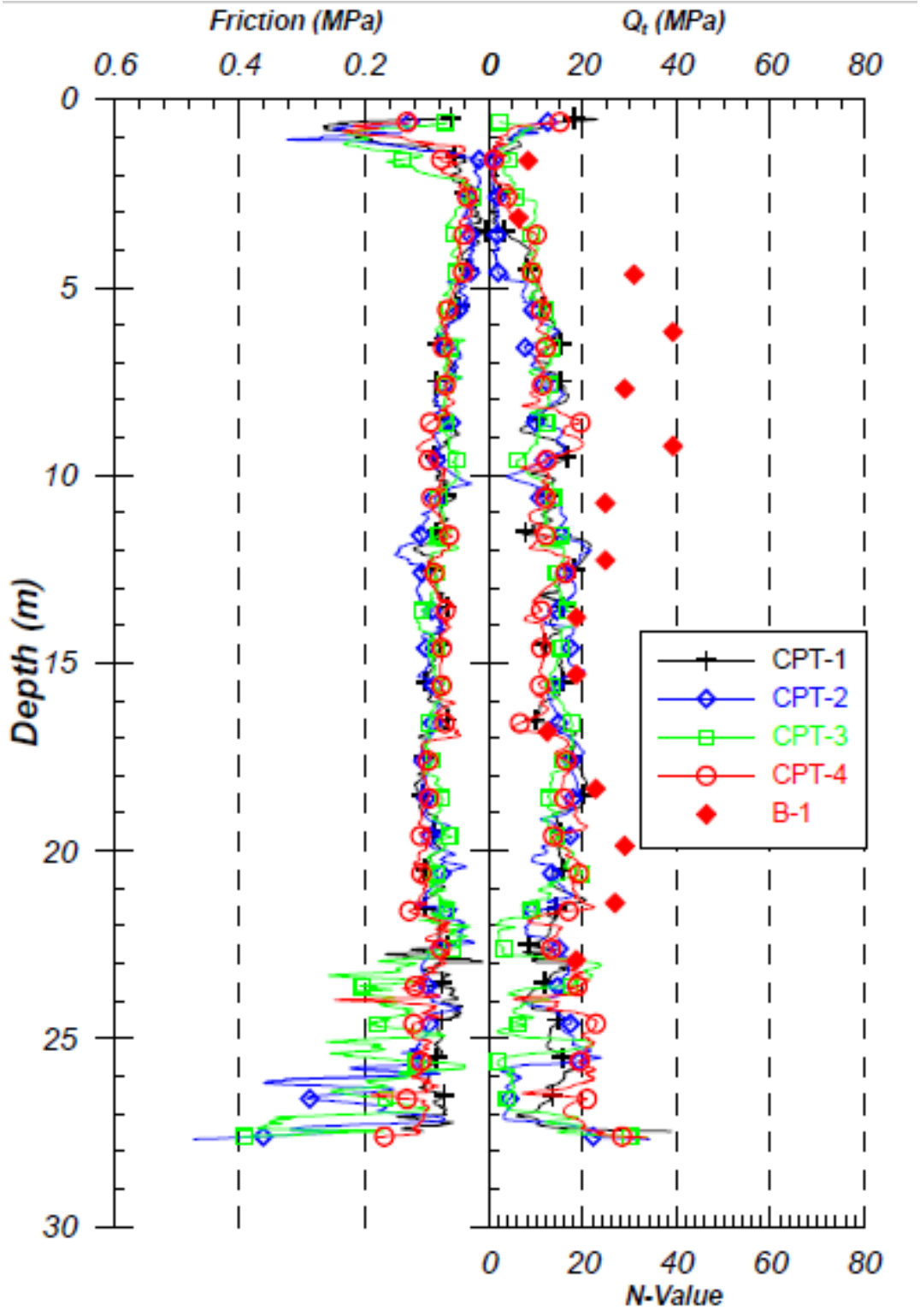

Figure 48. CPT measurements for Site 4 by Bastani (2012)

Table 22. Main inputs for DEEPSOIL model of Site 4

Main Inputs			PWP Model Inputs		
Dept (m)	Unit Weight (kN/m^3)	V_s (m/s)	α	β	ν
2	17	179.85	0.65	0.3	0.32
4	17	270.63	0.29		0.98
6	17	299.51	0.29		0.98
8	17	321.84	0.29		0.98
10	17	328.59	0.36		1.60
12	17	316.70	0.68		0.50
14	17	312.93	0.68		0.50
16	17	372.33	0.36		1.60
18	17	383.46	0.36		1.60
20	17	367.58	0.68		0.50
22	17	376.44	0.68		0.50
24	17	384.72	0.68		0.50

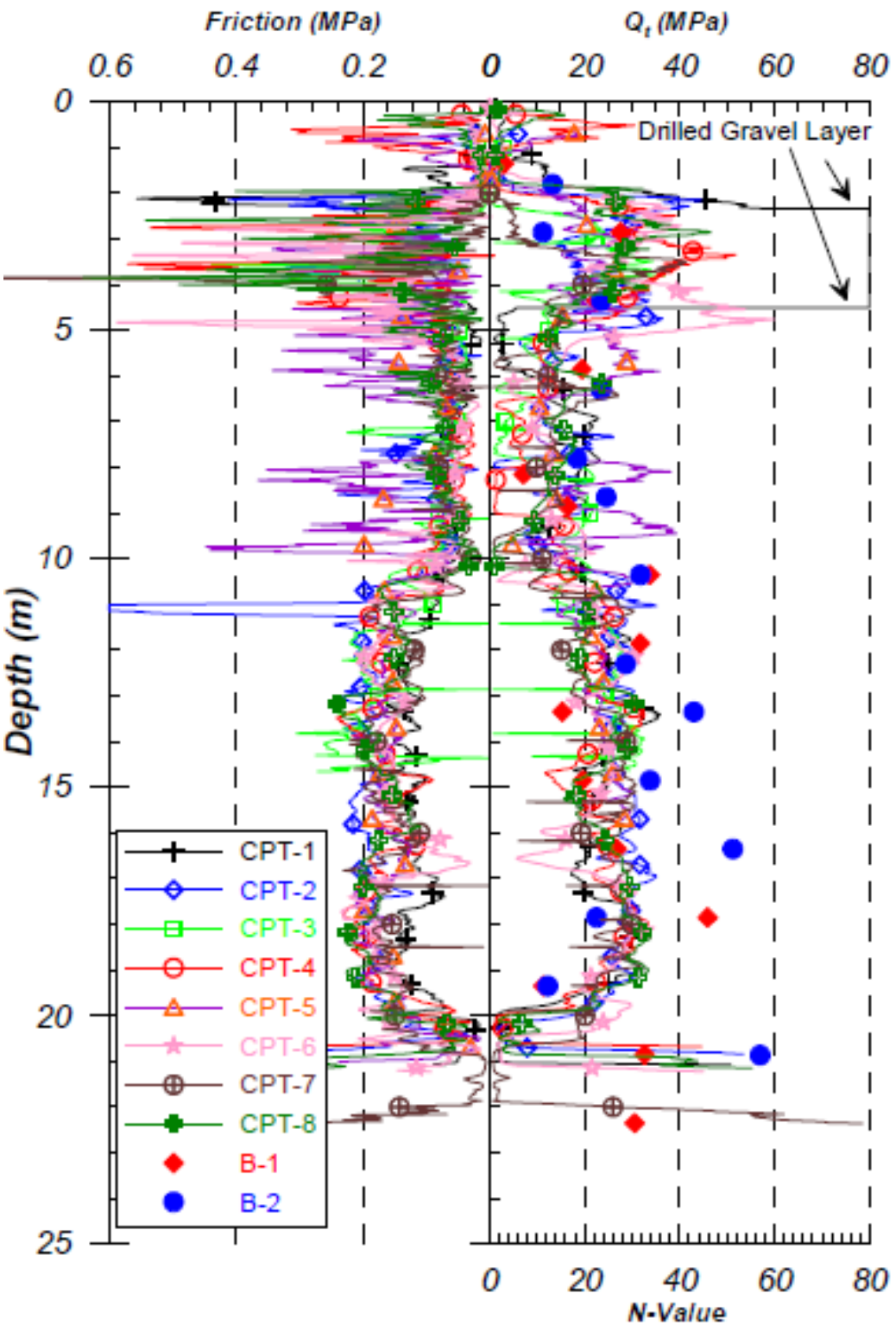

Figure 49. CPT measurements for Site 5 by Bastani (2012)

Table 23. Main inputs for DEEPSOIL model of Site 5

Main Inputs			PWP Model Inputs		
Dept (m)	Unit Weight (kN/m^3)	V_s (m/s)	α	β	ν
2	17	179.85	0.65	0.3	0.32
4	17	270.63	0.29		0.98
6	17	299.51	0.29		0.98
8	17	321.84	0.29		0.98
10	17	328.59	0.36		1.60
12	17	316.70	0.68		0.50
14	17	312.93	0.68		0.50
16	17	372.33	0.36		1.60
18	17	383.46	0.36		1.60
20	17	367.58	0.68		0.50
22	17	376.44	0.68		0.50
24	17	384.72	0.68		0.50

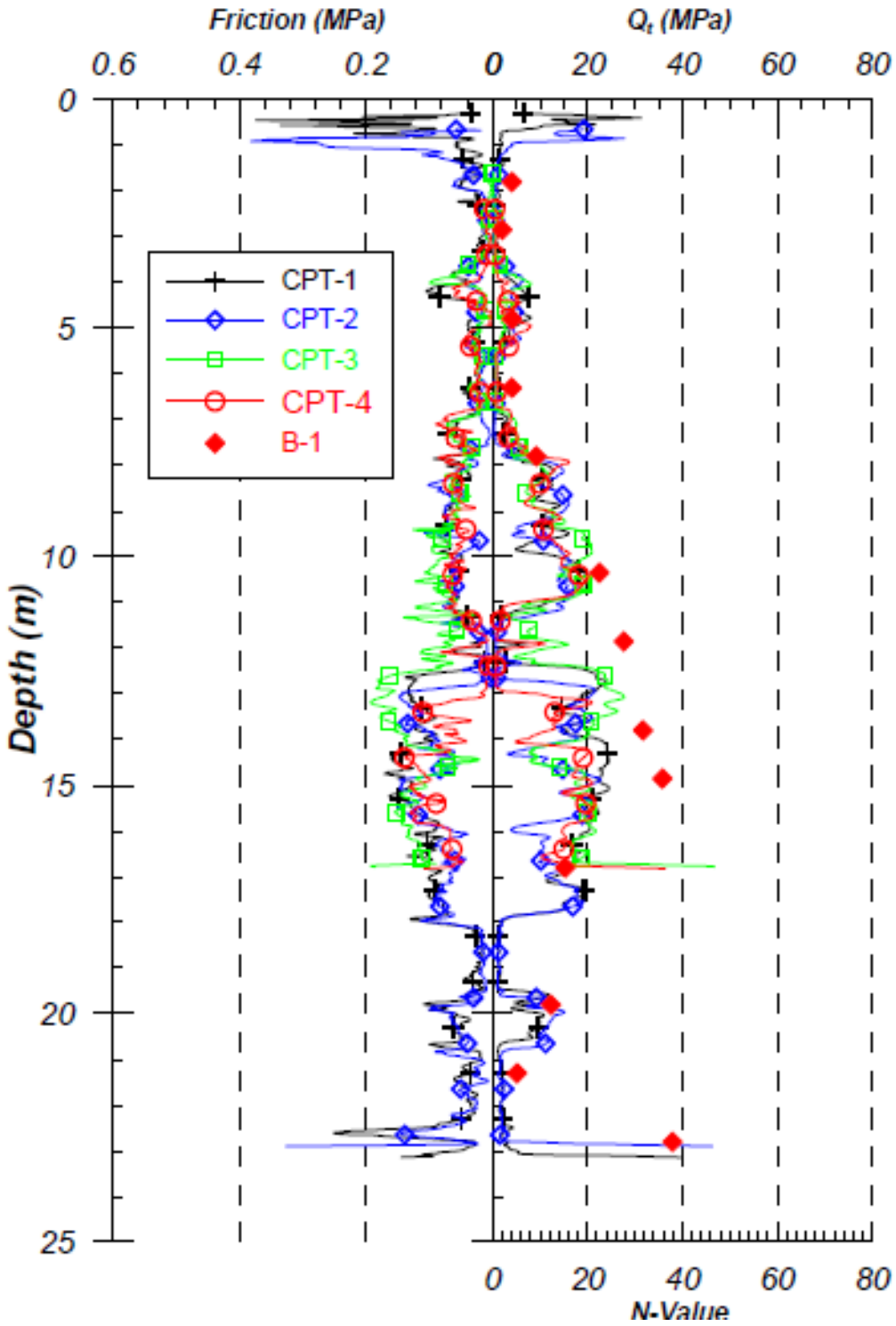

Figure 50. CPT measurements for Site 6 by Bastani (2012)

Table 24. Main inputs for DEEPSOIL model of Site 6

Main Inputs			PWP Model Inputs		
Dept (m)	Unit Weight (kN/m^3)	V_s (m/s)	α	β	ν
2	17	167.32	0.74	0.3	0.33
4	17	194.62	0.74		0.33
6	17	215.38	0.74		0.33
8	17	272.07	0.57		0.39
10	17	323.45	0.36		1.60
12	17	349.01	0.29		0.98
14	17	374.85	0.29		0.98
16	17	360.76	0.36		1.60
18	17	346.47	0.68		0.50
20	17	342.11	0.57		0.39
22	17	327.53	0.65		0.32
24	17	448.28	0.29		0.98

Table 25. Comparison of the volumetric-induced settlements for different locations after the 2011 Christchurch Earthquake

Location	Measured Settlement (cm)	Calculated Settlement Using the Proposed Method (cm)	Calculated Average Settlement Using the Zhang et al. Method (cm)	Calculated Average Settlement Using the Youd and Idriss Method (cm)
Site 1	10-20	13.5	12.6	23.1
Site 2	10-30	13.9	11.6	21.5
Site 3	0-20	11.2	8.1	49.7
Site 4	Unavailable	33.4	40.7	80
Site 5	20-30	3.1	7.8	4.3
Site 6	0-20	11.9	11.3	40

Chapter 8: Sensitivity Analyses

A series of simple profiles consisted of 3 layers and total thickness of 20 meters were created to analyze the effect of different parameters on the free-field settlement. Different soil conditions and ground motions were investigated. The studied soil conditions, were inspired by Bray and Macedo's 3-layered profile (20 meters in total) created to inspect the liquefaction-induced building settlement. The soil profile conditions are presented in Table 26. The top crust layer, which is above the water table, is a non-liquefiable with thickness (H_C) varying from 1 to 6 meters. The middle saturated liquefiable layer with relative density (D_r) ranging from 35% to 75%, has the thickness changing from 1 to 18 meters (H_L). The bottom layer consists of saturated soil with relative density of 90%. In total, 66 different 20-meter profiles were created. In many soil response studies, the maximum frequency of interest for shear waves is about 15 Hz. For the 20-meter profile under consideration the range for the shear wave velocity is $V_{S,\,min} \approx 113$ m/s and $V_{S,\,max} \approx 307$ m/s. We can calculate average wave length of propagating S-waves as:

$$V_{s,avg} = 210\ \frac{m}{s} \qquad \text{Equation 23.}$$

$$V_s = fL \ \rightarrow\ L = 14\ m \qquad \text{Equation 24.}$$

The sublayer thickness to transmit the 14-meters wave length can be calculated as:

$$L_{effective} = \frac{L}{5} = 2.8\ m \qquad \text{Equation 25.}$$

It should be noted that after liquefaction, the liquefiable soil layer losses strength and therefore, lower sublayer thickness is needed. The sublayer thickness used in the DEEPSOIL analyses described in Chapter 6 (0.5 m and 0.25 m) are much smaller than the limit (Equation 25). This means that a much higher frequencies can be transmitted through the 20-meter soil profile.

Table 26. Variation of different parameters for the proposed 3-layer soil profile

Parameter	Description	Values
H_C	Thickness of the unsaturated non-liquefiable crust layer, D_r = 90% (m)	1, 2, 4, 6
H_L	Thickness of the saturated liquefiable middle layer (m)	1, 2, 3, 6, 12, 18
H_B	Thickness of the saturated non-liquefiable bottom layer, D_r = 90%	20 - (HC + HL)
D_r	Relative density of the liquefiable middle layer (%)	35, 55, 75

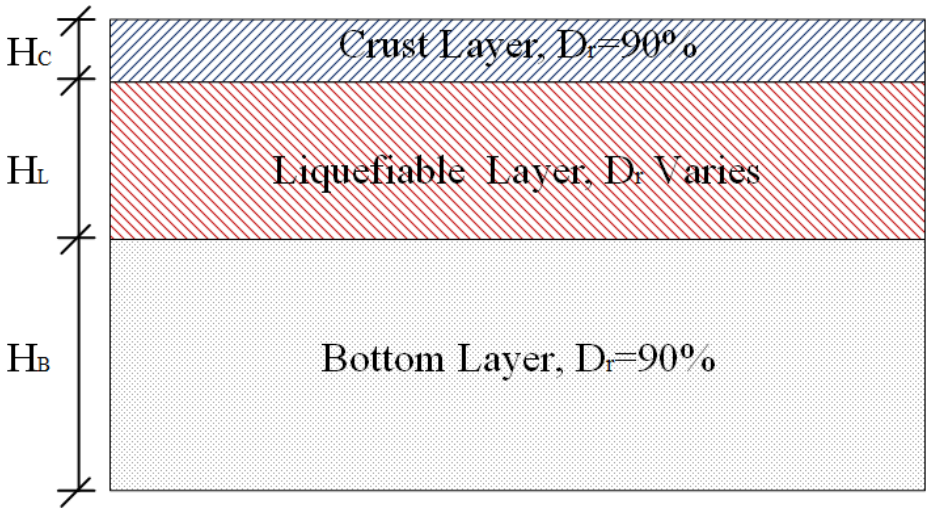

Figure 51. The proposed 3-layer soil profile

In order to obtain the shear strain history in the layered profiles, effective stress-based response analyses were conducted using DEEPSOIL. To get more realistic results and capture the layered soil response from propagating waves with higher frequencies, the main layers were divided into sublayers; the top and bottom layers were divided into sublayers with thickness of 50 centimeters and the middle liquefiable layer was divided into sublayers with thickness of 25 centimeters. For each sublayer, different inputs were needed to model the DEEPSOIL soil profile. It can be verified that the sublayers would be able to model high-frequency waves.

In order to determine the inputs, different equations from Seed and Idriss (1970) (Equations 15-18) Saturated unit weight of the soil was assumed between 18.8 (kN/m^3) and 21.8 (kN/m^3) depending on the relative density. The input values for this model were obtained from the values suggested in Table 2, based on the relative density of the soil sublayer calibrated to Boulanger and Idriss $P_L = 15\%$ curve. The effective-stress based analyses conducted using DEEPSOIL allows for a realistic modeling of the softening of the shear stiffness of the liquefiable layers during earthquake shaking.

8.1. Earthquake Ground Motion Database

Seismic response and dynamic behavior of layered ground, including liquefaction and volumetric-induced settlement, are heavily affected by different characteristics of ground motions. Bray and Macedo used an original list of 12 ground motions from shallow crustal earthquakes along active plate margins, plus a suite of 24 additional earthquake ground motions to explore the influence of wider range of ground motions on the liquefaction-induced foundation settlement. Most of those 36 time histories were modified by an amplitude scaling factor to study the influence of

liquefaction. For this study, the unscaled versions of the original and additional earthquakes from Bray and Macedo's work have been selected to study the effect of different ground-motion parameters on the earthquake-induced free-field settlement, which were also included in Carlton's original ground motion database (2014). The amplitude of these earthquakes were not scaled in order to examine cases with and without liquefaction. The list of these ground motion time histories is presented in Table 27.

Table 27. List of ground motions used for the nonlinear effective stress-based response analysis

Number	Earthquake	NGA #	M_w	PGA (g)
1	Montenegro	4455	7.1	0.255
2	Darfield	6928	7	0.356
3	Northridge	957	6.7	0.159
4	Kobe	1111	6.9	0.479
5	Imperial Valley	164	6.5	0.168
6	Hector Mine	1787	7.1	0.328
7	Denali	2111	7.9	0.581
8	Cape Mendecino	830	7	0.229
9	Northridge	952	6.7	0.621
10	Chi-Chi	1512	7.6	0.447
11	Cape Mendecino	3750	7	0.261
12	Morgan Hill	448	6.2	0.423

Number	Earthquake	NGA #	M_w	PGA (g)
13	Northridge	1012	6.7	0.263
14	Kocaeli	1162	7.5	0.137
15	Victoria	265	6.3	0.633
16	Loma Prieta	753	6.9	0.645
17	Whittier Narrows	690	6	0.262
18	Duzce	1612	7.1	0.152
19	Chi-Chi	2622	6.2	0.382
20	Parkfield	33	6.2	0.357
21	Tottori	3943	6.6	0.274
22	Parkfield	4132	6	0.367
23	Montenegro	4457	7.1	0.228
24	L'Aquila	4477	6.3	0.149
25	Northridge	1078	6.7	0.285
26	Friuli	125	6.5	0.357
27	Duzce	1618	7.1	0.16
28	New Zealand -02	587	6.6	0.241

8.2. Results and regression analysis

8.2.1. Settlement Trends

The response shear strain histories obtained by DEEPSOIL were used to calculate the total volumetric strain in layered soil profiles. The vertical volumetric strain (ε_{vi}) was calculated for

each sublayer based on their shear strain history and then was integrated with depth to compute the total free-field settlement ($D_{Surface}$). For a profile with n sublayers, it can be calculated as:

$$D_{Surface} = \sum_{i=1}^{n} h_i \,.\, \epsilon_{vi} \qquad \text{Equation 26.}$$

where h_i is the thickness of each sublayer. A MATLAB code was developed to estimate the surface settlement based on the volumetric strain histories of sublayers. The total number of the calculated free-field settlements was 1848.

This database of settlements enables the investigation of the the effect of different ground parameters. Figure 52 indicates the trends for free-field settlement versus the thickness of the liquefiable soil layer for ground motion records 1-10. The trends shows that the earthquake-induced free-field settlement increases as the liquefiable soil layer's thickness increases. This is in agreement with the expectations and similar to the ones observed by Macedo and Bray.

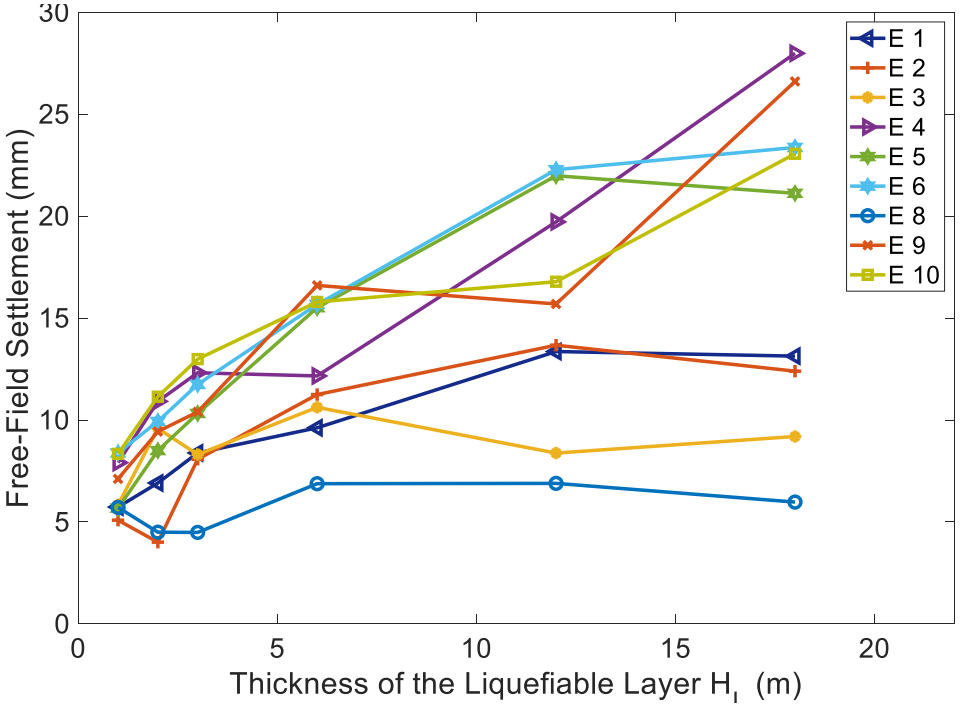

Figure 52. Free-field Settlement (%) versus thickness of the liquefiable layer (H_L) for earthquakes 1-10, $H_C = 2$ and $D_r = 35\%$

In Figure 53, the curves of free-field settlement versus the relative density of the liquefiable layer are demonstrated for ground motion records 1-10. The trend shows that the earthquake-induced free-field settlement decreases as the liquefiable soil layer's relative density increases, which is similar to our anticipations. Macedo and Bray also described similar trends.

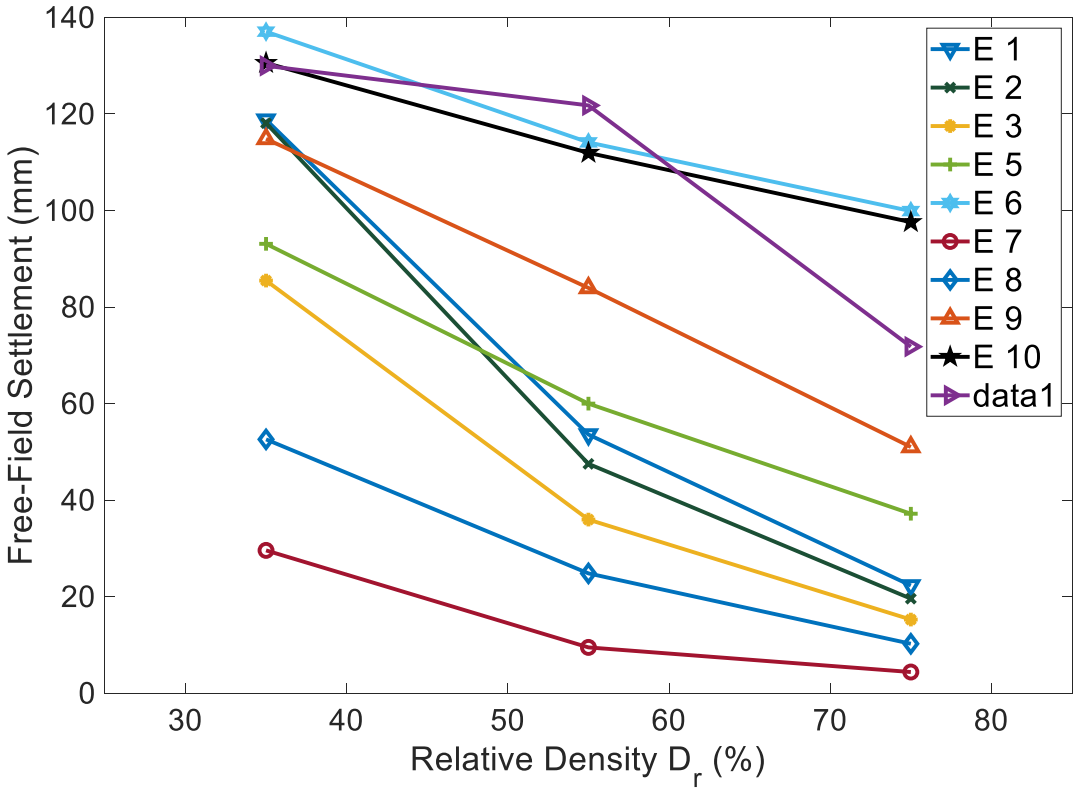

Figure 53. Free-field Settlement (%) versus relative density (D_r) of the liquefiable layer earthquakes 1-10, $H_C = 4$ and $H_L = 6$

Unlike the liquefiable layer, it can be observed that the effect of the thickness of the crust soil layer is minimal on the free-field settlement. Figure 54 shows that for ground motion records 1-10,

earthquake-induced free-field settlement is not showing any particular trends as the H_C increases. Macedo and Bray also reported a similar trend.

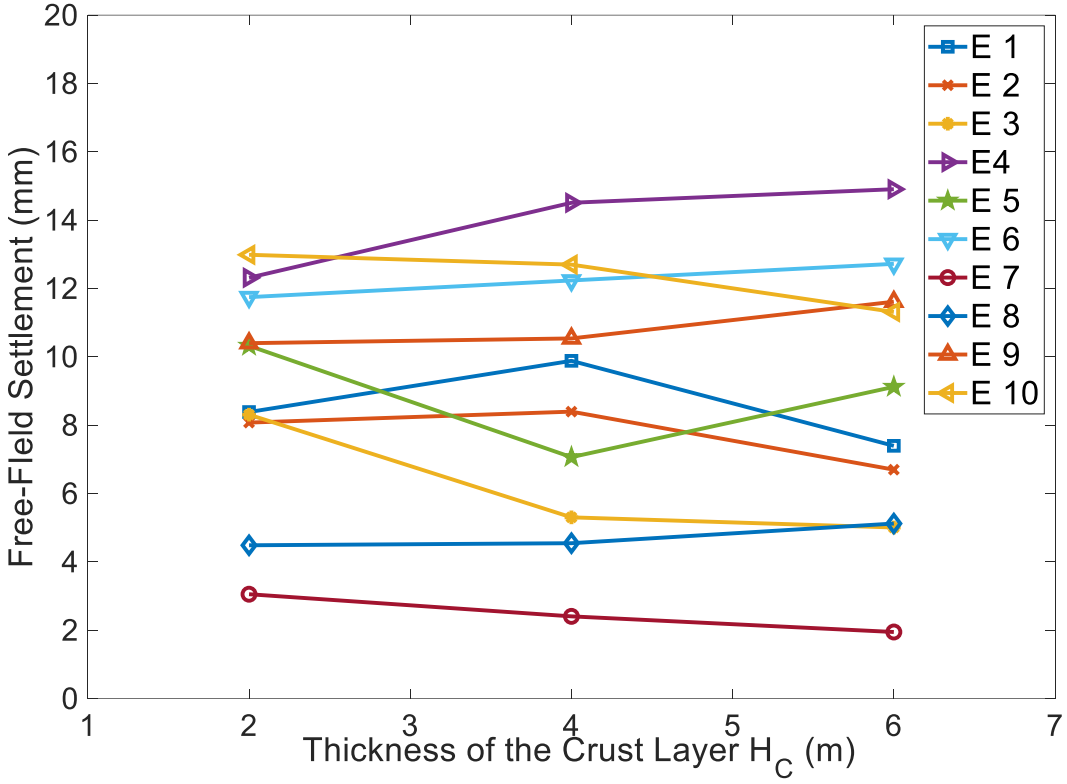

Figure 54. Free-field Settlement (%) versus thickness of the crust layer (H_C) for layer earthquakes 1-10, $H_L = 3$ and $D_r = 35\%$

8.2.2. Selection of variables

In order to propose an equation to estimate the earthquake-induced free-field settlement, a series of variables describing the soil profile or the earthquake ground motion were investigated. These variables were chosen based on the work of Dashti and Karimi and Bray and Macedo. The ground and soil parameters chosen to be studied were H_C, H_L, H_B and D_r . These parameters were also employed by both Bray and Macedo and Dashti and Karimi as a part of their efforts to evaluate

liquefaction-induced foundation settlement. In order to reflect the effect of ground motion on the free-field settlement, different ground motion intensity measures were considered. The ground motion parameters studied were also chosen based on the abovementioned studies. Those intensity parameters were PGA, PGV, CAV, CAVdp, Sa_1, T_m, I_a, $D_{5\text{-}95}$ and M_W. It is important to mention that the parameters were calculated for the outcrop rock, not the free-field ground surface.

Regression analyses were conducted using the analytical results and the selected ground motion parameters. The final equation is presented in form of a function (Equation 27) of those selected parameters:

$$\ln(D_v) = 2.75 - 4.92 * \ln(D_r) + 0.87 * \ln(H_L) + 0.81 * \ln(I_a) + 0.48 * \ln(T_m) \\ -0.33 * (\ln(T_m))^2 + 2.33 * (\ln(D_r))^2 + 0.47 * \ln(D_r) * \ln(T_m) \\ +0.28 * \ln(H_L) * \ln(T_m) + e$$

Equation 27.

where D_r (%) and H_L (m) the relative density and the thickness of the liquefiable layer (ground parameters), T_m (s) is the mean period and I_a (m/s) is the Arias Intensity (ground motion intensity variables), D_v is the volumetric-induced free-field settlement (in mm). This equation can be rewritten in terms of CPT measurements ($(q_{c1N})_{cs}$) as:

$$\ln(D_v) = 2.75 - 4.92 * \ln\left(0.405^{\sqrt[3.788]{\frac{(qc1N)cs}{0.9}}} - 1.063\right) + 0.87 * \ln(H_L) + 0.81 * \ln(I_a) \\ +0.48 * \ln(T_m) - 0.33 * (\ln(T_m))^2 + 2.33 * \left(\ln\left(0.405^{\sqrt[3.788]{\frac{(qc1N)cs}{0.9}}} - 1.063\right)\right)^2 \\ +0.47 * \ln\left(0.405^{\sqrt[3.788]{\frac{(qc1N)cs}{0.9}}} - 1.063\right) * \ln(T_m) + 0.28 * \ln(H_L) * \ln(T_m) + e$$

Equation 28.

The comparison of the settlement values estimated by the suggested equation and the method proposed by Zhang et al (2008) is shown in figures 55 and 56. It can be seen that in most cases,

the Zhang et al method tends to calculate larger settlements in comparison to both the proposed equation and the Incremental Volumetric Strain model.

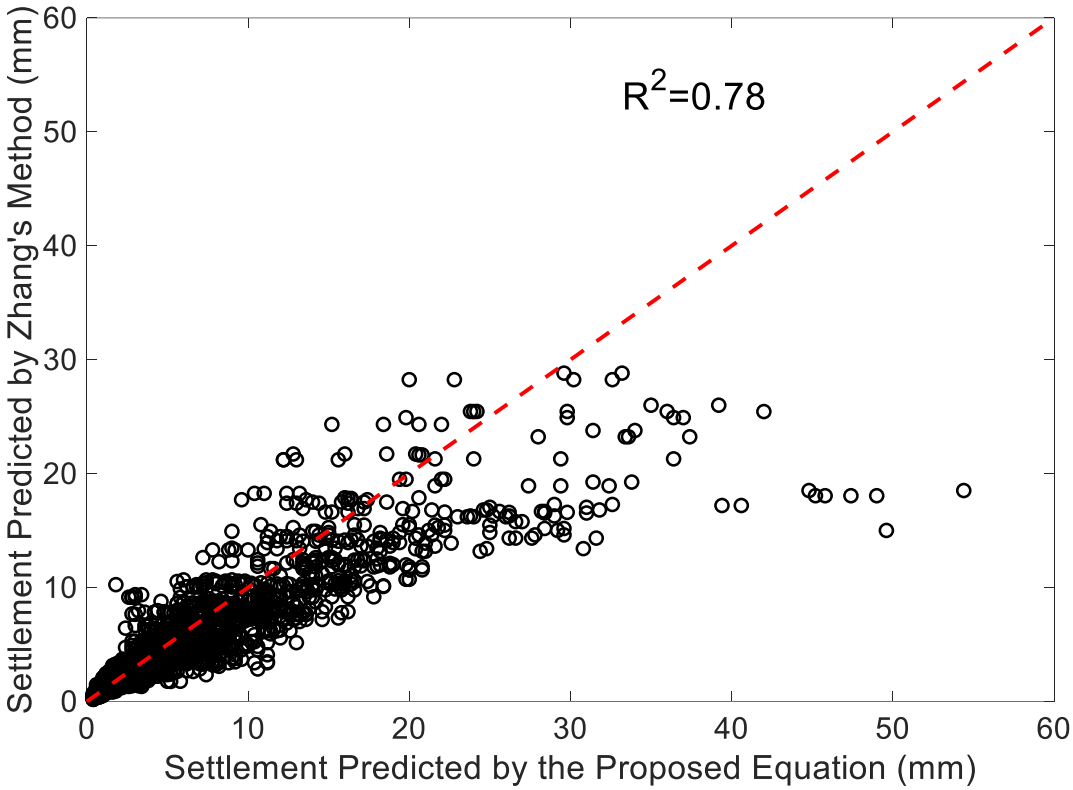

Figure 55. Comparison of earthquake-induced free-field settlement estimated using Equation 6 and calculated with the method proposed by Zhang et al. (2008)

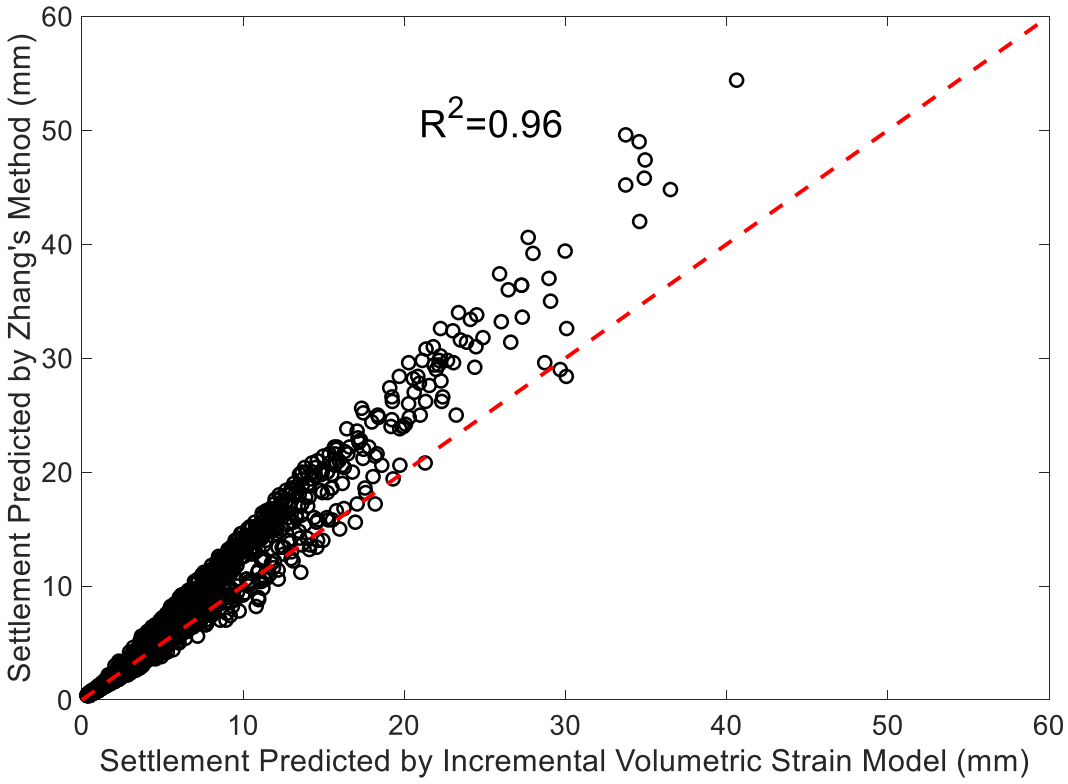

Figure 56. Comparison of earthquake-induced free-field settlement predicted by the Incremental Volumetric Strain model and calculated with the method proposed by Zhang et al. (2008)

It should be noted that since the proposed equation has been developed according to certain conditions, applicability when using this equation should be cognizant of the range of the variables. First of all, it should be mentioned that the settlement calculations were based on a 3-layer 20-meter-thick soil profile consisting of a surface crust layer, liquefiable middle layer and a dense bottom layer. Additional limits are shown in Table 28.

Table 28. Limiting values for the parameters of the proposed equation

Parameter	Minimum	Maximum
H_C (m)	1	6
H_L (m)	1	18
H_B (m)	0	18
D_r (%)	35	90
I_a (m/s)	0.07	5.79
T_m (s)	0.18	0.74

Chapter 9: Evaluation of the proposed equation by case histories

Among the earthquake-induced settlement measurements made at different sites, some have well-documented SPT or CPT records that can be used to calculate the volumetric strain. In order to evaluate the predictability of the equation proposed in this study, two case histories with high quality measurements and soil profiles that could be simplified into 3 main layers were chosen. The ground motions were chosen based on the nearest rock outcrop acceleration records to the sites.

In order to use the suggested equation to estimate the free-field settlement, the profiles were simplified according to the relative densities assessed based on the CPT or SPT measurements and the ground parameters used in the Equation 24 (D_r and H_L) were estimated accordingly. The ground motion intensity parameters (T_m and I_a) were calculated according to the strongest

horizontal acceleration time histories. It should be noted that even though the proposed equation was developed for cases with or without liquefaction, in all the case histories studied, liquefaction occurred at least in a partial manner.

9.1. 1989 Loma Prieta earthquake

USGS carried out a comprehensive inspection program after the 1989 Loma Prieta earthquake to evaluate the damages to the Marina District in the northern part of San Francisco. This investigation program included in-situ subsurface site investigations such as CPT and SPT tests. Severe damages were recorded in both artificial and natural sand deposits due to liquefaction and amplification of ground motion. Among the locations of these measurements, some indicated profiles that could be simplified to 3-layer soil deposits, suitable for evaluation of the proposed equation. Points M2 and M3 points were located within the arear where the top 8 meters of the soil deposit consisted of natural beach sand sitting on top of the bay mud. C4, C8, C10, and C15 points were located closer to the area where the top layer of the profile was mostly consisted of hydraulically filled sand and silty sand on top of the bay mud. Point M6 was located within the section which mostly consisted of dune sands. The simplified soil profiles and ground motion parameters used to evaluate the equation are presented in Table 28. For these locations, the ground motion used was RSN #765 from the NGA West 2 database with I_a = 1.69 m/s and T_m = 0.39 s.

The measured free-field volumetric-induced ground settlements and the values estimated using the proposed equation are presented in Table 29. The comparison shows a good agreement between these values. For further evaluation, the values estimated by Zhang et al. (2008) are also presented in this table.

Table 29. Simplified profiles for different locations in the Marina District

Location	H_C (m)	H_L (m)	H_B (m)	D_r (%)
M2	8	2	2	66
M3	6	1	5	72
M6	6	4	2	79
C4	1	7	0	51
C8	2	10	0	54
C10	0	16	2	55
C15	2	5	5	53

Table 30. Comparison of the volumetric-induced settlements for different locations at the Marina District after the 1989 Loma Prieta Eartquake

Location	Measured Settlement (cm)	Prediction by Zhang et al. Method (cm)	Prediction by the Proposed Equation (cm)
M2	0-3.4	1.9	3.2

M3	1.1	1	1.5
M6	0-1.6	2.3	2.3
C4	9.5	N/A	10.8
C8	13.5	N/A	10.4
C10	9.5	N/A	10.3
C15	9.6	9.4	8.9

9.2. 2011 Canterbury (Christchurch) earthquake

In 2010 and 2011, the city of Christchurch was damaged devastatingly due to liquefaction-induced settlement caused by a series of earthquake motions in grounds mainly consisted of silty and fine sands. These cases provided highly-detailed subsurface investigation, extensive documentation of ground settlement and high-quality ground motion records. For this study, 3 case histories from the 2011 earthquake from the report prepared by Bastani were evaluated due to the fact that the soil profiles in these sites could be simplified into 3 layers, as shown in Table 30. The measurements included SPT and CPT, and laboratory index tests and free-field settlement. All of these case histories were located within central business district of the city. For these locations, the ground motion used was RSN #8158 from the NGA West 2 database with I_a = 5.74 m/s and T_m = 0.21 s.

Table 31 compares the estimates using the proposed equation and measured settlements. Additionally, Bastani used different SPT and CPT-based methods to calculate the liquefaction-

induced settlement at these sites. Some of these estimates are also presented in this table. It can be noted that the settlements estimated using the proposed equation are in good agreement with the range of measurements at each of the sites.

It can be seen that in Site 5, both methods are underestimating the settlement by a considerable margin. It can be concluded that the measured settlement was not just caused by volumetric strain and some of it can be credited to either lateral spreading or ejecta. It should be noted that several ejecta-induced settlements were observed in different locations of Christchurch after the 2011 earthquake. In Figure 57, the comparison between earthquake-induced free-field settlement predicted by the proposed equation and the measured values are shown.

Table 31. Simplified profiles and ground motion parameters for different locations in the Christchurch

Location	H_C (m)	H_L (m)	H_B (m)	D_r (%)
Site 2	0	12	12	53
Site 3	0	12	12	48
Site 5	0	10	16	60

Table 32. Comparison of the volumetric-induced settlements for different locations at the city of Christchurch after the 2011 Eartquake

Location	Measured Settlement (cm)	Prediction by Zhang et al. Method (cm)	Prediction by the Proposed Equation (cm)
Site 2	20	11.6	11
Site 3	10	8.1	12.9
Site 5	25	7.8	8.4

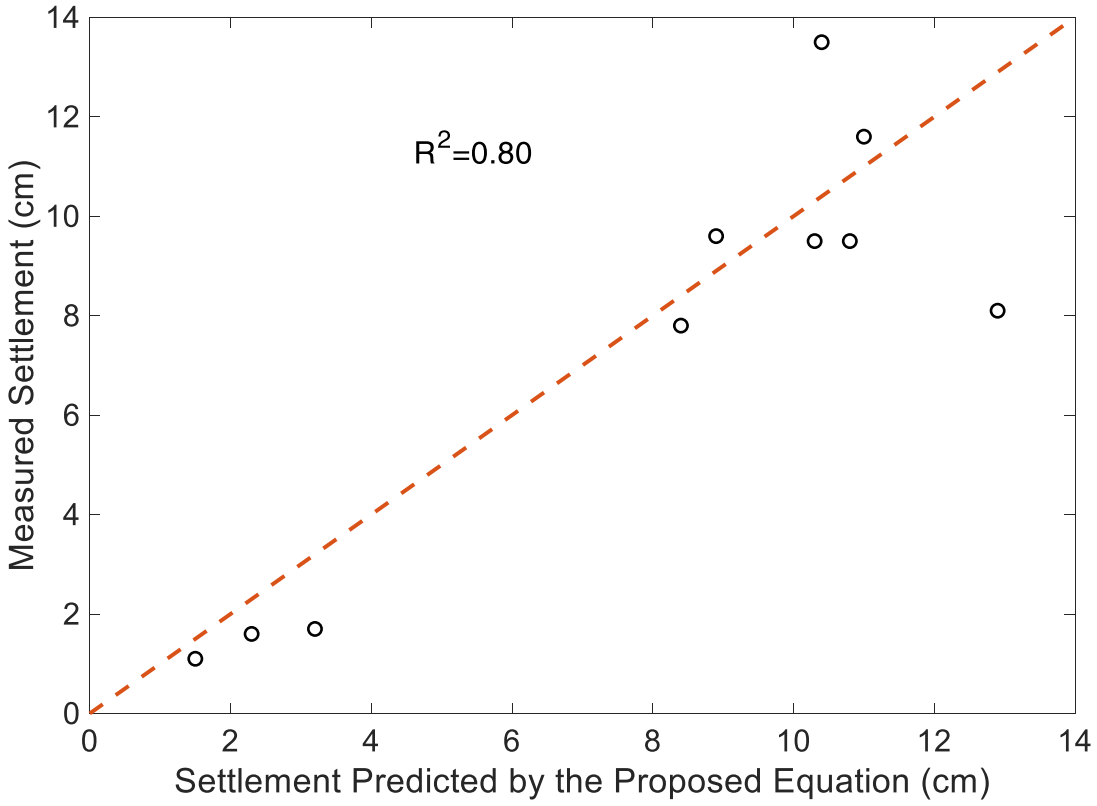

Figure 57. Comparison of earthquake-induced free-field settlement predicted by the proposed equation and the measured values

Chapter 10: Conclusions and recommendations

A new method is presented in this work that complements the recent research focusing on earthquake-induced building settlement, in which the free-field settlement is a component. This method focuses on the evaluation of free-field one-dimensional settlement history (pre- and post-liquefaction) in saturated layered soils. Such an approach enables the investigation of a number of plausible scenarios (post- and developing liquefaction) that entail multi-ensemble simulations of earthquakes of different hazard levels, which are needed to undertake PBE design.

The proposed method is based on an existing incremental shear-volume coupling equation. In this new method, each shear strain history is divided into phases of loading and unloading. Then, the volumetric strain is calculated for the unloading sequences. A single element model created in DEEPSOIL under effective stress-based mode was calibrated to the widely-used Seed and Idriss G/G_{max}-γ and D-γ curves. The porewater pressure model (generalized GMP) was calibrated to match with the probability-based liquefaction potential curves and the porewater generation rate obtained from laboratory test data. The use of simpler, yet robust soil and porewater pressure models gives the proposed method a practical advantage over the more complex models which require a larger number of inputs. The element created with DEEPSOIL is capable of reproducing the settlement values reported in laboratory tests by previous researchers, in both developing liquefaction conditions (FS<1.0) and post-liquefaction.

Soil profiles created with DEEPSOIL were used to obtain the shear strain history in the soil layers and a MATLAB script was developed to estimate the free-field settlement for three different case histories (1989 Loma Prieta, 1995 Kobe and 2011 Christchurch earthquakes). The proposed

method was able to make predictions that are in good agreement with the observed values and was compared to the predictions made using other methods.

The introduced method is then used in this paper to compute the one-dimensional free-field settlement in a series of 3-layered profiles under 28 different earthquake ground motions. These profiles were inspired by the work of Bray and Macedo and consisted of an unsaturated crust, liquefiable layer and a bottom non-liquefiable layer (20 meters in total).

The proposed profiles were created using DEEPSOIL and effective stress-based response analyses were conducted to obtain the soil layer shear strain histories, which were then used to calculate the volumetric utilizing the incremental volumetric strain model. The settlements were calculated using the method proposed by Zhang et al. (2008) as well and the results were compared. The effect of different ground parameters such as relative density (D_r), Thickness of the liquefiable layer (H_L) and the crust layer (H_C) were also investigated. The results show that the settlements predicted by the proposed method are smaller than the ones calculated using the Zhang et al. Method.

Based on the database derived from the prior analyses, a simplified equation has been developed to estimate the free-field one-dimensional settlement. The proposed equation consists of four parameters: two soil profile-related and two ground motion intensity measures. This equation was used to estimate the free-field settlement in 10 different sites after the 1989 Loma Prieta and the 2011 Christchurch earthquakes. These cases had profiles with high-quality site investigation reports and profiles that could be simplified into 3 layers. The estimates made using the proposed equation was compared to the predictions made by Zhang et al's method, which showed good agreement.

Further evaluation of this method with future earthquake scenarios is needed. Since the DEEPSOIL platform is being updated regularly, versions with newer and more advanced soil and porewater pressure models (e.g., silty soils), as they become available, can be used with the proposed method to study settlement behavior. These models could improve the predictions while taking advantage of the simplicity of the proposed method.

At the same time, the proposed equation needs further evaluation with additional existing and future earthquake scenarios. At the same time, since many of the real soil profiles are more complex and many of them cannot be simplified into a 3-layer soil profile. Such ground profiles could be investigated for proposing better equations and evaluation of different parameters. The free-field settlement and porewater pressure generation time history in these soil profiles could also be studied and compared to existing case histories.

10. References

Allen, J., Davis, C., Giovinazzi, S., Hart, D. E., Cochrane, T., Deam, B., ... and Johnson, L. (2014). Geotechnical & flooding reconnaissance of the 2014 March flood event post 2010-2011 Canterbury Earthquake Sequence, New Zealand. Report No. GEER035.

ASTM D6528-07. (2007). Standard test method for consolidated undrained direct simple shear testing of cohesive soils. ASTM International, West Conshohocken, PA

Bastani, S. A. Comparison of observed and calculated earthquake-induced settlements at 6 sites in Christchurch, NZ.

Bennett, M. J. (1990). Ground deformation and liquefaction of soil in the Marina District. Effects of the Loma Prieta Earthquake on the Marina District, San Francisco, California, US Geol. Surv. Open-File Rept. 90, 253.

Benuska, L. (1990). Ground motion, Loma Prieta Earthquake Reconnaissance Report. Earthquake Spectra, 6, 25-80.

Berrill, J. B., and Davis, R. O. (1985). Energy dissipation and seismic liquefaction of sands: revised model. Soils and Foundations, 25(2), 106-118.

Boulanger, R. W., and Idriss, I. M. (2014). CPT and SPT based liquefaction triggering procedures. Report No. UCD/CGM.-14, 1.

Boulanger, R. W., and Idriss, I. M. (2016). CPT-based liquefaction triggering procedure. Journal of Geotechnical and Geoenvironmental Engineering, 142(2): 04015065.

Bray, J. D., and Macedo, J. (2017). 6th Ishihara lecture: Simplified procedure for estimating liquefaction-induced building settlement. Soil Dynamics and Earthquake Engineering, 102, 215-231.

Bullock, Z., Dashti, S., Karimi, Z., Liel, A., Porter, K., & Franke, K. (2019). Probabilistic models for residual and peak transient tilt of mat-founded structures on liquefiable soils. Journal of Geotechnical and Geoenvironmental Engineering, 145(2), 04018108.

Bullock, Z., Karimi, Z., Dashti, S., Porter, K., Liel, A. B., & Franke, K. W. (2019). A physics-informed semi-empirical probabilistic model for the settlement of shallow-founded structures on liquefiable ground. Géotechnique, 69(5), 406-419.

Byrne, P. (1991). A cyclic shear-volume coupling and pore-pressure model for sand. Proceedings of Second International Conference on Recent Advances in Geotechnical Earthquake Engineering and Soil Dynamics, St. Louis, Missouri, 47-55.

Carlton, B. (2014). An improved description of the seismic response of sites with high plasticity soils, organic clays, and deep soft soil deposits. University of California, Berkeley.

Cetin, K. O., Bilge, H. T., Wu, J., Kammerer, A. M., and Seed, R. B. (2009). Probabilistic model for the assessment of cyclically induced reconsolidation (volumetric) settlements. Journal of Geotechnical and Geoenvironmental Engineering, 135(3), 387-398.

Geo-Engineering Extreme Events Reconnaissance (GEER). (2010). Effects of ground failure on bridges, roads, railroads, and lifeline systems. Chapter 9.0, Geo-engineering reconnaissance of the February 27, 2010 Maule, Chile earthquake, Ver. 1.

Green, R. A., Mitchell, J. K., Polito, C. P. (2000). An energy-based excess pore pressure generation model for cohesionless soils. In Proceedings of John Booker Memorial Symposium. Developments in Theoretical Geomechanics. Rotterdam, 383-390.

Hashash, Y. M. A., Musgrove, M. I., Harmon, J. A., Ilhan, O., Groholski, D. R., Phillips, C. A., and Park, D. (2017). DEEPSOIL 7.0, user manual. University of Illinois at Urbana-Champaign.

Idriss, I. M., and Boulanger, R. W. (2006). Semi-empirical procedures for evaluating liquefaction potential during earthquakes. Soil Dynamics and Earthquake Engineering, 26(2-4), 115-130.

Idriss, I. M., and Boulanger, R. W. (2008). Soil liquefaction during earthquakes. Earthquake Engineering Research Institute, California.

Idriss, I. M., and Boulanger, R. W. (2008). Soil liquefaction during earthquakes. Earthquake Engineering Research Institute, California.

Ishihara, K., and Yoshimine, M. (1992). Evaluation of settlements in sand deposits following liquefaction during earthquakes. Soils and Foundations, 32(1), 173-188.

Ishihara, K., Yasuda, S., and Nagase, H. (1996). Soil characteristics and ground damage. Soils and Foundations, 36, 109-118.

Iwasaki, T., Arakawa, T., and Tokida, K. I. (1984). Simplified procedures for assessing soil liquefaction during earthquakes. International Journal of Soil Dynamics and Earthquake Engineering, 3(1), 49-58.

Jahed Orang, M., Motamed, R., Prabhakaran, A., & Elgamal, A. (2021). Large-scale shake table tests on a shallow foundation in liquefiable soils. Journal of Geotechnical and Geoenvironmental Engineering, 147(1), 04020152.

Karimi, Z., & Dashti, S. (2016). Numerical and centrifuge modeling of seismic soil–foundation–structure interaction on liquefiable ground. Journal of Geotechnical and Geoenvironmental Engineering, 142(1), 04015061.

Karimi, Z., & Dashti, S. (2017). Ground motion intensity measures to evaluate II: the performance of shallow-founded structures on liquefiable ground. Earthquake Spectra, 33(1), 277-298.

Karimi, Z., Dashti, S., Bullock, Z., Porter, K., & Liel, A. (2018). Key predictors of structure settlement on liquefiable ground: a numerical parametric study. Soil Dynamics and Earthquake Engineering, 113, 286-308.

Konder, R. L., and Zelasko, J. S. (1963). A hyperbolic stress-strain formulation for sands. Proceedings of 2nd Pan-Am. Conference on Soil Mechanics and Foundation Engineering, 289-324.

Kramer, S. L. (1996). Geotechnical earthquake engineering. Pearson Education India.

Lee, K. L., and Albaisa, A. (1974). Earthquake induced settlements in saturated sands. Journal of the Geotechnical Engineering Division, 100(4), 387-406.

Liam Finn, W. D., and Byrne, P. M. (1976). Estimating settlements in dry sands during earthquakes. Canadian Geotechnical Journal, 13(4), 355-363.

Liam Finn, W. D., Lee, K. W., and Martin, G. R. (1977). An effective stress model for liquefaction. Journal of the Geotechnical Engineering Division 103(6), 517-533.

Macedo, J., & Bray, J. D. (2018). Key trends in liquefaction-induced building settlement. Journal of Geotechnical and Geoenvironmental Engineering, 144(11), 04018076.

Martin, G. R., Finn, W. L., and Seed, H. B. (1975). Fundementals of liquefaction under cyclic loading. Journal of Geotechnical and Geoenvironmental Engineering, 101(5), 423-438.

Matasović, N., and Vucetic, M. (1995). Generalized cyclic-degradation-pore-pressure generation model for clays. Journal of Geotechnical Engineering, 121(1), 33-42.

O'Rourke, T. D., Stewart, H. E., Gowdy, T. E., and Pease, J. W. (1991). Lifeline and geotechnical aspects of the 1989 Loma Prieta earthquake. Proceedings of 2nd International Conference on Recent Advances in Geotechnical Earthquake Engineering and Soil Dynamics, 1601-1612.

Polito, C. P., Green, R. A., and Lee, J. (2008). Pore pressure generation models for sands and silty soils subjected to cyclic loading. Journal of Geotechnical and Geoenvironmental Engineering, 134(10), 1490-1500.

Robertson, P. K., and Wride, C. E. (1998). Evaluating cyclic liquefaction potential using the cone penetration test. Canadian Geotechnical Journal, 35(3), 442-459.

Rollins, K. M., and McHood, M. D. (1998). Comparison of computed and measured liquefaction-induced settlements in the Marina District, San Francisco. The Loma Prieta, California Earthquake of October 17, 1989-Liquefaction, US Geological Survey Professional Paper 1551-B, 223-240.

Seed, H. B., and Idriss, I. M. (1970). Soil moduli and damping factors for dynamic response analyses. Report No. EERC 70-10, Earthquake Engineering Research Center, University of California, Berkeley, California.

Seed, H. B., Martin, P. P., and Lysmer, J. (1976). Pore-water pressure changes during soil liquefaction. Journal of the Geotechnical Engineering, 102(4), 323-346.

Toki, K. (1995). Committee of Earthquake Observation and Research in the Kansai Area.

Tokimatsu, K., and Seed, H. B. (1987). Evaluation of settlements in sands due to earthquake shaking. Journal of Geotechnical Engineering, 113(8), 861-878.

Wood, C. M., Cox, B. R., Green, R. A., Wotherspoon, L. M., Bradley, B. A., and Cubrinovski, M. (2017). Vs-based evaluation of select liquefaction case histories from the 2010–2011 Canterbury earthquake sequence. Journal of Geotechnical and Geoenvironmental Engineering, 143(9), 04017066.

Youd, T. L., and Idriss, I. M. (2001). Liquefaction resistance of soils: summary report from the 1996 NCEER and 1998 NCEER/NSF workshops on evaluation of liquefaction resistance of soils. Journal of Geotechnical and Geoenvironmental Engineering, 127(4), 297-313.

Zhang, G., Robertson, P. K., and Brachman, R. W. (2002). Estimating liquefaction-induced ground settlements from CPT for level ground. Canadian Geotechnical Journal, 39(5), 1168-1180.

Zhang, G., Robertson, P. K., and Brachman, R. W. (2002). Estimating liquefaction-induced ground settlements from CPT for level ground. Canadian Geotechnical Journal, 39(5), 1168-1180.

Ziotopoulou, K., and Boulanger, R. W. (2013). Numerical modeling issues in predicting post-liquefaction reconsolidation strains and settlements. Proceedings of 10th International Conference on Urban Earthquake Engineering, Tokyo Institute of Technology, Tokyo, 469–475.